ADDIS ABABA UNIVERSITY
SCHOOL OF GRADUATE STUDIES

Stability Study and Photovoltaic Application of Quinoxaline Based Polymers and Effect of Low Boiling Point Solvent Additives on Photovoltaic Performance of Bulk Heterojunction Polymer Solar Cells

Bedasa Abdisa

A Thesis Submitted to
The Department of Chemistry

Presented in Fulfillment of the Requirements for the Degree of

Doctor of Philosophy (Physical Chemistry)

Addis Ababa University, Addis Ababa, Ethiopia

October, 2016

Addis Ababa University

School of Graduate Studies

This is to certify that the thesis prepared by Bedasa Abdisa Gonfa, entitled: *Stability Study and Photovoltaic Application of Quinoxaline Based Polymers and Effect of Low Boiling Point Solvent Additives on Photovoltaic Performance of Bulk Heterojunction Polymer Solar Cells* and submitted in fulfillment of the requirements for the Degree of Doctor of Philosophy (Physical Chemistry) compiles with the regulations of the University and meets the accepted standards with respect to originality and quality.

Signed by Examining Committee

Name	Signature	Date
1. Prof. Teketel Yohannes (Advisor)	----------	25./10./2016/
2. Dr. Markus Clark Scharber (External Examiner)	----------	25./10./2016/
3. Prof. Theodros Solomon (Internal Examiner)	----------	25./10./2016/
4. Dr. Shimelis Admassie (Internal Examiner)	----------	25./10./2016/
5. Dr. Ahmed Mustefa (Chairman)	----------	25./10./2016/
_____	----------	----/----/--------/

Chairman, College Academic Commission

Abstract

Stability Study and Photovoltaic Application of Quinoxaline Based Polymers and Effect of Low Boiling Point Solvent Additives on Photovoltaic Performance of Bulk Heterojunction Polymer Solar Cells

Bedasa Abdisa

Addis Ababa University, 2016

In this study the photochemical stability and photovoltaic performance of two polymer families are presented; one based on a thiophene-quinoxaline unit and the other one on a thiophene-pyridopyrazine unit. Copolymerization of these monomers together with thiophene-hexylthiophene was performed in order to make the polymers more black, *i.e.* to fill the gap between the high- and the low-energy peak in the absorption spectra. The study has focused on how an increasing fraction of thiophene-hexylthiophene affects the photo-oxidative stability of these polymers, as well as the solar cell performance. Accordingly, thiophene-pyridopyrazine devices displayed increased device efficiency. In addition, the stability is retrained upon inclusion of the extra monomer of 30% and 50% mole fraction of thiophene-hexylthiophene. In contrast, it was found that for the thiophene-quinoxaline based copolymer both, device efficiency and stability, decreased with inclusion of 30%, 50%, and also 80% thiophene-hexylthiophene.

Furthermore, the effect of incorporation of low mole fraction of thiophene-hexylthiophene i.e 1% and 2.5% in to quinoxaline based polymer on photochemical and photovoltaic performance was also studied. In contrast to the incorporation of large fraction of thiophene-hexylthiophene in to quinoxaline based polymer, incorporation of low fraction of thiophene-hexylthiophene has improved both photochemical stability and photovoltaic performance of the copolymers.

Additionally, the effect of low boiling point solvent additives such as iodomethane, iodoethane, and diiodomethane on photovoltaic performance of bulk heterojunction polymer solar cells was studied. According to our findings, the efficiency of TQ1:[60]PCBM based devices have increased from 3.41% (control device) to 4.28, to 4.41, and 4.66% when the devices are processed from 3% (v/v) IMe, IEt, and DIMe, respectively. Similarly, the PCE of PCDTBT:[70]PCBM based devices have also showed enhancement from 3.08% (control device) to 3.39, 3.80, and 4.37% when processed from 3% (v/v) IMe, IEt, and DIMe, respectively. All the solvent additives have improved current density and fill factor leading to enhanced power conversion efficiency compared to control device fabricated without any additive. This is due to formation of nanomorphology creating large D-A interface area for better charge carrier dissociation and interpenetrated networks for efficient charge carrier transport to electrodes as confirmed from the AFM images. As confirmed by comparing UV-Vis absorption spectra of pristine blend films and blend films soaked in the additives for 5 seconds, the solvent additives selectively dissolved the PCBM aggregates leading to enhancing their misciblity/interaction in to the polymer domains of the

active layer. The enhanced misciblity and nanoscale formation of the blends were further confirmed by an increase of the quenching efficiency of the PL of the blends containing the solvent additives compared to the pristine blends. Therefore, the increase in interface area and formation of networks between the donors and acceptors up on addition of the low boiling point solvent additives are the main reasons for the improvement of current density and fill factor leading to enhanced PCEs.

Acknowledgements

First and foremost, I would like to express my sincere gratitude to my advisor Prof. Teketel Yohannes for his encouragement, guidance and valuable suggestions during the whole of my study and for the realization of the completion of this work.

My deepest gratitude also goes to Prof. Olle Inganäs for giving me the opportunity to do part of my research work in his laboratory at Linkoping University, Sweden. Thank you for your unreserved encouragement and best scientific experiences I got in your institute. I also would like to thank Prof. Olle Inganäs's organic electronics group Prof. Fengling Zhang, Dr. Zaifei Ma, Dr. Zheng Tang, Jonas Bergqvist, Armantas Melianas, Dr. Wolfgang Tress, Dr. Scott Mauger, and Dr. Feng Gao for making all my days in Linkoping University beautiful and enjoyable by your very friendly approach and for sharing me your scientific experiences.

I would like to thank also Prof. Mats Andersson and Dr. Patrik Henriksson from Chalmers University, Sweden, for providing me almost all the polymers I used in my study and Prof. Ergang Wang from Chalmers University, Sweden, for helping us in generating some of AFM data I used in this work.

I would like to express my thank to Adama Science and Technology University for sponsoring my study and Addis Ababa University, Chemistry Department, for hosting me as PhD student and facilitating administrative affairs and conducive working environment during all my study time. My appreciation and thanks also goes to academic staff members of Chemistry Department of Addis Ababa University: Prof. Theodros Solomon, Dr. Shimelis Admassie, Dr. Mesfin Redi, Dr. Ahmed Mustefa,

Prof. Wondimagegn Mammo, and Dr. Edwardo Pérez for their encouragement, comments, and scientific criticism for the success of my study. My thank goes also to technical staff members of Department of Chemistry of Addis Ababa University: Ato Sahlemichael Demie and the secretaries.

I thank also Dr. Siraye Esubalew, Dr. Getachew Adam, Dr. Sisay Taddese, and Dr. Fedlu Kedir for sharing their research experience in area of organic photovoltaics. I also thank my friends, Dr. Hagos Tesfay, Endale Tsegaye, Girma Erjabo, Zekarias Teklu, Hagos Tukue, and Dawit Tibebu for joyful time we had together at Addis Ababa University.

I would like also to express my heartfelt thank to my mother Likitu Tuge, father Abdisa Gonfa, sisters, brothers, and friends for your encouragement, moral and material support without which my success would not have been realized. You all have special place in all my life and thanks once more again!

Lastly but for most I would like to express my gratitude to my lovely wife Zinash Dame for her true love, care, encouragement, and support that strengthen me all the time. The long journey would have not been possible without you and you really shared the most for my success. My affection also goes to my little son Murti Bedasa and my baby daughter Wedu Bedasa who bring me the happiness I have never felt before in my life.

Bedasa Abdisa

Table of Contents **Page**

List of Figures

List of Tables

List of Symbols and Abbrevations

C_{60}	Buckminsterfullerene
CP	Conducting polymer
PE	Polyethylene
σ	Sigma
π	Pi
E_g	Energy bandgap
HOMO	Highest occupied molecular orbital
LUMO	Lowest unoccupied molecular orbital
E_{ox}	Oxidation potential
E_{red}	Reduction potential
PA	Polyacetylene
PPP	Poly(p-phenylene)
PT	Polythiophene
Ppy	Polypyrrole
PANI	Polyaniline
MIS	Metal-insulator-semiconductor

MS	Metal-insulator
Mw	Molecular weight
PD	Polydispersity
BHJ	Bulk heterojunction
OSC	Organic solar cell
OPV	Organic photovoltaics
PSC	Polymer solar cell
RH	Relative humidity
ITO	Indium-doped tin oxide
FTO	Fluorine-doped tin oxide
PEDOT:PSS	Poly(3,4-ethylenedioxythiophene):poly(styrenesulfonate)
LCA	Life cycle analysis
D-A	Donor-acceptor
P3HT	Poly(3-hexylthiophene)
L_D	Diffusion length
η_A	Absorption efficiency
η_{ED}	Exciton diffusion efficiency
η_{CT}	Charge transfer efficiency
η_{CC}	Charge collection efficiency
CT	Charge transfer
J-V	Current density-Voltage

V_{OC}	Open circuit voltage
J_{SC}	Short circuit current density
IPCE	Incident photon-to-current conversion efficiency
MPP	Maximum power point
J_M	Maximum current density
V_M	Maximum voltage
FF	Fill factor
P_{in}	Incident power
EQE	External quantum efficiency
PCE	Power conversion efficiency
λ	Wavelength
MDMO-PPV	Poly(2-methoxy-5-(3′,7′-dimethyloctyloxy)-1,4-phenylenevinylene)
TQ1	Poly[2,3-bis-(3-octyloxyphenyl)quinoxaline-5,8-diyl-*alt*-thiophene-2,5-diyl]
TQN	Poly[2,3-bis(3-(octyloxy)phenyl)pyrido[3,4-b]pyrazine-alt-thiophene]
THT	Poly(thiophene-hexylthiophene)
PCDTBT	Poly[*N*-9′-heptadecanyl-2,7-carbazole-*alt*-5,5-(4′,7′-di-2-thienyl-2′,1′,3′-benzothiadiazole)]
PCPDTBT	Poly[2,6-(4,4-bis-(2-ethylhexyl)-4H-cyclopenta [2,1-b;3,4-

	b′]dithiophene)-alt-4,7(2,1,3-benzothiadiazole)]
PFPA-1	Poly(3,3′-([(9′,9′-dioctyl-9H,9′H-[2,2′-bifluorene]-9,9-diyl)bis(4,1-phenylene)]bis(oxy))bis(N,N-dimethylpropan-1-amine))
[70]PCBM	[6,6]-phenyl-C_{71}-butyric acid methyl ester
[60]PCBM	[6,6]-phenyl-C_{61}-butyric acid methyl ester
IMe	Iodomethane
IEt	Iodoethane
DIMe	Diiodomethane
o-DCB	*Ortho*-dichlorobenzene
bp	Boiling point
DMSO	Dimethylsulphoxide
DMF	Dimethl formamide
THT	Tetrahydrofuran
HC-PEDOT:PSS	High conductive poly(3,4-ethylenedioxythiophene):poly(styrenesulfonate)
CN	Chloronaphthalene
AM	Air mass
AFM	Atomic force microscopy
PL	Photoluminescence
UV-Vis/NIR	Ultraviolet-Visible/Near infrared

SWV	Squarewave Voltammetry
A_{max}	Maximum absorbance
RMS	Root mean square

1. Introduction

1.1 The Need for Solar Energy

Continuous industrialization and urbanization of developing countries, growth in human population, and a general increase in human welfare is projected to increase the demands for energy in the future by a large proportion. By the year 2050, the anticipated level of energy consumption by humans is 28 - 35 TW, which is a challenge we currently cannot meet with the sources of energy available. Presently, more than 80% of the energy supply is derived from fossil fuels (coal, oil, and gas) [1]. However, these sources of energy largely pollute the environment and emit green house gases and have become the main cause for the global warming of the world. Besides the environmental problem they cause, fossil fuels are also largely decreasing from their reservoir and would not satisfy potentially the energy need of the world in the future [2 - 7]. As a result of this detrimental factor and their decrease from reservoir of fossil fuels, clean and renewable alternative energy sources have been under investigation by researchers for fulfilling the energy demand of the world. These renewable and clean energy sources include hydropower, solar energy, geothermal energy, wind energy, and ocean energy. Among the renewable and clean energy sources, solar energy outweighs most of the other renewable energy sources by orders of magnitude when comparing the theoretical potentials [1, 8, 9]. As a matter of fact the side of the earth that is exposed to the sun receives approximately 1.2×10^5 TW hour from the sun continuously, which is approximately 10,000 times the energy we consumed in the year 2004 i.e. more energy from the sun hits the earth in one hour than all of the energy consumed on our planet in an entire year [1, 9].

This indicates that there is a huge gap between our present use of solar energy and its potential which defines the grand challenge in energy research. Therefore, solar energy is a renewable and clean energy source with a large potential for fulfilling the increasing energy demand of the world and this has motivated many scientists working in this field.

1.2 History of Photovoltaics

Photovoltaics also called solar cells are devices that convert solar energy into electrical energy. The photovoltaic effect, the conversion of light into electrical power, can be traced back to Becquerel's 1839 pioneering studies that discovered a photocurrent when platinum electrodes, covered with silver bromide or silver chloride, was illuminated in aqueous solution. Strictly speaking this is a photoelectrochemical effect [10].

In the modern era, the tipping point that transformed photovoltaics into a technology, to convert sun light into electricity, was the 1954 report by Chapin et al. [11] of a silicon based single p-n junction solar cell device. This type of silicon solar cell absorbs light and generates electron-hole pairs that diffuse to the p-n junction and driven efficiently to respective electrodes in opposite directions by an electric field produced at the boundary and generated electric current. With this pioneering work of photovoltaics a solar power conversion efficiency of 6% was achieved [11]. Since then, this clean and sustainable energy technology have been expected to play a major role in meeting the global energy challenge and drawn the attention of scientists to carry out in depth research work to improve the solar energy-to-electric current

conversion efficiency of the technology. Decades after this pioneering work, intensive research work on the area has boosted the power conversion efficiency of single crystalline silicon solar cells to about 25.6% at present [12, 13]. As a result of this the current solar technologies are dominated by wafer-size single-junction solar cells based on crystalline silicon that are assembled into large area modules.

Furthermore, the monocrystalline silicon solar cells, the so called first-generation photovoltaics, exhibited little degradation in performance during operations. Therefore, from the birth of the solar cell as a technology it was thus not an integral part of the understanding that such a device could exhibit instability. However, the drawback of the monocrystalline silicon solar cell was the significant loss in material when sawing the ingots into wafers and also the appreciable thickness of the wafers (~0.25 mm - 1 mm). In an effort to decrease the manufacturing cost of the technology, massive research efforts were dedicated towards realizing thin film solar cell with the idea of lowering the thermal budget and the materials usage [14].

Thin film solar cells, referred to as second-generation photovoltaics, have been under active investigation in order to further reduce the cost of produced electricity. This was intended to be done by increasing the power conversion efficiency, reducing the amount of absorbing material needed, and lowering the assembly cost of modules. Thin film photovoltaic technologies are based on inorganic semiconductor materials that are more absorbing than crystalline silicon and can be processed directly onto large area substrates [15]. Such semiconductors include amorphous silicon, II-VI

semiconductors such as CdS or CdTe, and chalcogenides such as $CuInSe_2$ (CIS) or $CuInGaSe_2$ (CIGS) [16]. Despite the laboratory demonstration of cells with high efficiencies, 20.5% for CIGS and 21% for CdTe, the controlled manufacturing of second generation cells remains a challenge and their commercial use is growing but not as widespread yet as their price is still high to enter the market on a large scale [12, 13]. Therefore, other solar cell technology alternative which takes in to account ease of fabrication and cost has been investigated. These photovoltaic technologies are the organic solar cells.

The basis for organic solar cells, referred to as the third-generation photovoltaics, was the finding of dark conductivity in halogen doped organic compounds in 1954 [17]. In the late 1970s, the conductivity of the polymer polyacetylene, again by doping with halogens, was discovered [18], for which its three main contributors Shirakawa, Heeger and MacDiarmid were awarded the Nobel Prize in Chemistry in 2000. It is the semiconducting and light absorbing properties that make conjugated organics a very interesting choice for photovoltaics.

The first organic solar cells were based on an active layer made of a single material, sandwiched between two electrodes of different work functions. The typical device configuration is shown in Figure 1.2.1 (left). By the absorption of light, strongly Coulomb-bound electron-hole pairs are created, so-called singlet excitons. The binding energy of excitons in organic semiconductors is usually between 0.5 and 1 eV as their effective dielectric constant is much lower than the corresponding inorganic

materials. To generate photocurrent, the e/h forming exciton has to be separated from each other. In order to overcome the exciton binding energy, one has either to rely on the thermal energy, or dissociate the exciton at the contacts [19]. Unfortunately, both processes have a rather low efficiency. Under the operating conditions of solar cells, the temperature is not high enough, and the sample thickness is much higher than the exciton diffusion length. The consequence is that not all excitons are dissociated, but can as well recombine radiatively by photoluminescence. Consequently, the single layer organic solar cells had power conversion efficiencies of far below 1% for the solar spectrum [20]. Therefore, the introduction of a second organic semiconductor layer, that can accept the excited electron, was required to enhance the power conversion efficiency leading to the concept of bilayer organic solar cell.

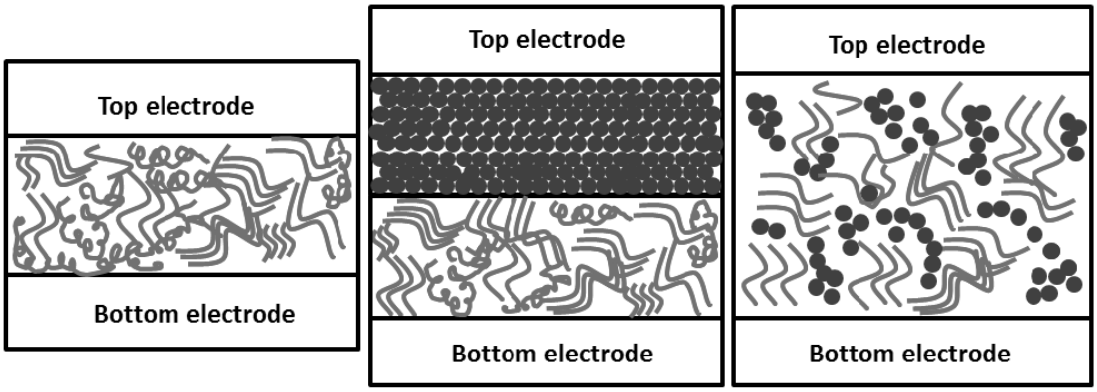

Figure 1.2.1. *Polymer solar cells constructed with three different active layer structures: single layer (left), bilayer (middle), and bulk heterojunction (right).*

The first organic bilayer solar cell was presented by Tang in the mid-1980s [21]. The typical device configuration is shown in Figure 1.2.1 (middle). The light is usually

absorbed in the so-called donor material, a hole conducting small molecule such as copper phthalocyanine. In bilayer devices, the photogenerated singlet excitons could diffuse within the donor towards the planar interface to the second material, the acceptor, buckminsterfullerene (C_{60}) which is usually chosen to be strongly electronegative. The acceptor material provides the energy needed for the singlet exciton to be separated, as the electron can go to a state of much lower energy within the acceptor. This charge transfer dissociates the exciton, the electron moves to the acceptor material, whereas the hole remains on the donor [22]. This charge transfer, or electron transfer, is reported to be very fast. Indeed, it was found to be faster than 100 fs in polymer-fullerene systems, and very efficient, as the alternative loss mechanisms are much slower [23]. Thus, the exciton is dissociated and the resulting charge carriers are spatially separated. Then the separated charge carriers are driven to their respective electrodes by electric field. Accordingly, the organic bilayer solar cells invented by Tang achieved a power conversion efficiency of about 1% [21]. The limiting factor in this concept is that for a full absorption of the incident light, the layer thickness of the absorbing material has to be of the order of the absorption length, approximately 100 nm. This is much more than the diffusion length of the excitons, about 10 nm in disordered and semicrystalline polymers and small molecules. As mostly the exciton diffusion length is much lower than the absorption length, the potential of the bilayer solar cell is difficult to exploit.

In the early 1990s a novel concept bulk heterojunction solar cell was introduced accounting for the low exciton diffusion length in disordered organic semiconductors

and the required thickness for a sufficient light absorption [24]. This approach, shown in Figure 1.2.1 (right), features a distributed junction between the donor and the acceptor material forming interpenetrated materials through the bulk of the film. This concept is implemented by spin coating a polymer-fullerene blend, or by co-evaporation of conjugated small molecules. Bulk heterojunctions have the advantage of being able to dissociate excitons very efficiently over the whole extent of the solar cell, and thus generating electron-hole pairs throughout in the film. The disadvantages are that it is somewhat more difficult to separate these still strongly Coulomb bound charge carrier pairs due to the increased disorder, and that percolation to the contacts is not always given in the disordered material mixtures. Furthermore, in bulk heterojunction based solar cells it is also more likely that trapped charge carriers recombine with mobile ones. However, the positive effects on the device performance outweigh the drawbacks [24] and currently power conversion efficiency exceeding 11% and 12% for single-and multi-junction polymer solar cells have been reported, respectively [12, 13].

Generally, the low-temperature processing of either organic small molecules from the vapor phase or polymers from solution confers organic semiconductors with a critical advantage over their inorganic counterparts. For inorganic based solar cells high-temperature processing requirements limit the range of substrates on which they can be deposited. Particularly attractive for organic semiconductors are flexible plastic substrates that can lead to applications and consumer products with lower cost, highly flexibility, and light weight. Low-temperature processing also cuts on energy use

during manufacturing, further reducing the energy payback time which is defined as the operating life of a power-generating device needed to produce the amount of energy invested during manufacturing, installation and maintenance. These attributes, combined with the ability to tune the physical properties of organic materials by fine tuning their chemical structure, constitute the main drivers boosting research and industrial interest in organic photovoltaics [25].

1.3 Conjugated Organic Polymers

Conventional polymers, plastics, have been used traditionally because of their attractive chemical, mechanical, and electrically insulating properties, and not for their electronic properties. A polymer, material containing a long chain of molecular structures, is first and foremost an insulator. The idea that polymers or plastics could conduct electricity is considered absurd for decades ago. Their wide application as an insulating material is the reason they are studied and developed in the first place. In fact, these materials are commonly used for surrounding copper wires and manufacturing the outer structures of electrical appliances that prevent humans from coming in direct contact with electricity [26 - 29].

However, over three decades ago researchers showed that certain class of polymers exhibits semiconducting properties [30, 31]. Accordingly, studies showed that polypyrroles exhibit signs of conductivity and its conductivity changed following the adsorption of electron acceptor or donor molecules in relation to the concentration of donor nitrogen atoms in polypyrrole. This brought the researchers to the conclusion that the polymer may behave as an intrinsic or extrinsic semiconductor with n- or p-

type characteristics. Charge-transfer complexes of strength sufficient to cause partial ionization induce extrinsic behavior by changing the ratio of the number of electrons to the number of holes. Furthermore, substituent groups such as the hetero atoms like nitrogen in polypyrrole which interact with the π-electron system inductively or through resonance affect only the relative mobility of the charge carriers and induce intrinsic behavior [32]. This discovery was followed by the work of Shirakawa and co-workers in 1977 who reported the first synthesis of doped polyacetylene which was formed accidentally. This incident took place when one of the co-workers mistakenly added excessive amounts of catalyst in the reaction vessel for the polymerization of acetylene which resulted in the formation of a silver film instead of the expected black powder. When analyzed, the new product had different optical properties compared to the normal black powder. Hence, by using iodine vapor they attempted to oxidize polyacetylene in order to obtain its normal optical properties. However, that only resulted in an increase in the conductivity of the polymer [18]. It was since this discovery reported by Shirakawa and co-workers, conducting polymers (CPs) have received much attention in the field of material Science.

By the mid-1980s, several research teams in both academia and industry were investigating π-conjugated small molecules and polymers to gain benefit of their unique optical and semiconducting properties leading to the emergence of the fields of plastic electronics and photonics. Technologies depending on conjugated polymers are thought to compliment current inorganic-based optoelectronic devices, which greatly impacted our society starting from the second half of the 20th century. The

goal of organic based opto-electronic devices is not that of attaining or exceeding the level of performance of silicon technologies but of enabling the fabrication of certain optoelectronic devices or part of them at far reduced costs and/or enabling completely new device functionalities such as: mechanical flexibility and optical transparency, that are challenging to achieve with silicon [33].

1.3.1 Nature of Conjugated Organic Polymers

Since carbon has the electronic structure, $1s^2 2s^2 2p^2$, carbon atoms form four nearest-neighbor bonds. In σ-bonded polymers, the C-atoms are sp^3 hybridized, as in polyethylene (PE), and each C-atom has four σ-bonds. In such non-conjugated polymers, the electronic structure of the chain of atoms which comprises the backbone of the macromolecule consists of only σ-bands. However, in this kind of polymers there is a possibility for π-electronic levels to be localized on side groups as, for example, in polystyrene. The bandgap ($E_g(\sigma)$) for these kind of polymers is the energy difference between the anti-bonding and bonding sigma (σ) bonds which is expected to be large. Therefore, the large electron energy band gaps in σ-bonded polymers, $E_g(\sigma)$, renders these polymer materials electrically insulating, and generally non-absorbing to visible light. In polyethylene, for example, which consists of a monomeric repeating unit -(CH_2-CH_2)-, the optical band gap is on the order of 8 eV [27].

However, in conjugated polymers, there exists a continuous network of a simple chain of adjacent unsaturated carbon atoms i.e. carbon atoms in the sp^2 hybridized

state. Each of these sp^2 C-atoms has three σ-bonds. The remaining fourth p_z atomic orbital, which is perpendicular to the plane of the three sp^2 hybridized orbitals, exhibits π-overlap with the p_z-orbitals of the nearest neighbor sp^2 hybridized C-atoms. This chain of atoms with π-overlap of the atomic p_z-orbitals leads to the formation of π-states delocalized along the polymer chain which is the origin of conductivity in these conjugated organic compounds [27, 34]. In a system with one-dimensional periodicity, these π-states form the frontier electronic bands, with a π-band gap, $E_g(\pi) < (E_g(\sigma)$, accounting for optical absorption at lower photon energies. The bonding and antibonding π and π^* orbitals, also called the highest occupied molecular orbital (HOMO) and the lowest unoccupied molecular orbital (LUMO), are formed, respectively.

The essential properties of the delocalized π-electron system, which differentiate a typical conjugated polymer from a conventional polymer with π-bands, are (i) the electronic band gap, E_g, is relatively small (1 - 3 eV), leading to low-energy electronic excitations and semiconductor behavior; (ii) the polymer chains can be rather easily oxidized or reduced, usually through charge transfer with molecular dopant species; (iii) carrier mobilities are large enough that high electrical conductivities are realized in the doped state; and (iv) charge carrying species are not free electrons or holes, but quasi-particles, which may move relatively freely through the material, or at least along uninterrupted polymer chains [27, 34, 35]. Figure 1.3.1 shows some of the most common conjugated polymers.

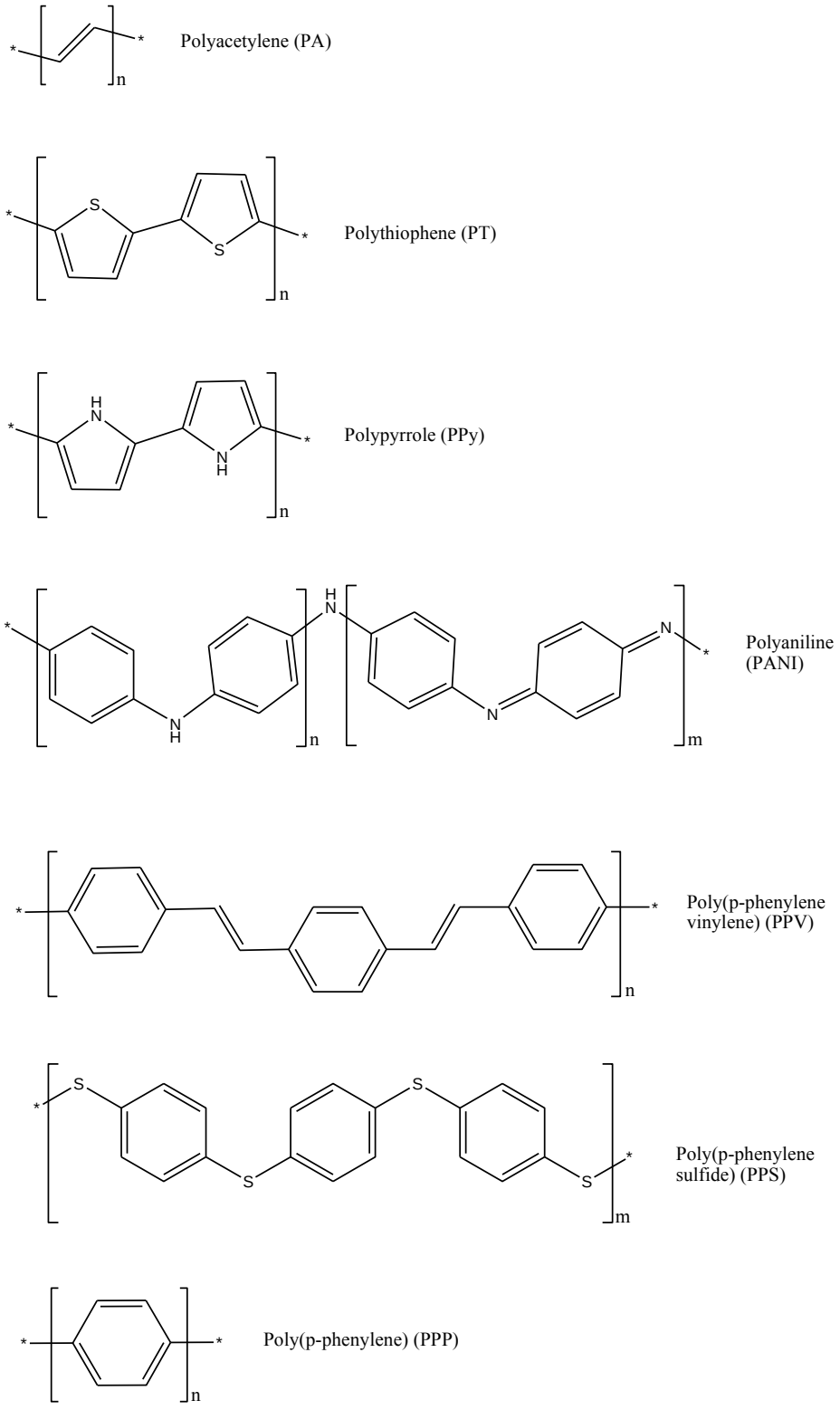

Figure 1.3.1. *Some common conjugated polymers.*

1.3.2 Doping of Conjugated Organic Polymers

Conjugated organic polymers are either electrical insulators or semiconductors. Those that can have their conductivity increased by several orders of magnitude from the semiconductor regime are generally referred to as electronic polymers and have become of very great scientific and technological importance since 1990. The concept of doping is the unique, central, underlying, and unifying theme, which distinguishes conducting polymers from all other types of polymers. During the process, an organic polymer, either an insulator or semiconductor having a small conductivity, typically in the range from 10^{-10} to 10^{-5} S/cm is converted to a polymer, which is in the metallic conducting regime (1 - 10^{4} S/cm). The controlled addition of usually small ($\leq$ 10% w/w) non-stoichiometric quantities of chemical species, for chemical doping, causes dramatic changes in the electronic, electrical, magnetic, optical, and structural properties of polymer. Doping is reversible with little or no degradation of the polymer backbone [36, 37]. Reversible doping of conducting polymers, with associated control of the electrical conductivity over the full range from insulator to metal, can be accomplished either by chemical doping, or by electrochemical doping. By controllably adjusting the doping level, a conductivity anywhere between that of the non-doped (insulating or semiconducting) and that of the fully doped (highly conducting) form of the polymer can be easily obtained. During chemical and electrochemical doping, charge neutrality is maintained by the introduction of counter ions. The electrical conductivity results from the existence of charge carriers, obtained through doping, and from the ability of those charge carriers to move along the π-bonded back bone of the polymers. Figure 1.3.2 shows conductivity of

conjugated polymers in neutral and doped state compared to other common materials. Doping can be accomplished in a number of ways [31, 38]. These include chemical doping by charge transfer, electrochemical doping, acid-base chemistry doping, photodoping, and doping by charge injection at metal-semiconductor interface. Among these the most commonly used doping methods are described below [31, 36 - 38].

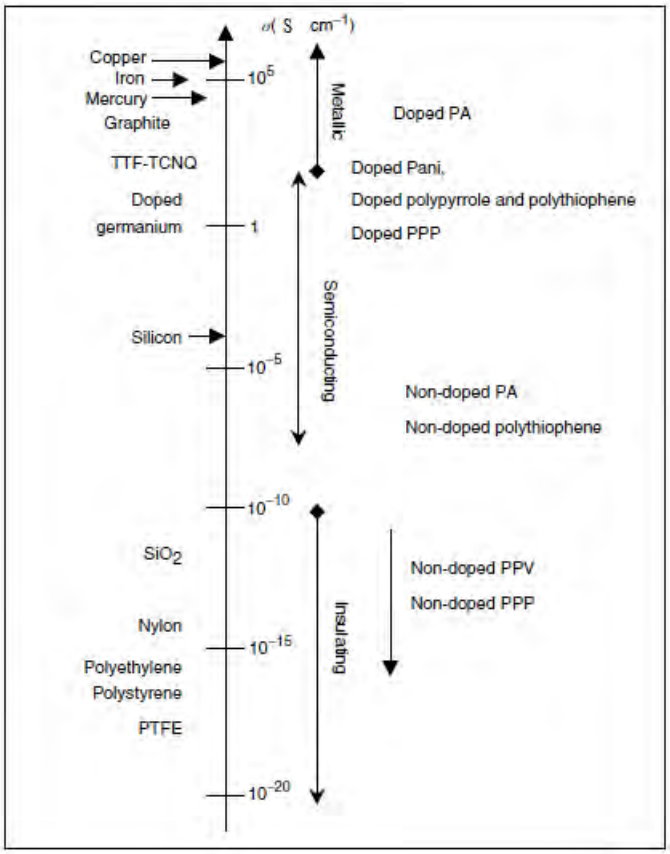

Figure 1.3.2. *Conductivities of conjugated polymers compared with other common materials [38].*

Chemical doping: The chemical doping by charge transfer involves partial oxidation (p-type doping) and partial reduction (n-type doping) of π-backbone of the polymer. When the doping level is sufficiently high, the electronic structure evolves to that of a metal. Examples of p- and n-type chemical doping are shown below.

p-type doping: $(\pi\text{-polymer})_n + \frac{3}{2}\,ny(I_2) \rightarrow [(\pi\text{-polymer})^{+y}(I_3^-)_y]n$

n-type doping: $(\pi\text{-polymer})_n + [Na^+(\text{naphthalide})^-]_y \rightarrow [(Na^+)_y(\pi\text{-polymer})^{-y}]_n + (\text{naphthaline})^0$

Electrochemical doping: Although chemical doping is an efficient and straight forward process, it is typically difficult to control. Complete doping to the highest concentrations yields reasonably high quality materials. However, attempts to obtain intermediate doping levels often result in inhomogeneous doping. In electrochemical doping, the electrode supplies the redox charge to the conducting polymer, while ions diffuse into (or out of) the polymer structure from the nearby electrolyte to compensate the electronic charge. The doping level is determined by the voltage between the conducting polymer and the counter electrode. At electrochemical equilibrium the doping level is precisely defined by that voltage. Thus, doping at any level can be achieved by setting the electrochemical cell at a fixed applied voltage and simply waiting as long as necessary for the system to come to electrochemical equilibrium, the state where the current through the cell going to zero. Electrochemical doping is illustrated by the following examples:

p-type: $(\pi\text{-polymer})_n + [Li^+(BF_4^-)]_{soln} \rightarrow [(\pi\text{-polymer})^{+y}(BF_4^-)_y]_n + Li\ (electrode)$

n-type: $(\pi\text{-polymer})_n + Li\ (electrode) \rightarrow [(Li^+)_y(\pi\text{-polymer})^{-y}]n + [Li^+(BF_4^-)]_{soln}$

Photodoping: This is a doping process which does not involve dopant ions. The semiconducting polymer is locally oxidized and reduced by photoabsorption and creates electron-hole bound excitons. When trans-$(CH)_x$ for example, is exposed to radiation of energy greater than its band gap, electrons are promoted across the gap and the polymer undergoes photo-doping. However, the electron-hole pairs disappear rapidly because of the recombination of electrons and holes when irradiation is discontinued. If a potential is applied during irradiation, then the electrons and holes separate and photoconductivity is observed. Photodoping is illustrated in the following example.

$(\pi\text{-polymer})_n + h\nu \rightarrow [\{\pi\text{-polymer}\}^{+y} + \{\pi\text{-polymer}\}^{-y}]_n$

where *y* is the number of electron-hole pairs

Charge-injection doping: This type of doping conjugated polymers also does not involve dopant ions. Charge-injection doping is most conveniently carried out using a metal/insulator/semiconductor (MIS) configuration involving a metal and a conducting polymer separated by a thin layer of a high dielectric strength insulator. In this type of doping, electrons and holes can be injected from metallic contacts into the π^*- and π-bands, respectively, as shown below.

Hole injection into filled π-band: $(\pi\text{-polymer})_n - y(e^-) \rightarrow [(\pi\text{-polymer})^{+y}]_n$

Electron injection into an empty π*-band: $(\pi\text{-polymer})_n + y(e^-) \rightarrow [(\pi\text{-polymer})^{-y}]_n$

For charge injection doping method at a metal-semiconductor (MS) interface, electrons reside in the π*-band and/or holes reside in the π-band only as long as the biasing voltage is applied. This type of doping make conjugated polymers to be widely used in light-emitting diodes applications.

1.3.3 Conjugated Organic Polymers for Optoelectronic Devices

Conducting polymers have wide range of applications in day-to-day life of human being. Among the wide applications of these materials the major ones include: supercapacitors, light emitting diodes, field effect transistors, solar cells, and sensors [39 - 41]. Insulator materials, such as polyethylene, are dielectric and display forbidden bands at energy levels situated well outside the optical spectrum. The energy separation between molecular bonding (σ) and antibonding (σ*) orbitals joining-CH_2 -groups is due to the considerable axial overlapping of these orbitals permitted by the polymer geometry. Therefore, to prepare organic optoelectronic components, one has to go beyond using these passive insulator materials. In contrast to insulator materials, the energy separation between π-bonding and π*-anti-bonding orbitals in conjugated organic polymers is relatively small, as lateral orbitals exhibit limited overlapping. As a result, band gap for polymeric solids containing such orbitals is typically between 1 and 3 eV, a value which covers the optical domain well. This electronic property of conjugated organic polymers makes them suitable

for optoelectronic device applications. Furthermore, doping of such polymers gives rise to semiconducting materials, and the metallic state can also be reached with certain materials such as polyaniline or its derivatives (Figure 1.3.2). With these optical and electrical properties of conjugated organic polymers, it becomes possible to envisage the fabrication of polymer optoelectronic devices [35, 38].

Furthermore, conjugated organic polymers must present two essential structural features for optoelectronic applications. The first is a π-conjugated backbone composed of linked unsaturated units resulting in extended π-orbitals along the polymer chain enabling proper charge transport and optical absorption [42, 43]. The second is the functionalization of the polymer core with solubilizing substituent, which is essential for inexpensive manufacture by solution methods as well as to enhance solid state core interactions [44, 45]. The extent of conjugation/interaction between these units determine the polymer solution/solid state electronic structure, which in turn control key polymer properties such as optical absorption/emission, redox characteristics, and frontier molecular orbital energy levels which in turn affects the performance efficiency of the optoelectronic devices.

Other important conjugated organic polymer architecture parameters to be considered for optoelectronic applications are the molecular weight (Mw) and the polydispersity (PD) index which influence solubility, solution aggregation, and formulation rheology, as well as the thin film formation and morphology for both pristine and blended materials. The electronic structure, thermal properties, and microstructure of

polymers generally vary considerably when going from low (oligomers) to high (polymer) molecular weights. Therefore, it is important to achieve Mw/PD regime where certain property stabilizes, so that greater reproducibility of the polymer property from batch to batch can be achieved which are very important for device applications. This value is likely to be strongly dependent on the polymer structure. For example, most soluble thiophene-based polymers with a number average molecular weight value of about 20 - 30 kDa and a PD of 1.2 - 1.8 are reasonable for this threshold values [46]. Since polymers do not vaporize before decomposition and thus have negligible vapor pressure, they are not susceptible to interlayer diffusion during the typical device-fabrication thermal cycles and typically exhibit robust mechanical properties, making nanometer-thick semiconductor films potentially compatible with roll-to-roll fabrication on flexible substrates for optoelectronic devices fabrications [45 - 46].

1.4 Bulk Heterojunction Polymer Solar Cells

Since the first discovery of bulk heterojunction (BHJ) solar cells by research groups of Heeger [24] and Friend [47] using polymer-fullerene and polymer-polymer as components of the active layer blend, respectively, several research works have been revealed showing the potential of this architecture for replacing the inorganic based solar cells. The BHJ device configuration is achieved by blending the n-type and p-type materials to increase the number of interfaces between the donor and acceptor phases in order to provide more exciton dissociation/charge separation sites to generate more charge carriers compared to the bilayer architecture [24]. Bulk heterojunction based polymer solar cells have become a promising alternative to

inorganic materials due to their advantages of being cheaper, light weight, flexible, and made into large areas by roll-to-roll processing [48 - 54]. However, there are three main issues to overcome before OSC devices and technologies can be competitive with other energy generation systems.

First of all, the crucial efficiency value of organic solar cells (OSCs) is still inferior to all inorganic counterparts. Currently, a combination of novel polymer development, nanoscale morphology control, and processing optimization has led organic solar cells to have over 10% power conversion efficiencies (PCEs) both in single and multijunction architectures [55 - 59].

The second issue to overcome is device stability under ambient operating conditions. The manufacturers of commercial crystalline silicon solar cells usually assure a 25 years lifetime warranty. However, so far there are few OSC devices that can pass a 1000-hour test in damp heat (85°C and 85% relative humidity, RH) with less than 10% degradation of PCE. While it is possible to protect the devices through cell encapsulation and device packaging, it will no doubt increase overall production costs. A good solution is to search for stable materials that are less sensitive to oxygen and moisture so that only minimal encapsulation and packaging is required [60 - 63]. Another elegant way to overcome such an issue is the so-called “inverted” bulk heterojunction (BHJ) polymer solar cells (PSCs), a device geometry in which the charge collection is reverted in comparison with the standard geometry device *i.e.* the electrons are collected by the bottom electrode and the holes by the top electrode

which is in contact with air [64]. The detail of this architecture in comparison to the conventional geometry, which uses bottom high work function and top low work function electrodes, is discussed in the next section.

The third issue is processing technologies for mass production. State-of-the-art OSCs with high efficiencies are usually made in research laboratories. These champion cells usually have very small active areas (less than 1 cm^2) and are typically fabricated by multiple steps utilizing many different processing techniques. Indeed, these techniques suitable for research purposes in the laboratory may not be able to scale up to large-area and low-cost mass production. Although OSC technology can potentially offer a credible solution to the problem of high-cost fabrication encountered for other photovoltaic technologies, there are still a lot of issues to be solved and finding suitable technologies that allow processability and mass production without sacrificing power conversion efficiency (PCE) are required [60].

1.4.1 Polymer Solar Cells Device Architecture

There are two device architectures in polymer solar cells. These are the conventional and inverted device architectures. Therefore, all lab-scale fabrication of polymer solar cells uses either conventional or inverted device architecture. The basic difference of the two device architectures is the polarity of the charge carriers during photocurrent generation. In conventional device architecture, holes are collected by bottom high work function anode electrode and electrons are collected by top low work function cathode electrode. However, in inverted device architecture, holes are collected by the top high work function anode electrode and electrons are collected by low work

function bottom cathode electrode [65 - 69]. Figure 1.4.1 shows schematic representation of conventional and inverted device architectures.

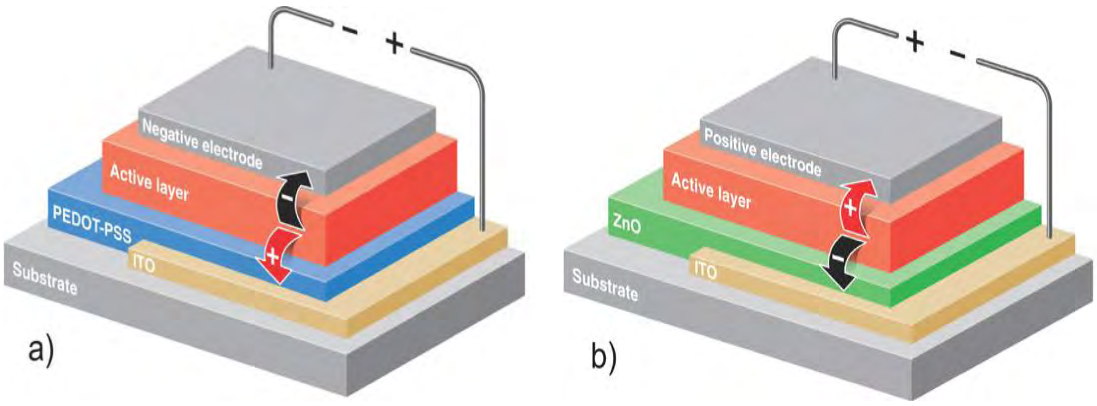

Figure 1.4.1. *(a) Conventional geometry of a BHJ solar cell and (b) Inverted geometry that causes electrons and holes to exit the device in the opposite direction.*

1.4.1.1 Conventional Device Architecture

This is the most commonly used and pioneering device structure for a BHJ organic solar cell. This architecture comprises a conductive transparent substrate such as indium tin oxide (ITO) or fluorine-doped tin oxide (FTO) coated on glass or plastic substrates at the bottom. The conductive substrate is then covered by a thin hole conducting layer poly(3,4-ethylenedioxythiophene):poly(styrenesulfonate) (PEDOT:PSS) over which the active layer is deposited typically from a solution by means of spin coating. Finally, a thin metal layer such as Al, Ca/Al, or LiF/Al is usually thermally evaporated to complete the device for characterization [70 - 74]. In general, the normal configuration of OSCs are made of an active BHJ layer or planner heterojunction layers sandwiched by a high work function transparent metal oxide as

the bottom anode and a low work function metal as the top cathode. The schematic device structure is shown in Figure 1.4.1a. For efficient charge collection, work functions of anode and cathode should be matched to the highest occupied molecular orbital (HOMO) of donor and the lowest unoccupied molecular orbital (LUMO) of acceptor, respectively. However, low work function metals undergo very fast oxidation when exposed to air losing their conductivity and suddenly turning a working device into a faulty one. Furthermore, evaporation of the top electrode needs high vacuum and energy consuming which increases cost and fabrication complexity. This architecture is also not compatible for large scale roll-to-roll fabrication of polymer solar cells. Moreover, the hole conducting PEDOT:PSS is acidic and hygroscopic in nature and is thus detrimental to the underlying metal oxide layer. This acidic PEDOT:PSS etches the ITO and make indium to diffuse in to the active layer resulting in change in morphology of the active layer and fast degradation of the performance of the solar cell device [75, 76]. Finally, it has been widely reported that polymer/fullerene, as well as polymer/polymer blends, are characterized by a stratified composition i.e. vertical phase separation during the film formation [77, 78]. This vertical phase separation of the components of the blend results in fullerene phase, electron transporting phase, to be concentrated at the bottom of the film and polymer phase, hole transporting phase, to be concentrated at the top of the film. The vertical phase separation is attributed to the surface energy difference of the components and their interactions with the substrates. Thus, the film vertical phase structure is opposite to the ideal one where the electron-conducting phase must face the top low work function electrode and the hole conductive phase must face the

bottom high work function electrode [79, 80]. The above problems can be avoided by reversing the collection process *i.e.* collecting the holes by the top electrode and the electrons by the bottom electrode. The architecture compatible with reversing the collection process of charge carriers is the inverted architecture [60, 64, 81 - 83].

1.4.1.2 Inverted Device Architecture

In contrast to the conventional device architecture, inverted device architecture of polymer solar cell comprises low work function bottom cathode electrode and high work function top anode electrode in between which the active layer is sandwiched. As a result, this architecture reverses the charge carriers collection process i.e. holes are collected by the top electrode and electrons are collected by the bottom electrode. Figure 1.4.2b shows the schematic device representation of inverted architecture polymer solar cell. Inverted structure was first exploited in the fabrication of organic light emitting diodes and initially referred to as an "upside-down" structure [78]. It was after this work that inverted architecture started to be exploited also in the photovoltaic field. After these pioneering works, it has been demonstrated that the inverted structure allows one to reach performances even better than the standard polymer solar cell [84 - 87]. Moreover, inverted polymer solar cells have several advantages over the conventional architecture polymer solar cells.

Firstly, the inverted device architectures removes the use of acidic hole collecting PEDOT:PSS layer at the ITO interface which is one of the detrimental factor for the stability of conventional polymer solar cells. Furthermore, Ameri et al. [86] has shown that the PEDOT:PSS absorbs about 20% of the solar radiation reducing the

fraction of photons reaching the active layer. Therefore, avoiding PEDOT:PSS layer enhances stability of the solar cell devices and also increases the fraction of photons reaching the active layer. For ITO based inverted polymer solar cells n-type metal oxides such as ZnO and TiO_x are more commonly utilized as the interface modification layer for ITO and reverse the polarity of the charge carriers. These n-type metal oxides used in inverted polymer solar cells are advantageous due to their high optical transparency in the visible and near infrared, high carrier mobility, high environmental stability, and solution processibility which make this architecture compatible for large scale roll-to-roll fabrication of polymer solar cells. Furthermore, the LUMO and HOMO energy levels of these metal oxides have been reported to be around -4.4 eV and -7.6 eV, respectively. The low LUMO and high HOMO levels allow these materials to be good electron selective and hole-blocking layers [81]. Moreover, the application of n-type metal oxides used as ITO-surface modification in inverted polymer solar cells also act as optical spacers for redistributing radiation inside the active layer enhancing light absorption inside the active layer that may contribute to the enhancement of current density [88 - 92]. Besides these n-type metal oxides, there are also several solution processable and cheap polymer materials such as polyelectrolytes which have been applied for ITO-surface modification in inverted polymer solar cells and potentially reversed the polarity of the charge carriers [93 - 97].

Secondly, inverted polymer solar cells use high work function top metal electrodes such as Au and Ag that are in contact to air and stable enhancing the stability of

inverted polymer solar cell device [98 - 100]. The inverted architecture also uses non-vacuum deposited high work function metal electrodes at the top interface which reduces cost and fabrication complexity. As the fabrication process for OSCs will be solution processing, in which different cell layers are deposited onto flexible substrates to tailor for the ultimate simple roll-to-roll type printing, inverted architecture is an ideal geometry for large scale fabrication and commercialization of polymer solar cells [101 - 104].

Thirdly, inverted architecture polymer solar cells give an opportunity to use indium tin oxide (ITO) free polymer solar cells [105 - 111]. ITO is a commercially dominant transparent conductor with relatively high conductivity (sheet resistance of 10 - 20 Ω/cm^2) and transmission (> 80%) in the visible region of the solar spectrum and as a result it is the material-of-choice for transparent conductors in any optoelectronic application. However, scarce resources of indium and high market demand of ITO have created large price fluctuations and future supply concerns. Apart from the volatility of indium prices, its incorporation in the processing of ITO requires high preparation temperatures and vacuum-based highly energy intensive deposition techniques such as sputtering, thus further increasing the cost of ITO [112]. As life cycle analysis (LCA) showed in polymer solar cells (PSCs), ITO is the single-most cost driving factor due to expensive raw materials and processing [113 - 115]. ITO, besides being expensive, has also very poor performance under mechanical stress because of its fragile oxide nature [116]. Given the limited lifetime and stability of PSCs as compared with other mature technologies such as silicon-based solar cells,

the technological future of PSCs beyond that of academic interests rests in reducing cost of production. In this regard, replacing ITO has the potential to dramatically reduce material and processing cost and the energy payback time of PSCs. Several alternatives to ITO in inverted architecture polymer solar cells have been presented in literature that potentially reduce further the cost of polymer solar cells compared to inorganic based solar cells and even compared to ITO-based polymer solar cells [112].

Therefore, the inverted configuration OSCs is the best candidate to meet all requirements including high efficiency, stability, low-cost and high-speed production into one system compared to conventional architecture. Furthermore, the inverted device architecture has also been investigated as a suitable architecture tailoring for solution processing, which allows various cell layers to deposit onto flexible substrates and is promising for scale-up production *via* industrial roll-to-roll type fabrication [81, 82].

1.4.2 Working Principles of Polymer Solar Cells

Operation of polymer solar cells involves series of steps that make the devices convert solar energy in to useful electrical energy. These operational steps in organic solar cells are absorption of light by photoactive layer, creation of electrostatically bound excitons, diffusion of excitons to donor-acceptor (D-A) interface, exciton dissociation into charge carriers, transportation of charge carriers through the bulk of the active layer to electrodes, and collection of charge carriers by electrodes to generate photocurrent through the external wire. Figure 1.4.2 shows schematic

representation of the working mechanism of polymer solar cells. The detail of each steps during operation of polymer solar cells are described below [117].

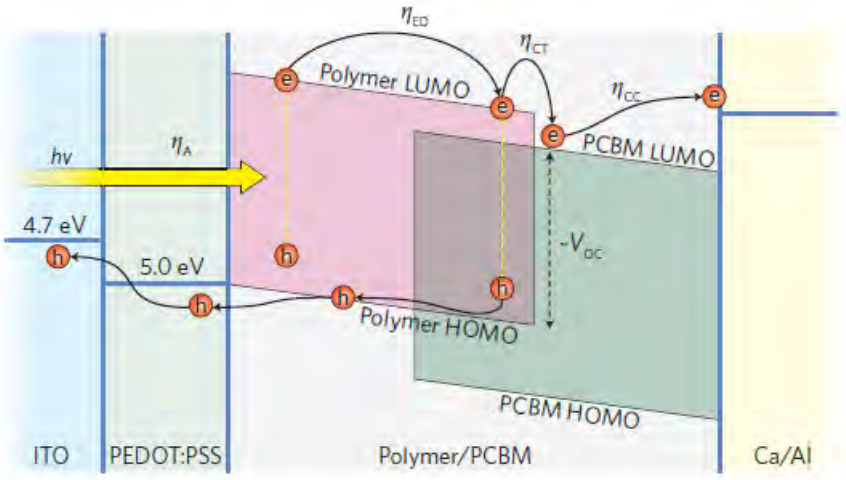

Figure 1.4.2. *Operating mechanism of polymer solar cells [117].*

1.4.2.1 Light Absorption

The strength and width of the absorption spectrum of a photoactive layer determines to a large extent its potential for harvesting incident solar radiation. In an organic donor-acceptor solar cell, light is usually absorbed mostly in the donor material i.e. conjugated polymer and molecule. Organic semiconductors often exhibit very high absorption coefficients above 10^7 m^{-1} so that high optical densities can be achieved at peak wavelength. Consequently, very low thicknesses between 100 - 300 nm are sufficient for a good absorption yield in organic photovoltaic devices [34, 118]. In contrast, solar cells based on the inorganic polycrystalline semiconductor $CuInSe_2$ need few micron thick active layers for good absorption, and crystalline silicon solar

cells require more than 100 microns. This is due to their low absorption coefficient compared to that of the organic semiconductor materials. Thus, lower material amounts are needed for organic solar cells which are one of the reasons they are called relatively cheap. Unfortunately, many organic materials have a rather narrow absorption width with low or no absorption at longer wavelength spectrum regions. Conjugated polymers commonly used in organic solar cells typically cover the visible optical spectrum only although polymers with wider absorption bands exist [119 - 124]. The narrow absorption coverage of conjugated polymers is due to their well-defined electronic transitions that are typically quite narrow [125, 126]. In contrast, the inorganic semiconductors silicon and $CuInSe_2$ absorb across the whole visible spectrum of the sun light, and beyond to more than 1000 nm with optical bandgap of 1.1 eV. To increase the photon absorption of active layer in BHJ polymer solar cells low-bandgap conjugated polymers which covers wider solar spectrum have been used which doubled harvesting of sun's photon from about 20% for P3HT, which absorbs between 450 nm - 600 nm, to 41% if the absorption range is extended between 350 nm - 826 nm [127 - 129].

Other strategies to increase light absorption include reduction of reflection losses, either by adding antireflection coatings or by structuring the interfaces, and engineering the optical interference inside the device to maximize the electromagnetic field in the active region by using optical spacers [130 - 134].

Upon absorption of a photon of sufficient energy by the organic semiconductor, an electron is promoted from highest occupied molecular orbital (HOMO) into the lowest unoccupied molecular orbital (LUMO) leaving behind a hole [118]. The generated electron-hole pairs in the organic semiconductors exhibit significant electrostatically binding energy of about 0.3 - 1 eV which is much larger than the thermal energy at room temperature of about 25 meV [19, 135 - 137]. Consequently, unlike inorganic semiconductors, optical absorption in organic materials does not directly lead to free electron and hole carriers that could readily generate an electrical current. The exciton with high binding energy is therefore given the name Frenkel exciton. Thus, in contrast to inorganic semiconductors which generate charge carriers up on photon absorption, the absorption of a photon at room temperature in conjugated materials does not lead to free charge carriers but to neutral bound electron-hole pairs. This is the reason why two components, an electron donor and an electron acceptor, are required to promote the generation of charge carriers in organic solar cells.

1.4.2.2 Exciton Diffusion

In order to generate separated negative and positive charges, the excitons need to diffuse to the donor-acceptor interface where they can dissociate [138]. Since excitons are neutral species, their motion is not influenced by any electric field and they diffuse *via* random hops [12]. The fraction of excitons that reach the D-A interface is determined by the exciton diffusion length (L_D), the product of diffusion constant and exciton life time [125]. Several values have been reported for exciton diffusion lengths in organic semiconductors, ranging between 1 and 20 nm [135, 139

- 143] which are significantly shorter than device thicknesses. Exciton diffusion can be limiting in that decay routes are in competition with charge carrier generation. In bilayer polymer solar cells, for example, the small exciton diffusion length limits the thickness of the absorbing donor layer [144]. Excitons generated further away from the planar interface to the acceptor than the exciton diffusion length are lost by recombining radiatively. Consequently, the dimensions of the donor layer should ideally be chosen to be thin that in turn limit the amount of photon flux to be absorbed. Here, the reason why bulk-heterojunctions usually perform better than bilayer architectures becomes clear. Due to the small exciton diffusion length, the real active region of the bilayer device is limited to a very narrow region close to the D-A interface, while the remaining thickness only contributes to increase series resistance and to filter part of the light intensity before it reaches the active zone. On the other hand, in cells where the donor and acceptor are mixed, such as in BHJs, exciton diffusion is not normally considered a major limitation as donor (acceptor) phase domains tend to be of the order of the diffusion length. However, generated charges have to be transported as well and very small domain sizes may lead to limited percolation and increased recombination losses [145, 146].

1.4.2.3 Exciton Dissociation

Once the exciton, diffusing within the donor phase, has reached the interface to the acceptor material within its diffusion length, it can transfer its electron to the electronegative acceptor [2, 34]. In suitable materials combination this charge transfer is very fast. The process can be very efficient, with reported internal quantum efficiency values close to 100% [147]. This is because the kinetics of charge transfer

in optimized polymer-fullerene devices is ultrafast, around 40 - 45 fs [24, 148 - 150], and in this time regime there is no competing decay process for the optically excited electron-hole pair. However, excitons dissociate only at energetically favorable acceptor molecules such as the fullerenes, when the energy gain is larger than the exciton binding energy. Briefly, the exciton can dissociate when its energy is larger than the energy of the electron-hole pair after the electron transfer, often called charge transfer complex/state [151 - 152]. Only then an electron or charge transfer takes place, dissociating the singlet exciton into an electron residing on LUMO of the fullerene acceptor and a hole on the HOMO of the polymer. However, in such a case, since they remain in close proximity, the electron and the hole are still rather strongly coulombically bound. Charge separation can also be influenced by concentration and morphology gradients near the heterojunction that take place during the formation of the organic films, or can be assisted by local electric fields [12, 153]. Generally, charge separation process in organic semiconductors must be energetically favorable i.e. the change in Gibbs free energy on converting a neutral species into two separated charged species must be negative [154].

1.4.2.4 Charge Carrier Transport

Following exciton dissociation, electrons are found in the acceptor phase whereas holes remain in the donor phase. As a result, the charge carriers can drift and diffuse through the bulk of the organic materials towards their respective electrodes. Current density in organic photovoltaics is composed of drift and diffusion components. During this transport holes move to the anode electrode through donor material and electrons move to the cathode electrode through cathode electrode, respectively. Due

to the lack of long-range order in the solution processed and evaporated organic semiconductors, the electrical transport mostly takes place by hopping from one localized state to the next [155], instead of band transport found in crystalline inorganic semiconductors. Efficient charge transport is important as it will be in competition with interfacial recombination, and will therefore limit device thickness [2, 34]. Therefore, the charge carriers need a driving force to be transported through the bulk and reach their respective electrodes and generate current. This internal electrical field determines the maximum open circuit voltage (V_{OC}) and contributes to a field-induced drift of charge carriers. Also, the usage of asymmetrical contacts, low work-function metal for the collection of electrons and high work-function metal for the collection of holes, is proposed to lead to an external field under short circuit condition. Another driving force can be the concentration gradients of the respective charges. It leads to diffusion current. During this bulk transport process, trapping of carriers can occur. However, if carriers are trapped for a finite time, the mobility is affected and carriers can finally be collected at electrodes without losses and the charge transport efficiency reaches up to unity. Conversely, if the carriers are trapped for an infinite time, they are lost with respect to electrical current. Thus the charge carries' mobility not only depends on inherent characters, but also has correlation with charge traps effect [118].

1.4.2.5 Charge Carrier Extraction

Once charges drifting and diffusing through the bulk of the active layer of the organic solar cell and reach the electrode, they need to be extracted with minimum loss for the generation of photocurrent through external wire. The simplest picture for charge extraction would be a hopping [155] or tunnelling [156] step, from the organic material, HOMO level for holes and LUMO level for electrons, to the Fermi levels of the electrodes. However, the nature of the electrode/organic layer interfaces is complex. The efficiency of the charge collection process cannot be simply determined from the difference between the work function of the isolated electrode and the donor ionization potential or acceptor electron affinity. The deposition of organic layers on electrodes or *vice versa* leads to interfacial charge-density redistributions and/or geometry modifications that strongly affect the alignment of the organic frontier electronic levels versus the electrode Fermi level [157]. Therefore, in real devices charge extraction is also a much more complex problem. Ion or metal diffusion into the organic layer [158], interfacial dipoles at the contact [159], band bending [160], and chemical reaction [161] can all affect the energetic at the interface and influence the injection process.

1.4.3 Characterization of Polymer Solar Cell Performance

The following terms are often used to characterize solar cells. Some of the terms are also shown on the *J-V* graph (Figure 1.4.3) [148, 162 - 167].

Open Circuit Voltage (V_{OC}): The maximum possible voltage across a photovoltaic cell. The voltage across the cell in sunlight when no current is flowing i.e., under the

open circuit condition when all photo-generated charges are recombined inside the cell. In organic solar cells, V_{OC} is found to be linearly dependent on the energy difference between the HOMO of the donor and the LUMO of the acceptor. Accordingly, those donor materials with low HOMO level and acceptors with high LUMO levels are usually applied in organic photovoltaic (OPV) devices in order to achieve high V_{OC} and efficiency. For the ideal diode, the V_{OC} increases logarithmically with light intensity and is given by:

$$V_{OC} = \frac{nkT}{q} \ln\left(\frac{J_{sc}}{J_o} + 1\right) \qquad (1)$$

Where *n* is the diode ideality factor (typically between 1 and 2); J_o is the saturation current density of the diode (caused by diffusion of minority carriers from the neutral region to the depletion region); q is the elementary charge, 1.6 x 10^{-19} C; k is Boltzman constant of value 1.38 x 10^{-23} J/K, T is the Kelvin temperature of the cell and J_{SC} is short circuit current density.

Short Circuit Current Density (J_{SC}): This is the current that flows through an illuminated solar cell when there is no external resistance i.e. when the electrodes are simply connected or short-circuited. The short circuit current density is the maximum current that a device is able to produce. Under an external load, the current will always be less than J_{SC}. At short circuit the photo-generated charges are expected to flow into the external circuit with unit efficiency. According to diode equivalent circuit, the short circuit current, J_{SC}, is equal to the difference between the photo-

generated current J_{ph} and that lost in the diode and shunt resistance (J_D) i.e. $J_{SC} = J_{ph} - J_D$ and can also be expressed as:

$$J_{SC} = q_e \int_{\lambda min}^{\lambda max} Jphoton(\lambda) IPCE(\lambda) d\lambda \qquad (2)$$

where q_e is the electron charge and IPCE is defined as the incident monochromatic photon-to-electron conversion efficiency

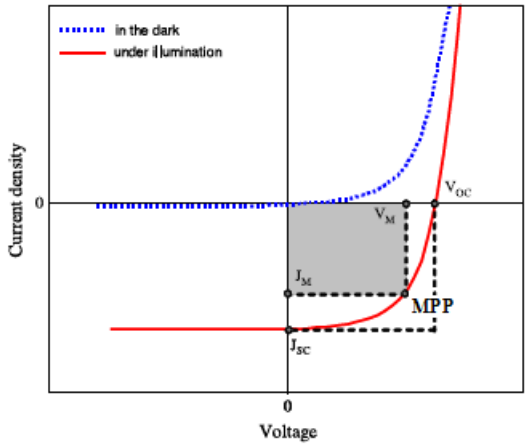

Figure 1.4.3. *Current-voltage (J-V) curves of an organic solar cell [2].*

Maximum Power Point (MPP): This is the point on the *J-V* curve where the area of the resulting rectangle is largest. The point (J_M, V_M) on the *J-V* curve is where the maximum power is produced. Power (P) is the product of current and voltage (P = I*V) and is illustrated in Figure 1.4.3 as the area of the rectangle formed between a point on the *J-V* curve and the axes.

Fill Factor (FF): FF characterizes how ‘‘square’’ the *J-V* curve is and it represents how ‘‘difficult’’ or how ‘‘easy’’ the photogenerated carriers can be extracted out of a photovoltaic device. The ideal value for FF is unity (100%), when the *J-V* curve is a rectangle. Only a small voltage deviating from the V_{OC} (< V_{OC}) can make the current density rise perpendicularly to the maximum value (J_{SC}), and keep constant during the applied voltage changes from V_{OC} to zero and even a large reversed bias. In fact, FF cannot reach 100%. Even in the inorganic solar cells, the PCE of which is far larger than OSCs, the maximum FF reported is about 90%. Fill factor is the ratio of a photovoltaic cell’s actual maximum power output to its theoretical power output if both current and voltage were at their maxima, J_{SC} and V_{OC}, respectively. The formula for FF in terms of the above quantities is:

$$FF = \frac{J_M V_M}{J_{SC} V_{OC}} \qquad (3)$$

Power Conversion Efficiency (PCE): The ratio of power output to power input. In other words, PCE measures the amount of power produced by a solar cell relative to the power available in the incident solar radiation (P_{in}). P_{in} here is the sum over all wavelengths and is generally fixed at 100 W/cm^2 when solar simulators are used. This is the most general way to define efficiency. The formula for PCE, in terms of quantities defined above, is:

$$PCE\ (\%) = \frac{J_M V_M}{P_{in}} = \frac{J_{SC} V_{OC} FF}{P_{in}} \qquad (4)$$

External Quantum Efficiency (EQE): The external quantum efficiency or incident photon to current conversion efficiency (IPCE) is simply the number of electrons collected under short circuit conditions divided by the number of incident photons at a given wavelength. IPCE is calculated using the following formula:

$$\text{IPCE}\ (\%) = \frac{1240 J_{SC}}{\lambda P_{in}} \qquad (5)$$

where λ *(*nm) is the incident photon wavelength, J_{SC} (A/cm^2) is the photocurrent of the device, and P_{in} (W/cm^2) is the incident power.

1.5 Photochemical Stability of Conjugated Polymers and Device Stability

In order to achieve commercial viability for organic solar cells, both the efficiency and stability are important research areas. Currently the lab-scale efficiency of organic solar cell devices is exceeding the milestone limit i.e. a power conversion efficiency of 10% before large scale commercialization is viable [55 - 59]. Most of the high performance devices presented in the literature are prepared and studied under inert atmosphere conditions. To transfer to practical use and large scale production of organic solar cells, combination of high efficiency and good stability in the same device is essential. With much progress and encouraging advancement in the device efficiency, stability is becoming a crucial issue for the development of OSC. Over recent years, the lifetime of OSC has greatly improved from a matter of minutes to thousands of hours [14, 168 - 171]. However, for well-encapsulated devices under controlled temperature conditions, the lifetime is estimated to reach up to 5 - 10 years [14, 172, 173]. This encapsulation of devices of course can be done by

using glass, which is very effective in blocking out ambient air. Encapsulation of organic solar cells with glass however result in the disadvantages of being bulky and inflexible while organic solar cells are claimed to have advantages over the inorganic solar cells by their light weight and flexibility [48 - 54]. To avoid the bulkiness and inflexibility of the glass encapsulated organic solar cells, plastic encapsulation have been tried and such device lifetimes are likely to be less than for glass-encapsulated devices. In addition, the presence of thermal stress during outdoor exposure can further decrease the device operating lifetimes regardless of encapsulation. Overall, the stability of OSC is still significantly poorer than conventional silicon photovoltaic which typically exhibits over 25 years of operating lifetime [174].

In polymer solar cells different components undergo degradation and affect the life time of the devices. Degradation in polymer solar cells is the net sum of chemical degradations from the electrodes [75, 175, 176], PEDOT:PSS [177 - 179], and photo-oxidative degradation of active layers. The active layer component in the organic solar cell is the part of the device that is very prone to degradation since it is integral to the device functionality. This translates directly into a degradation of the power conversion efficiency. Even though photo-oxidative reaction contributes strongly to the degradation of the active layers in polymers, thermal degradation cannot also be ignored [180, 181]. Polymer photochemical degradation contributes the most in degradation of active layer in polymer solar cells compared to the polymer-acceptor blend photochemical degradation in which the acceptor acts as stabilizing material. In the last years, several studies have been published in literatures comparing the

photochemical stability of polymers and polymer-acceptor blend films for polymer solar cell applications [63, 181 - 183]. These works revealed that photochemical stabilities of polymers depend on several factors such as length and nature of side chains [183 - 187]. Additionally, the nature of the backbone of the polymers i.e. the distance of highest occupied molecular orbital (HOMO) and lowest unoccupied molecular orbital (LUMO) from vacuum level [181, 188, 189] are among the major factors affecting the photochemical stability of polymers. The studies showed that increase in the side chain length of polymers has negative impact on the photochemical stability of the polymers [183 - 187]. Furthermore, the architecture of the side-chain has also influence on the nature of thin film formed. Short and branched side-chains are advantageous in forming compact and ordered films that decreases rate of diffusion of oxygen and moisture in to the film and hence enhance stability of the polymer film. With regard to the energy levels of the polymers, polymers with HOMO and LUMO close to the vacuum energy level can readily photo-oxidize compared to those polymers with HOMO and LUMO energy levels far away from the vacuum energy level. A notable study by Manceau et al [181] compared the photochemical stability for a systematic and wide range of semiconducting polymers and is used as rule of thumb for photochemical stability of polymers. Through this study, several parameters in terms of chemical structures that may undergo faster rates of photo-oxidation have been identified. For instance, the presence of readily cleavable bonds such as C-N, C-O and exocyclic double bonds like in MDMO-PPV can lead to poor stability and moieties with quaternary sites have been suggested to be unstable due to the high oxidizability of such sites.

Therefore, overcoming the stability issue of polymer solar cells before large scale production and commercialization is important. There are several approaches used to overcome the stability issues in polymer solar cells. These include using encapsulation technology to minimize the availability of oxygen and water [172, 173], tuning the electronic energy levels of the polymers to make more resistant to oxidation [188, 189], making the polymers "harder" by tuning their glass-transition temperature or with cross-linking, using thermo-cleavable polymers the side chain of which can be removed post processing [181], using less reactive electrodes or capping reactive metal electrodes with less reactive ones and using inverted device architecture [98 - 100]. Encapsulation and using inverted device architecture were the most successful approaches.

1.6 Effect of Solvent Additives on Photovoltaic Performance of Polymer Solar Cells

One of the factors limiting PCEs of BHJ device in organic solar cells is the morphology of the interpenetrating networks of donor and acceptor materials in the photoactive layer [190]. Multiple interfaces for efficient charge separation and long percolation pathways of the network for efficient charge transfer are among the requirements for efficient OSCs. Multiple interfaces of the network requires an ideal BHJ donor/acceptor domain length scale of $\leq$ 10 nm [191] which is the diffusion length limit of the excitons before decaying. Many processing methods have been explored to achieve the required morphologies in organic solar cells. These include postproduction annealing [192], solvent annealing [193], using mixed solvents [194], and the introduction of processing additives [190, 195 - 198]. Among these many processing methods, using additives offer an attraction over annealing processes in that they do not require an additional fabrication step which makes it cost effective and compatible with large scale production. For solvent additives to be used in OSCs processing, there are two widely accepted design rules. The first is the boiling point must be significantly greater than that of the processing solvent to maximize the interaction time between the additive and the active layer components during thin film formation. And the second is, one active layer component must be significantly more soluble in the additive than the other component to enhance the miscibility [190, 195, 199]. Figure 1.6.1 shows schematic depiction of the role of the processing additive in the self-assembly and selective solubility of either of the components of bulk heterojunction blend materials.

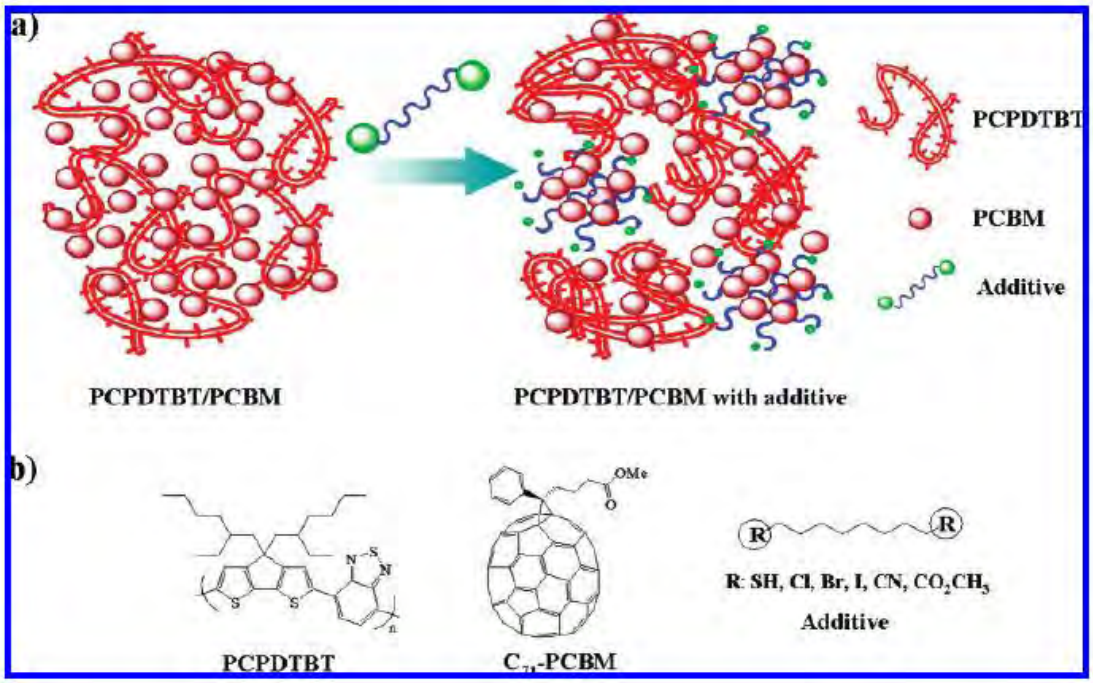

Figure 1.6.1. *Schematic depiction of the role of the processing additive in the self-assembly of bulk heterojunction blend materials (a) and structures of PCPDTBT, C_{71}PCBM, and additives (b) [195].*

2. General and Specific Objectives

The general objective of this study is photo-oxidative stability study and photovoltaic application of quinoxaline based copolymers and study of effect of low boiling point solvent additives on photovoltaic performance of bulk heterojunction polymer solar cells.

Specific objectives:

- to study the effect of incorporation of thiophene-hexylthiophene in to quinoxaline based donor polymers on photochemical stability and photovoltaic performance
- to study the effect of incorporation of thiophene-hexylthiophene in to pyridopyrazine based donor polymers on photochemical stability and photovoltaic performance
- to study the effect of incorporation of small fraction of thiophene-hexylthiophene in to quinoxaline donor polymers on photochemical stability and photovoltaic performance
- to study the effect of low boiling point solvent additives on photovoltaic performance of bulk heterojunction polymer solar cells

3. Experimental Section

This section describes materials used in the experiments for the study. The chemical structures of some of the materials which are thought to be necessary are also included. This section also includes experimental procedures and equipments used for the study.

3.1 Materials

3.1.1 Photoactive Donor Polymers

Photoactive polymers used as donor materials include: poly[2,3-bis-(3-octyloxyphenyl)quinoxaline-5,8-diyl-*alt*-thiophene-2,5-diyl] (TQ1) with molecular weight M_n = 17; copolymers of TQ1 with different hexylthiophene fraction named as TQTHTs: f_{THT} = 1 (M_n = 18.8), f_{THT} = 2.5 (M_n = 33.7), f_{THT} = 30 (M_n = 15), f_{THT} = 50 (M_n = 17), and f_{THT} = 80 (M_n = 10); poly[2,3-bis(3-(octyloxy)phenyl)pyrido[3,4-b]pyrazine-alt-thiophene] (TQN) with molecular weight M_n = 20.2; copolymers of TQN with different hexylthiophene fraction named as TQNTHTs: f_{THT} = 30 (M_n = 20.7), f_{THT} = 50 (M_n = 15.6); Poly(thiophene-hexylthiophene) (THT) with molecular weight M_n = 5.9; and poly[*N*-9′-heptadecanyl-2,7-carbazole-*alt*-5,5-(4′,7′-di-2-thienyl-2′,1′,3′-benzothiadiazole)] (PCDTBT) with molecular weight (M_w = 20 - 100) The molecular weights expressed here are in kg mol^{-1}. Except PCDTBT, which was purchased from sigma-Aldrich, all the other polymers were synthesized by collaborating groups at Chalmers University, Sweden. Figure 3.1.1 shows the molecular structures of the donor polymers.

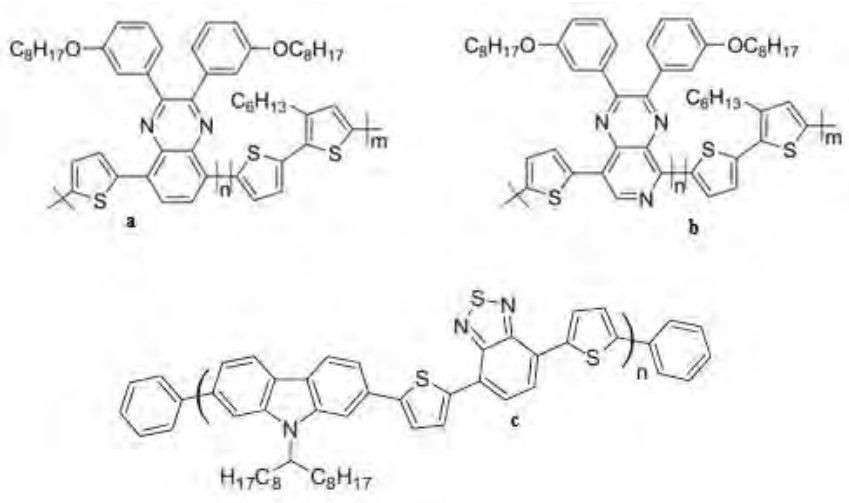

Figure 3.1.1. *Molecular structure of: a) TQ1 (m = 0), TQTHT (f_{THT} = 30) (n = 0.7, m = 0.3), TQTHT (f_{THT} = 50) (n = 0.5, m = 0.5), TQTHT (f_{THT} = 80) (n = 0.2, m = 0.8), TQTHT (f_{THT} = 2.5) (n = 0.975, m = 0.025), and TQTHT (f_{THT} = 1) (n = 0.99, m = 0.01); b) TQN (m = 0), TQNTHT (f_{THT} = 30) (n = 0.7, m = 0.3), and TQNTHT (f_{THT} = 50) (n = 0.5, m = 0.5). n = 0 represents molecular structure of THT; c) PCDTBT.*

3.1.2 PEDOT:PSS, PFPA-1 and PCBM

Conductive PEDOT:PSS (H.C. Starck) was used as interlayer to modify the surface of indium doped tin oxide (ITO) and used as hole transporting layer for conventional geometry bulk heterojunction solar cell devices fabricated for the study. However, the high conductive (HC-)PEDOT:PSS (H.C. Starck) was used as anode electrode for inverted geometry solar cell devices. Poly(3,3′-([(9′,9′-dioctyl-9H,9′H-[2,2′-bifluorene]-9,9-diyl)bis(4,1-phenylene)]bis(oxy))bis(N,N-dimethylpropan-1-amine)) (PFPA-1) (synthesized by collaborating group at Chalmers University, Sweden) is a polymer used as an interlayer to modify the surface of TiOx electron collecting layer in inverted geometry bulk heterojunction solar cell devices [200]. [6,6]-phenyl-C_{71}-butyric acid methyl ester ([70]PCBM) and [6,6]-phenyl-C_{61}-butyric acid methyl ester

([60]PCBM) were used as electron acceptor in this study. Figure 3.1.2 shows the molecular structures of PEDOT:PSS, PFPA-1, and PCBMs.

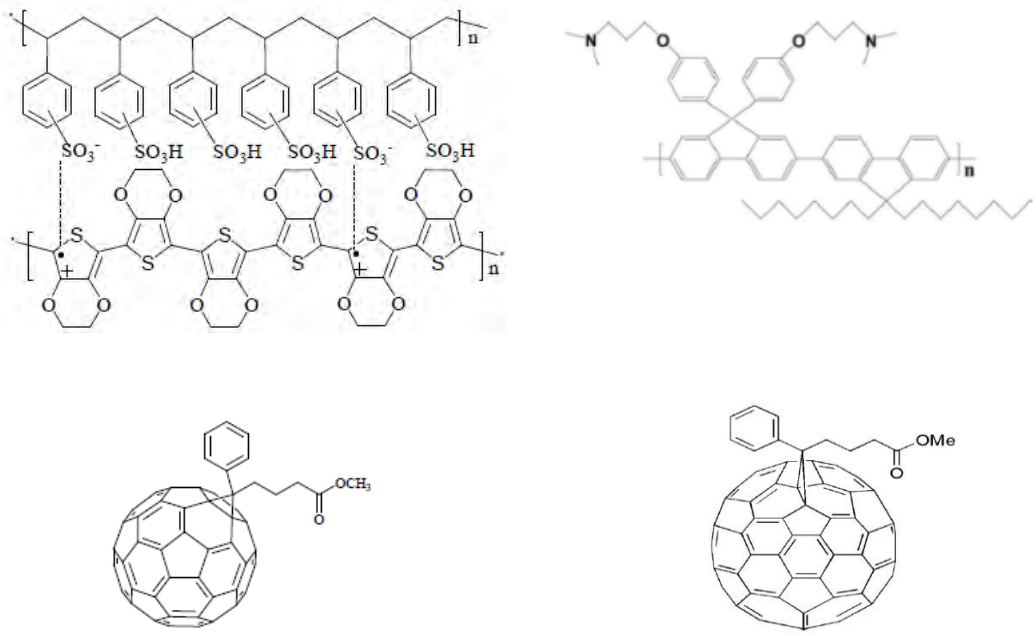

Figure 3.1.2. *Molecular structure of PEDOT:PSS (top left), PFPA-1 (top right), [60]PCBM (bottom left), and [70]PCBM (bottom right).*

3.1.3 Solvents

The low boiling point solvent additives used in this study were: Iodomethane (IMe, bp = 42°C), Iodoethane (IEt, bp = 72°C), and Diiodomethane (DIMe, bp = 181°C). The host solvent used was 1,2-dichlorobenzene (*o*-DCB, bp = 186°C). Figure 3.1.3 shows the chemical structures of the low boiling point solvent additives.

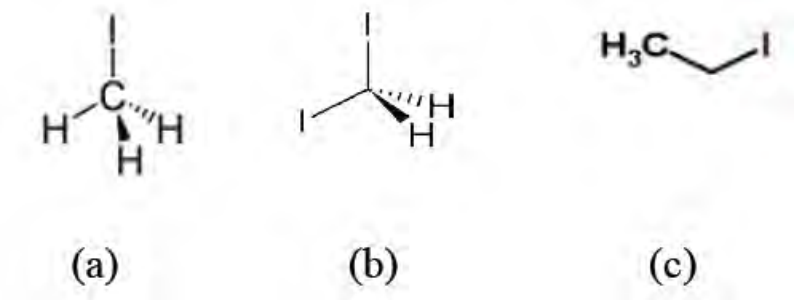

Figure 3.1.3. *Chemical structure of: a) Iodomethane, b) Diiodomethane, and c) Iodoethane.*

Other solvents such as acetone, isopropanol, dichloromethane, ammonia, hydrogen peroxide, and distilled water were also used for cleaning purposes in this study. Toluene, chloroform and chlorobenzene were also used for thin film preparation of polymers. Furthermore, dimethylsulfoxide (DMSO) and Zonyl FS-300 surfactant were used as additives to enhance the conductivity of HC-PEDOT:PSS.

3.1.4 Other Materials and Chemicals

Other materials and chemicals used in this study include: Glass substrate, indium doped tinoxide (ITO) as anode electrode for conventional geometry bulk heterojunction solar cell devices, aluminum metal rod used for evaporating cathode electrode both in conventional and inverted geometry solar cell devices, titanium metal used as interlayer for electron transporting in inverted geometry solar cell devices, and silver paste used for contact during device characterization both in conventional and inverted geometry bulk heterojunction solar cell devices.

3.2 Sample Preparation and Characterization

3.2.1 Thin Film Preparation for Photochemical Stability Measurement

The polymers were dissolved in a solvent mixture of 90 vol% chloroform and 10 vol% chlorobenzene and then spin-coated onto 2 x 2 cm cleaned glass substrates. The glass substrates were cleaned by sonication in acetone and isopropanol, respectively, followed by rinsing with water, acetone, dichloromethane and isopropanol, consecutively. Unless otherwise stated the film thickness was ~100 nm. For photochemical stability of TQTHTs with low fraction of THT (f_{THT} = 2.5 and f_{THT} = 1) compared with TQ1, all the films were prepared from solution of the same concentration in *o*-DCB with same spin speed to roughly manage the thickness. Prior to the stability measurements the films were annealed for 10 - 15 min at 100°C in ambient atmosphere to remove residual solvents but with light protection to avoid prior photochemical degradation. Thickness determination was done with a Digital Instrument Nanoscope IIIa equipped with a type G scanner (Digital Instrument Inc., Santa Barbara, CA, USA). The measurements were done in tapping mode and in air using a Micro Masch NSC 15 silicon cantilever.

3.2.2 Photochemical Stability Measurements of Polymer Films

Samples were illuminated under 1 sun in ambient atmosphere using an Educational/Research benchtop open array solar simulation system from Eye Lighting International (AM 1.5 spectral matching filter, 1000 W m^{-2}) for films of copolymers with large fraction of thiophene-hexylthiophene and SolSim solar simulating photodetector (AM 1.5 spectral matching, 1000 W m^{-2}) for copolymers

with low fraction of thiophene-hexylthiophene. During illumination, the samples were placed on a heating plate at 85°C [181]. The samples were removed periodically and the UV-visible absorbance spectra were recorded from 300 to 900/1100 nm with a Perkin Elmer Lambda 900 UV-Vis-NIR and Perkin Elmer Lambda 950 UV-Vis/NIR, USA, absorption spectrophotometer to monitor the degradation.

3.2.3 Solar Cell Device Fabrication

ITO-free inverted polymer solar cells were fabricated with the following device geometry: glass/Al (80 nm thick)/TiO_x (2 nm thick)/PFPA-1/Active layer/HC-PEDOT:PSS PH1000. Prior to cathode electrode deposition, the glass substrates were cleaned with detergents followed by a TL1 treatment, *i.e.* the substrates were put into a mixture of deionized water, ammonia solution (25%), and hydrogen peroxide solution (28%) in the ratio 5:1:1 by volume and heated to 85°C during 5 min to remove organic adsorbents. The Al/Ti-bilayer was thermally evaporated onto the glass substrate through a shadow mask at a pressure of less than 10^{-5} mbar. The electrode was subsequently exposed to air for 12 hours to form TiO_x [200]. PFPA-1 was spin-coated onto the electrode from a toluene solution inside a glove box, followed by rinsing with toluene to remove residual PFPA-1 that is not chemically bonded to the TiO_x surface. PFPA-1 was synthesized according to previous literature [200]. All polymer/$PC_{71}BM$ blend solutions were spin-coated inside a glove box from *ortho*-dichlorobenzene (*o*-DCB) onto the PFPA-1 modified cathode. After deposition of the active layer all samples were taken out of the inert atmosphere and aqueous HC-PEDOT:PSS PH1000 (H.C. Starck) mixed with 5% dimethyl sulfoxide (DMSO) and 0.25% surfactant (Zonyl FS-300) was spin-coated on top of the active layer and

annealed for 5 - 10 min at 60^{o}C in ambient atmosphere to remove residual water and then used as anode electrode. The complete devices were then taken back to the glove box for encapsulation using glass lids and light sensitive adhesive glue and lastly silver paste paint was used for contact. All solar cells had an active area of ~ 4 mm^2, as measured by optical microscopy.

For conventional geometry bulk heterojunction solar cell devices the device structure was Glass/ITO/PEDOT:PSS/Active Layer/LiF/Al. As a buffer layer, the conductive polymer PEDOT:PSS (H.C. Starck) was spin-coated at 3500 rmp onto ITO-coated glass substrates, followed by annealing at 120°C for 10 minutes to remove residual water. The thickness of the PEDOT:PSS layer was about 45 nm. Thicknesses of blend films and PEDOT:PSS were determined by a Dektak 6M surface profilometer. The active layer, blend of donor polymer and [70]PCBM, was spin coated from *o*-DCB solution onto the PEDOT:PSS layer. The active layers were spin-coated in a glove box and directly transferred to a vapor deposition system mounted inside of the glove box. LiF (0.6 nm) and Al (80 nm) were used as top electrodes and were deposited *via* a mask in vacuum onto the active layer. The accurate area of every device defined by the overlap of the ITO and metal electrode was about 4 mm^2. Figure 3.1.4 shows the device architecture of inverted and conventional bulk heterojunction solar cell used in this study.

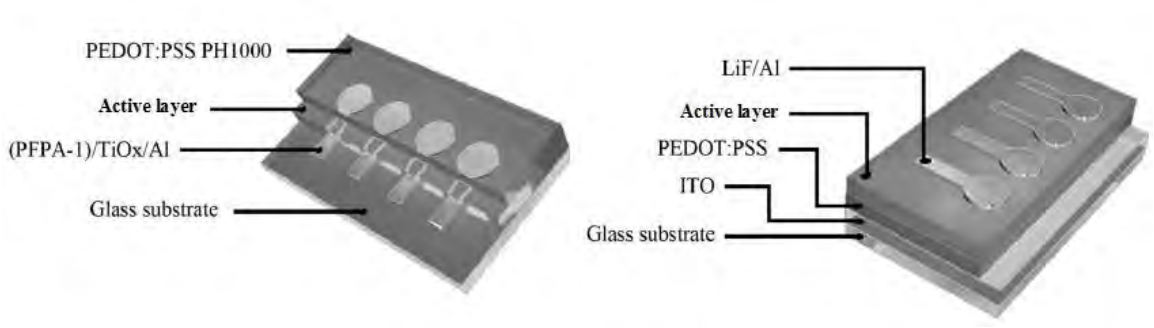

Figure 3.1.4. *Device architecture of inverted (left) and conventional (right) solar cell devices [200].*

For the study of effect of low boiling point solvent additives on photovoltaic performance of BHJ solar cells a 1:2 (w/w) ratio of TQ1:$PC_{61}BM$ blend solution (25 mg/mL) was prepared by mixing 1 mg of TQ1 and 2 mg of $PC_{61}BM$ in *o*-DCB host solvent. Blend solutions containing 2% (v/v), 3% (v/v), and 4% (v/v) low boiling point solvent additives (iodomethane, iodoethane, and diiodomethane) in the host solvent were also prepared by the same procedure. In addition to 2% (v/v), 3% (v/v), and 4% (v/v), 10% (v/v) DIMe was also prepared to get more insight of effect of the solvent additives on morphology. To enhance solubility and miscibility of the blends, cleaned magnetic stirrer was introduced into the solutions for stirring and the solutions were left over night under stirring at 40^{o}C. The device structure of the solar cell fabricated was glass/ITO/PEDOT-PSS/Active layer/Al in the absence of LiF interlayer. Prior to spin coating the hole transporting layer PEDOT-PSS film, the pre-patterned ITO glass substrates with a sheet resistance of 15 Ω/cm^2 were washed manually in detergent. Furthermore, the substrate was ultrasonically cleaned by distilled water, acetone and isopropanol sequentially for 15 min and dried with a hot

air gun. A dispersion of aqueous solution of PEDOT-PSS was then spin coated (CHEMAT TECHNOLOGY SPINCOATER KW-4A) onto cleaned ITO substrates at 3500 rpm for 60 s in ambient atmosphere and baked at 120°C on hot plate for 10 min to remove residual water. Then, the active layers, both pristine and containing the solvent additives, were spin coated from the blend solution of TQ1:$PC_{61}BM$ at 1000 rpm and PCDTBT:[70]PCBM at 1500 rpm, respectively, for 60 s on top of PEDOT:PSS layer in ambient atmosphere. The devices were completed for measurement after thermal deposition of aluminum film (~100 nm) as the cathode on top of the active layer by thermal evaporator (Edwards 306) through a shadow mask under vacuum pressure of $\sim 5 \times 10^{-6}$ mbar. Lastly, to avoid easy scratching of the Al electrode during characterization, silver paste paint was used for contact. The area of each device was defined by the overlap of the ITO and metal electrode and was about 6 mm^2. The device structure used for this study is similar to the conventional solar cell architecture stated (Figure 3.1.4, right) except the absence of LiF buffer layer.

3.2.4 Solar Cell Device Characterization

Current density-Voltage (*J-V*) curves were measured by using Keithley 2400 Source Meter under illumination of AM 1.5 filtered light with intensity of 100 mW cm^{-2} from a SS 50A Photoemission Tech. solar simulator. For inverted solar cell devices illumination took place from the top side i.e. from HC-PEDOT:PSS PH1000 while the same phenomenon took place from bottom (ITO) side for conventional solar cell devices. EQE spectra were obtained using a Newport Merlin lock-in with the solar cells illuminated with chopped monochromatic light. Atomic Force Microscopy

(AFM) images were recorded on a Dimension 3100 system (Digital Instruments/Veeco) in taping mode.

For the study of the effect of low boiling point solvent additives, the current density-voltage (*J-V*) measurements of the solar cell devices was performed using a computer-controlled CHI600A Electrochemical Analyzer, and a 250 W xenon lamp regulated by an Oriel power supply (Model 68830) which was used to illuminate the solar cells. Before illumination of the device, the white light intensity was set to 100 mW/cm^2 using Gigahertz-Optik X11 Optometer. For incident photon-to-current conversion efficiency (IPCE) measurement, a grating monochromator (Model 77250) placed into the light path to select a wavelength between 300 and 800 nm, was used. The photocurrent spectral response of the lamp was corrected using a standard silicon photodiode (Hamamatsu, Model S1336-8BK). Photoluminescence (PL) spectra of polymers and blend films were measured using Flouromax-4 spectroflourometer. To check that the additives selectively dissolve the acceptor or donor materials, films prepared from pristine blends of TQ1:[60]PCBM and PCDTBT:[70]PCBM were soaked in each additive for 5 seconds and their UV-Vis spectra were taken and compared with that of the un soaked pristine films of the same blends [195].

4. Results and Discussion

4.1 Study of Photochemical Stability and Photovoltaic Application of Quinoxaline Based Copolymers

It is desirable to improve the absorption of the active layer in order to increase the amount of generated charge pairs. This can be achieved by several means, for example by making the active layer thicker or by designing the polymer structure to absorb more light, *i.e.* to make the polymers more black [201]. The latter could be realized by incorporation of a new moiety in the conjugated backbone of the polymer *via* copolymerization. Another route that has been employed successfully to increase the absorption is by using [6,6] phenyl-C_{71}-butyric acid methyl ester ($PC_{71}BM$) instead of [6,6] phenyl-C_{61}-butyric acid methyl ester ($PC_{61}BM$) as the acceptor material [175, 202]. Quinoxaline based copolymers with incorporation of THT are therefore synthesized to improve absorption of the active layer for photovoltaic applications and their photochemical stabilities are also investigated in this work. The first photovoltaic application of quinoxaline based polymer, TQ1, was reported by Wang et al. [203]. The interest in photovoltaic investigation of this polymer was based on the interesting photophysical properties of the polymer disclosed by Yamamoto et al. [204]. Accordingly, the initial high power conversion efficiency (PCE) of an easily synthesized TQ1 blended with [6,6]-phenyl-C_{71}-butyric acid methyl ester ([70]PCBM) acceptor has been reported to be about 6% [203] in conventional geometry. In inverted geometry the polymer has shown a PCE of ~5.2% [200]. Furthermore, Kim et al. [196] has also reported a PCE of higher than 7% by means of engineering active layer nanomorphology using chloronaphthalene (CN)

solvent additive. With regard to the photochemical stability, an earlier stability study by Carlé et al. [205] has shown that the quinoxaline based polymer, TQ1, is five times more stable than P3HT when comparing the decrease in absorbed photons after being subjected to 1 sun and 85°C at ambient conditions. The ease of synthesis of TQ1, promising stability, and its promising power conversion efficiency of its device [196, 203, 205] would make it a good candidate material for large scale production of polymer solar cells.

Therefore, in this study, varying amounts of thiophene and hexylthiophene monomers were used in a semi-random copolymerization process with quinoxaline monomer to increase the absorption in the gap between the high- and the low-energy absorption peaks of the thiophene-quionoxaline polymer TQ1 *i.e.* to make the polymers more black. Therefore, this work explores how the incorporation of hexylthiophene affects the photochemical stability and the broadening of the spectra will affect the photovoltaic performance of these copolymers.

4.1.1 Photophysical and Electrochemical Properties

By copolymerizing the monomers of thiophene and hexylthiophene with quinoxaline monomer, the resulting polymer should become more black than TQ1 since THT absorbs light in the area where TQ1 lack absorption. The absorption spectra of the synthesized copolymers and TQ1 are shown in Figure 4.1.1 (top). The absorption spectrum of TQ1 shows two distinct peaks. The high energy peak of the spectrum is due to π-π^* electronic transition and the low energy peak of the spectrum is due to intramolecular charge transfer between the donor and acceptor moieties of the

polymer along the backbone [203, 204]. Similarly, the copolymers also show two distinct peaks at high and low energy regions due to π-π* and intramolecular charge transfer between donor and acceptor moieties along the backbone of the copolymers, respectively.

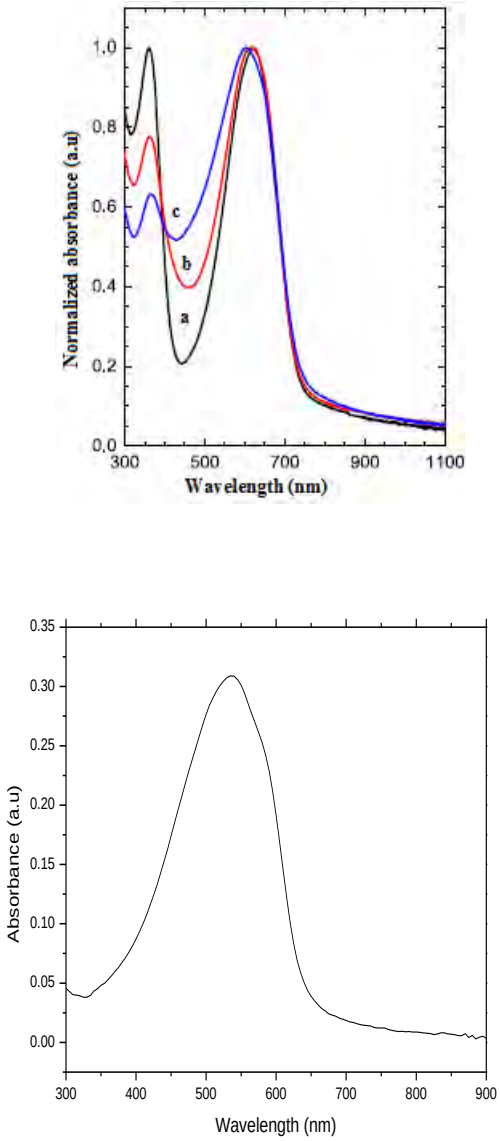

Figure 4.1.1. *Top: Normalized UV-Vis absorption spectra for TQ with 0 mol% (a), 30 mol% (b), and 50 mol% (c) hexylthiophene. Bottom: UV-Vis absorption spectra of THT.*

From the absorbance spectra it could be seen that by incorporation of a THT fraction (f_{THT}) of 30 or 50 mol% the absorbance between 400 nm and 600 nm is indeed increased as the absorption of thiophene-hexylthiophene lies between the two distinct peaks (Figure 4.1.1, bottom). In addition, the high energy peak around 360 nm is decreased. The increased photoabsorption between the two peaks by incorporation of THT in quinoxaline based copolymers is expected to harvest more photons to increase the photovoltaic performance by generating more excitons [201]. Figure 4.1.2 shows the UV-Vis spectra of the copolymers and THT blended with $PC_{70}BM$ acceptor. As it is observed from Figure 4.1.2, the presence of the acceptor increases the plateau nature of the spectra by contributing to absorption at low wavelength region [175, 202].

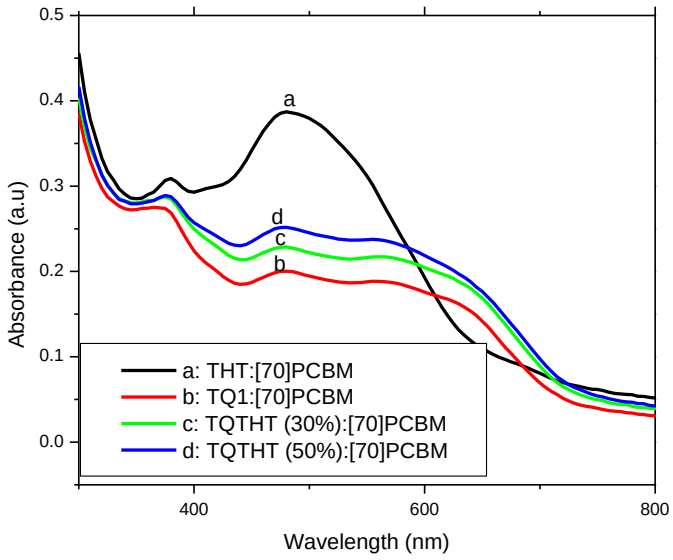

Figure 4.1.2. *UV-Vis spectra of TQ1, TQTHT copolymers, and THT blended with [70]PCBM acceptor.*

This enhancement of absorption due to the presence of acceptor could also enhance photon generated excitons and hence the photovoltaic performance of the solar cells made of the copolymers.

Table 4.1.1 shows the electrochemical parameters of TQ1, TQTHT copolymers, and THT obtained from the square wave voltammetry (SWV) [206]. HOMO and LUMO were determined from the third oxidation and reduction scans, respectively, using the peak value and setting the oxidative potential of Fc/Fc^{+} *versus* the normal hydrogen electrode (NHE) to 0.630 V [207] and the NHE energy level relative to vacuum to 4.5 V [208] with the following equation: HOMO = -(E_{ox} + 5.13) eV and LUMO = -(E_{red} + 5.13) eV [209].

Table 4.1.1. *Electrochemical parameters of TQ1, TQTHTs, and THT.*

S.No	Polymer	f_{THT}	E_{ox} (eV)	HOMO (eV)	E_{red} (eV)	LUMO (eV)
1	TQ1	0	0.67	-5.8	-1.73	-3.4
2	TQTHT	30	0.47	-5.6	-1.83	-3.3
3	TQTHT	50	0.37	-5.5	-1.93	-3.2
4	TQTHT	80	0.37	-5.5	-1.83	-3.3
5	THT	100	0.27	-5.4	-2.13	-3.0

The lying positions of the highest occupied molecular orbital (HOMO) and the lowest unoccupied molecular orbital (LUMO) of the photoabsorber materials (polymers)

with respect to the corresponding HOMO and LUMO energy levels of the acceptor is important in determining photovoltaic performance of solar cells [188, 189].

Furthermore, for efficient charge transfer and dissociation of photogenerated excitons in polymer solar cells, sufficient LUMO (polymer)-LUMO (acceptor) offset equivalent to the exciton binding energy of ~0.3 eV [137] has also to be maintained. This indicates that electronic structure of polymer materials plays major role in photovoltaic performance of polymer solar cells. For example, Wang et al. [203] calculated HOMO and LUMO energy levels of TQ1 from oxidation and reduction peak potentials of SWV to be -5.7 eV and -3.3 eV, respectively, and came to the conclusion that the high LUMO level of TQ1 ensures a downhill driving force for charge separation to PCBM whose LUMO level has been reported to be -4.1 eV measured under the same experimental conditions [210].

The gap between the HOMO of the polymer and the LUMO of the acceptor has also direct relationship with open circuit voltage (V_{OC}) and is its experimental limit in polymer solar cells. Hence, low lying HOMO value of polymers can be expected to produce high V_{OC} [167]. Furthermore, the energy gap between the HOMO and LUMO of polymers could also be used to determine the electrochemical bandgap which is an informative parameter to know the extent to which the photoabsorbers covers electromagnetic radiation for photons harvesting.

In addition, the positions of the HOMO and LUMO energy levels with respect to the vacuum energy level are one of the factors which determine the photochemical stability of polymers for photovoltaic applications [188, 189]. Accordingly, polymers possessing low lying HOMO and LUMO energy levels are expected to be photochemically stable and are preferable for solar cell application. In summary, as can be seen from Table 4.1.1, as the fraction of THT is increased the HOMO and LUMO energy levels of the copolymers are up-shifted towards the vacuum level. This is most probably because of the electron donating property of the THT which increases the electron density in the polymer and as a consequence resulted in up-shifting of the energy levels. This is of course one of the factors that could hamper the open circuit voltage and performances of solar cells made from the polymers unless and otherwise this would be compensated by the increased photon absorption as the THT fraction is increased.

4.1.2 Photochemical Stability

The degradation of the neat polymer, TQ1, was studied by monitoring the bleaching of the UV-Vis absorption spectra as shown in Figure 4.1.3. In addition, a thiophene-hexylthiophene (THT) polymer was synthesized and used as a reference. During the test, the sample was subjected to solar simulator light with an intensity of 1 sun and annealed at 85°C [181].

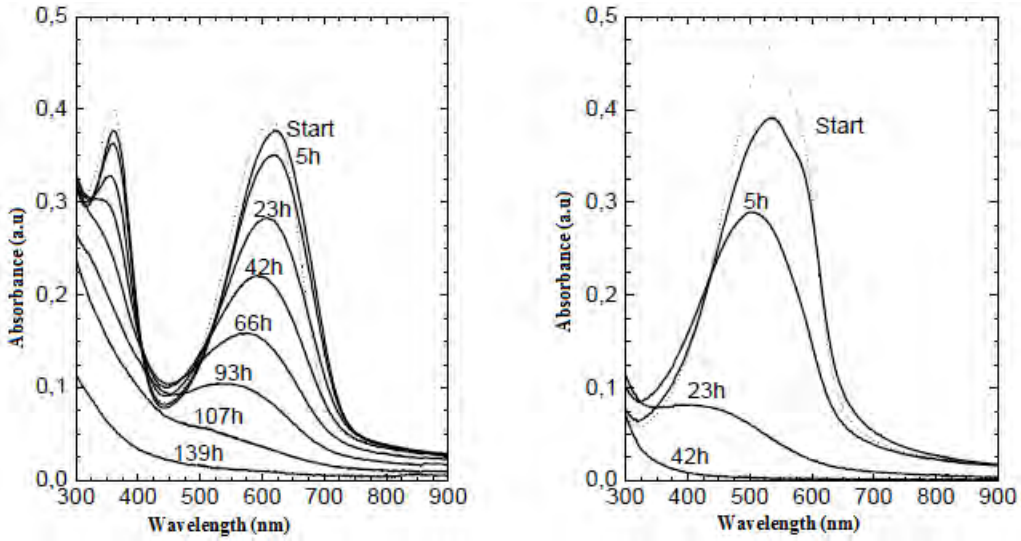

Figure 4.1.3. *UV-Vis spectra measured after ageing for indicated times under the solar simulator for TQ1 (left) and THT (right). Dotted line indicates the spectra before pre-heating.*

By comparing UV-Vis spectra measured at several times (Figure 4.1.3), it could be concluded that TQ1 is much more stable than THT. The remaining peak absorbance ($A_{max,\ remaining}$) at low energy peak was used to monitor the degradation for TQ1 compared to THT. This remaining peak absorbance is determined using the following expression:

$$A_{max,\ remaining} = \frac{A_{max}}{A_{max,\ start}} \times 100\% \qquad (6)$$

where A_{max} is the absorbance at the peak at each time and $A_{max,\ start}$ is post-heating start value of the peak absorbance. It should be kept in mind that the thicknesses of the films decreased during the experiment probably due to loss of degraded materials,

which also contributes to the decrease in maximum absorbance. For THT, $A_{max,\ remaining}$ is reduced to 74% after 5 h and after 24 h $A_{max,\ remaining}$ is as low as ~ 25%. For TQ1 $A_{max,\ remaining}$ was ~ 93% after 5 hours and after 50 hours $A_{max,\ remaining}$ ~ 53%. From the UV-Vis absorbance spectra, it can be seen that the low-energy peak decreases faster than the high-energy peak (Figure 4.1.3) i.e. the ratio between the peaks is changed for TQ1. This indicates that the conjugation length is decreased when the polymer is subjected to photo-induced oxidation, probably due to chain scission, that hinders the interamolecular charge transfer of the polymers along the backbone.

To investigate if the increasing of f_{THT} influences the stability of the copolymers, the same stability test as described above, was performed on the copolymers. Since the photo-induced degradation of THT is faster than that of TQ1, it would be expected that the stability of the copolymers would decrease with increasing f_{THT}. In Figure 4.1.4 it can be seen that this is true for the TQTHTs, which could be explained by the fact that both HOMO and LUMO levels of TQTHTs are closer to vacuum than for TQ1 as shown in Table 4.1.1. Therefore, incorporation of 30% and 50% mole fraction of THT in to TQ1 polymer decreased stability of the copolymers and resulted in negative impact with regard to the stability of the polymer materials.

Figure 4.1.4. $A_{max,\ remaining}$ *measured by UV-Vis after ageing under simulated solar irradiation is plotted against time for TQ with 0 mol% (stars), 30 mol% (diamonds), 50 mol% (triangles), and 80 mol% (pentagons) THT with respect to TQ1. As a reference the normalized maximum peak absorbance (circles) for THT is added.*

4.1.3 Photovoltaic Performance

Photovoltaic devices of the copolymers were prepared according to the description in the experimental section. In all devices $PC_{71}BM$ is used as the electron acceptor. It has been shown that the D-A ratio greatly influences the performance of the organic BHJ solar cell as it strongly affects the crystalline order, phase separation, and morphology of the thin film bicontinuous percolation pathways with maximal interfacial area [211]. Hence, optimization of donor-acceptor ratio is an important step for fabrication of efficient polymer solar cells. Accordingly, for devices prepared

with TQTHTs and reference devices prepared with THT the optimal ratio between polymer and electron acceptor was found to be 1:2.

Table 4.1.2 shows the summary of the donor-acceptor blend optimization done to obtain optimum efficiency of polymer solar cells fabricated from TQ1, TQTHT, and THT copolymers. TQTHTs based devices show lower device efficiency compared to TQ1 based devices. Furthermore, the J_{SC} of the optimized TQTHTs based devices were not improved, even though this was expected from absorption contribution of THT in the copolymers, compared to TQ1 based devices. The decrease in J_{SC} and device efficiency of TQTHTs compared to the TQ1 based once could be due to the morphology difference of the blends. As observed from AFM images (Figure 4.1.6 a, b, and c) the grain size of the TQTHTs based blend is larger than that of the TQ1 based blend limiting the diffusion of excitons to D-A interfaces to be dissociated in to free charge carriers. Both copolymers with f_{THT} = 30 and f_{THT} = 50 mol% show a substantial decrease in efficiency but the efficiency of the devices with $f_{THT} = 50$ mol% are slightly higher. The increase in photovoltaic performance of device fabricated from $f_{THT} = 50$ mol% compared to that of f_{THT} = 30 is due to significant improvement of its FF and descent increase in short circuit current density (J_{SC}). The better J_{SC} and FF obtained could be due to good nanomorphology and interpenetrating network formation of the donor and acceptor materials (Figure 4.1.6 b and c). In addition, even with a f_{THT} = 80 mol% the efficiency of the solar cells is still more than twice as high as THT devices.

Table 4.1.2. *Performance of solar cells fabricated with different donor-acceptor ratios for TQ1, TQTHTs, and THT polymers.*

S.No	Polymer	Polymer: [70]PCBM ratio	J_{SC} (mA/cm^2)	V_{OC} (V)	FF	PCE (%) (max)
1	THT	1:1	2.95	0.59	0.36	0.62
		1:2	5.01	0.49	0.41	1.0
		1:3	5.19	0.47	0.36	0.87
		1:4	5.42	0.44	0.36	0.85
2	TQ1	1:2	10.18	0.78	0.54	4.27
		1:3	10.12	0.74	0.52	3.89
3	f_{THT} = 30	1:2	7.28	0.68	0.47	2.32
4	f_{THT} = 50	1:2	8.18	0.64	0.54	2.83
5	f_{THT} = 80	1:1	5.21	0.69	0.49	1.77
		1:2	6.88	0.62	0.53	2.28
		1:3	6.78	0.61	0.53	2.24
		1:4	6.44	0.55	0.53	1.88

Figure 4.1.5 shows *J-V* curve of the best performing device fabricated from THT, TQ1, and TQTHTs blended with [70]PCBM. As observed from the graph and Table 4.1.3, which shows the summary of the photovoltaic parameters of Figure 4.1.5, the V_{OC} of the solar cells made from TQTHT polymers has largely decreased as the fraction of THT is increased compared to the pristine TQ1. This is one of the factors which hampered the photovoltaic performance of TQTHTs based solar cells. One

reason for the decrease in V_{OC} is due to the electron energy level modification [212] of the copolymers as introduction of THT up-shifted the HOMO energy level of the copolymers.

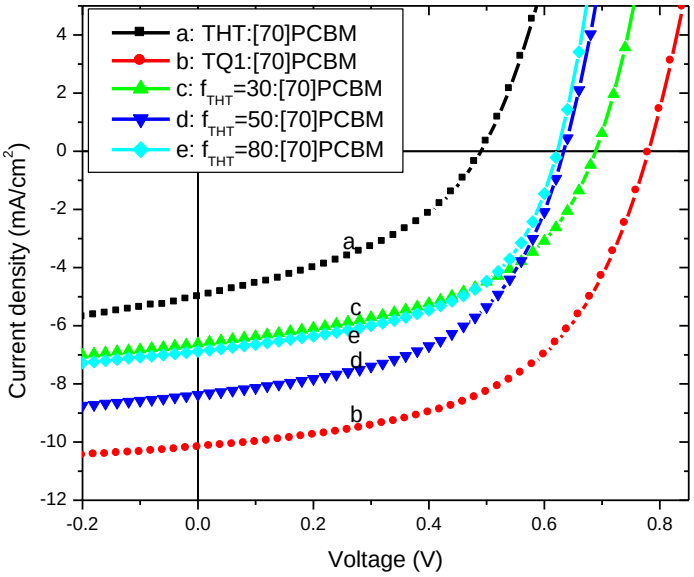

Figure 4.1.5. *J-V curves of solar cells with maximum performance fabricated from TQ1, TQTHTs, and THT blended with [70]PCBM acceptor.*

Furthermore, the current densities of the devices made of the TQTHT copolymers compared to the pristine TQ1 were not increased as expected from the UV-Vis spectra as the fraction of the THT is increased. However, as stated above, slight current density and FF increment has been observed when the THT fraction has increased from f_{THT} = 30 to f_{THT} = 50 and led device made of f_{THT} = 50 to possess better performance compared to devices made of the other TQTHT copolymers. In fact, current density in solar cells is not solely depends on the absorption of

photoactive materials but also can largely be affected by exciton diffusion to the donor-acceptor interface, charge carrier dissociation at the interface, and charge carriers transportation to respective electrodes.

Table 4.1.3. *Summary of the photovoltaic parameters of the best performing devices fabricated from THT, TQ1, and TQTHTs.*

S. No	Polymer	Polymer: [70]PCBM ratio	J_{SC} (mA/cm^2)	V_{OC} (V)	FF	PCE (%) (max)
1	THT	1:2	5.01	0.49	0.41	1.0
2	TQ1	1:2	10.18	0.78	0.54	4.27
3	f_{THT} = 30	1:2	7.28	0.68	0.47	2.32
4	f_{THT} = 50	1:2	8.18	0.64	0.54	2.83
5	f_{THT} = 80	1:2	6.88	0.62	0.53	2.28

To see the effect of THT fraction on the blend morphology of the photoactive materials atomic force microscope (AFM) and photoluminescence, to complement AFM data, have been generated. The AFM image of the blends with different THT fraction is shown in Figure 4.1.6. As it is indicated in the caption of Figure 4.1.6, the root mean square (RMS) roughness values are more or less very similar and are low. This indicates that all the polymers are well dissolved and mixed with the acceptor material in the organic solvent (*o*-DCB) used to prepare the films. Furthermore, as observed from the AFM images, the grain size of blend films of copolymers with f_{THT} = 30 and f_{THT} = 50 look larger than that of pristine blend. This might have contributed

for the low current density of devices fabricated from the copolymers limiting the diffusion length of generated excitons [139 - 143] even though the copolymers posses better absorbance coverage.

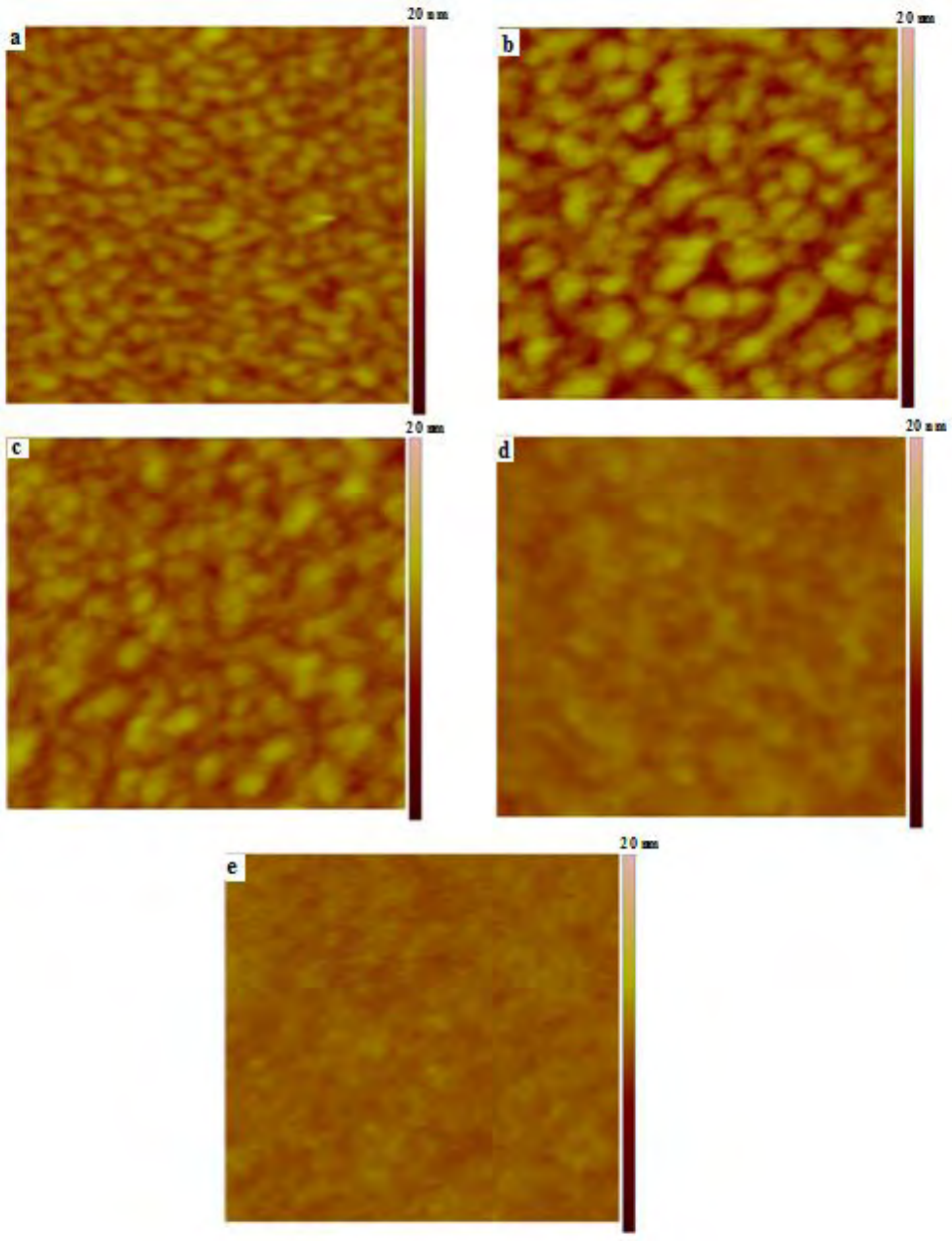

Figure 4.1.6. *AFM height image (1µm x 1µm) of: a) TQ1, b) f_{THT} = 30, c) f_{THT} = 50, d) f_{THT} = 80 and e) THT blended with [70]PCBM. The root-mean-square (RMS) values are 0.840, 1.470, 0.951, 0.461 and 0.365, respectively.*

However, the AFM image of film prepared from f_{THT} = 80 looks blurred showing the smallest RMS (0.461 nm) among the copolymers and is very similar to that of reference film made of THT (0.365 nm). This may be due to the increase in solubility of the copolymer and miscibility with acceptor as increase in fraction of hexylthiophene results in increase in side chain proportion [213] of the copolymer. Of course miscibility beyond the limit is also a disadvantage for photovoltaic performance of organic solar cells as it breaks percolation of acceptor and donor materials to respective electrodes for efficient charge carrier transport and collection [214, 215]. This then can lead to charge carriers recombination before collection by respective electrodes. This can also be put as one possible reason for the low current density of f_{THT} = 80:[70]PCBM based solar cells while its donor absorbance cover large portion of the solar spectrum compared to the other donor polymers of the family.

Figure 4.1.7 shows photoluminescence (PL) spectra of pristine polymer and their corresponding blend films. As it can also be observed from the PL spectra (Figure 4.1.7, top) of the polymers, the fluorescence of all donor copolymers are well quenched when they are blended with the [70]PCBM acceptor. This also indicates that donors and acceptor materials are soluble in the host solvent *o*-DCB and well mixed contributing for formation of better nanomorphology [216]. The same phenomena has also been observed for the reference film formed from THT polymer blended with [70]PCBM acceptor (Figure 4.1.7, bottom).

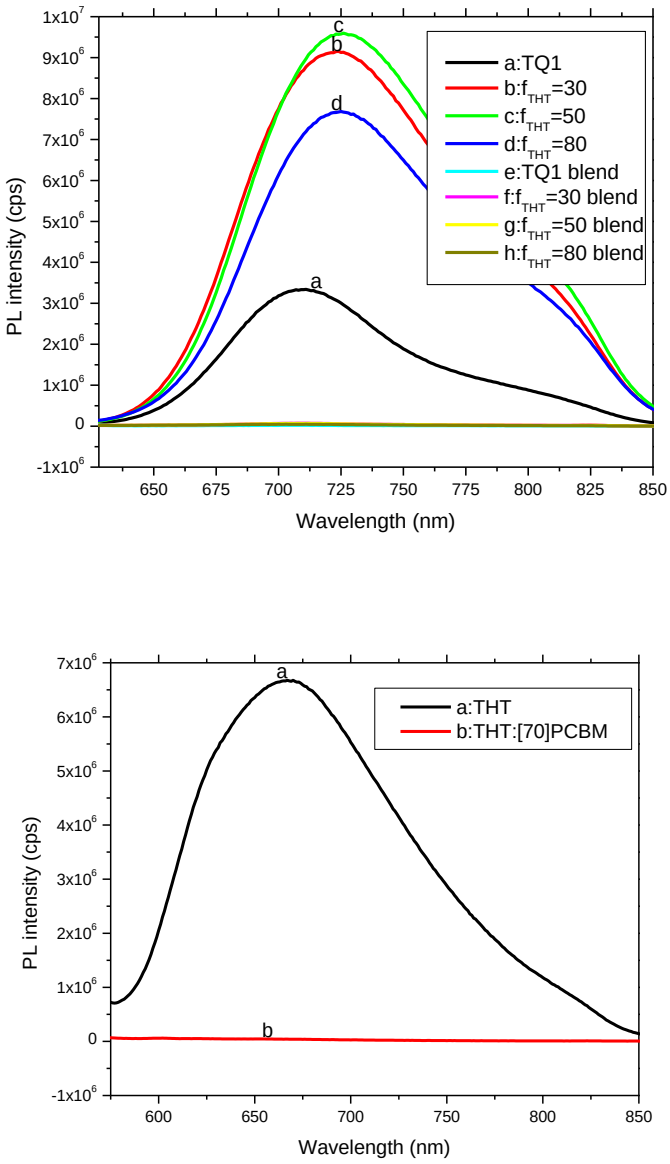

Figure 4.1.7. *Photoluminescence spectra of TQ1, TQTHTs, THT, and their blends with [70]PCBM. Top: TQ1, TQTHT, and their blends. Bottom: THT and its blend.*

Furthermore, as observed from Figure 4.1.8, the stability of the solar cell devices fabricated from the copolymers was also compared to device made of pristine TQ1 polymer. During the stability measurement of the solar cell devices, the PCE of the devices stored in ambient atmosphere were measured starting from the date of fabrication at fixed interval of time as shown in Figure 4.1.8. Figure 4.1.8 shows that devices fabricated in inverted geometry have shown greater stability compared to their corresponding devices fabricated in conventional geometry.

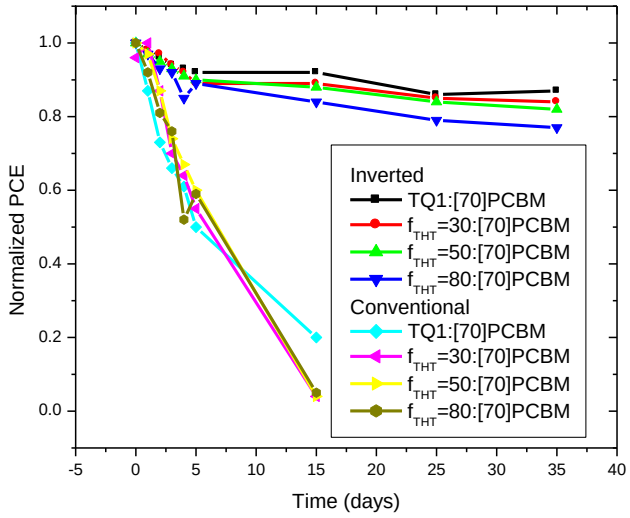

Figure 4.1.8. *Device stability of inverted (Glass/Al/TiOx/PFPA-1/active layer/HC-PEDOT:PSS/Ag paste and conventional (ITO/PEDOT:PSS/active layer/Al) polymer solar cells fabricated from TQ1 and TQTHTs.*

Accordingly, devices fabricated in inverted geometry have retained more than 80% PCE after 35 days storage in ambient atmosphere. However, the corresponding devices fabricated in conventional geometry have almost lost their performance after

15 days storage in similar air condition. This brings us to the conclusion made that fabrication of polymer solar cells in inverted geometry is more advantageous than conventional polymer solar cells for large scale printing and commercialization [82].

4.1.4 Conclusion

Copolymerization of quinoxaline and thiophene-hexylthiophene monomers has resulted in copolymers with enhanced absorption in the valleys between the two absorption peaks of the pristine polymer, TQ1. As determined from square wave voltammetry (SWV) the copolymers have shown up-shifted HOMO and LUMO energy levels as expected because of the electron donating property of the copolymerized monomer, thiophene-hexylthiophene. Furthermore, the incorporation of the thiophene-hexylthiophene in to the TQ1 polymer has negatively affected the photochemical stability of the copolymers. This could be due to the up-shifting of the copolymers compared to the TQ1 polymer which make the copolymers more sensitive to photo-oxidation. Moreover, the incorporation of the thiophene-hexylthiophene has also affected the photovoltaic performance of the copolymers negatively. Therefore, the incorporation of the thiophene-hexylthiophene in to the TQ1 polymer has resulted in neither photochemical stability nor photovoltaic performance improvement.

4.2 Study of Photochemical Stability and Photovoltaic Application of Pyridopyrazine Based Copolymers

Pyridopyrazine based copolymer (poly[2,3-bis(3-(octyloxy)phenyl)pyrido[3,4-b]pyrazine-alt-thiophene](TQN)) was first synthesized by Kroon et al. [217]. They investigated the influence of structural alteration on physical and electronic properties by making slight modification on quinoxaline based polymer, TQ1, either on the acceptor structure directly or on pendent side chains. Accordingly, they synthesized pyradopyrazine based polymer, poly[2,3-bis(3-(octyloxy)phenyl)pyrido[3,4-b]pyrazine-alt-thiophene] (TQN), by incorporation of an extra electron withdrawing imine-nitrogen directly on the acceptor moiety to increase acceptor strength and hence intramolecular charge transfer. This structural alteration resulted in red-shift of the UV-Vis absorption of the polymer because of increased intramolecular charge transfer between donor-acceptor moieties due to the incorporation of stronger acceptor group [218]. Similar to TQ1, TQN also displays two distinct absorption peaks, one high-energy peak originating from the absorption in aromatic structures and one low-energy peak from the intramolecular charge transfer along the backbone of the polymer. Furthermore, for TQN polymer the low energy peak exhibits some vibronic feature commonly attributed to some degree of ordering in the solid state. This UV-Vis spectra feature was not observed in quinoxaline based polymer [203, 204]. The reported device performance when the polymer, TQN, is blended with [6,6]-phenyl-C_{61}-butyric acid methyl ester ([60]PCBM) was ~ 1%. However, the stability study of TQN polymer has not been reported.

Here, varying amounts of thiophene and hexylthiophene monomers were used in a semi-random copolymerization process with pyridopyrazine monomer. This was done, in similar manner with the quinoxaline based polymers, in order to increase the absorption in the gap between the high- and the low-energy absorption peaks of the thiophene-pyridopyrazine polymer TQN; *i.e.* to make the polymers more black. Therefore, this work explores how the incorporation of hexylthiophene affects the photochemical stability and the broadening of the spectra will affect the photovoltaic performance of these copolymers.

4.2.1 Photophysical and Electrochemical Properties

Figure 4.2.1 shows the UV-Vis absorption spectra of TQN in comparison with that of TQ1. As can be seen from Figure 4.2.1, incorporation of strong electron withdrawing imine-nitrogen in to the acceptor moiety of the TQ1 polymer has red-shifted the absorption peak at low energy region.

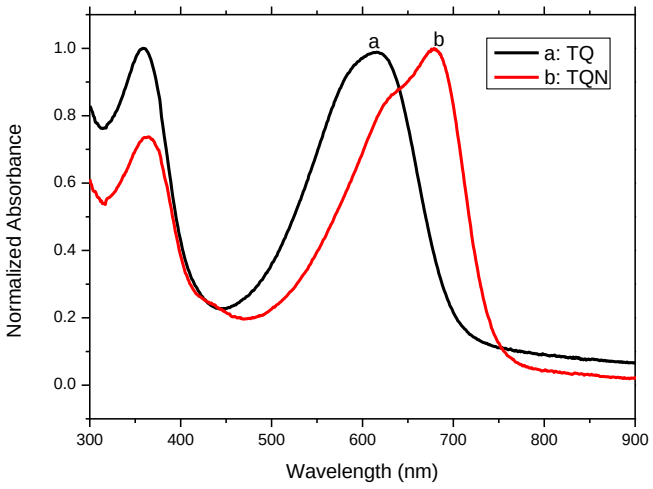

Figure 4.2.1. *UV-Vis spectra of films of TQ1 and TQN polymers in o-DCB.*

Figure 4.2.2 shows the UV-Vis spectra of TQN and copolymers of TQN with 30% and 50% THT mole fraction and that of THT.

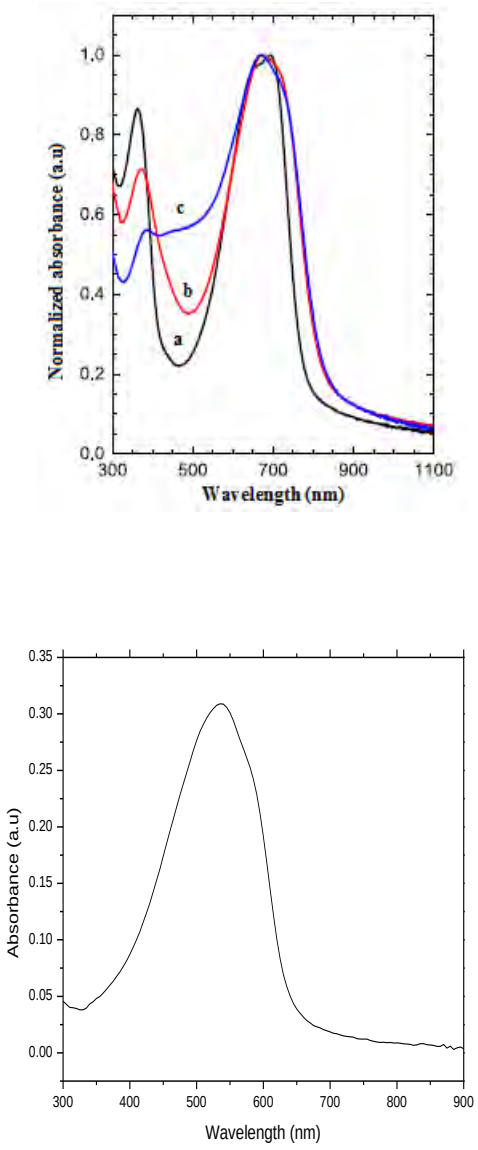

Figure 4.2.2. *Top: Normalized UV-Vis absorption spectra for TQN with 0 mol% (a), 30 mol% (b), and 50 mol% (c) THT and bottom: UV-Vis of THT as reference.*

Similar to TQTHT copolymers, copolymerization of thiophene and hexylthiophene monomers with pyridopyrazine monomer has resulted in increase in light absorption between the low energy peak and the high energy peak since THT absorbs light in the area where TQN lacks absorption (Figure 4.2.2). Figure 4.2.2 also shows that as the THT fraction of the copolymer increases from $f_{THT} = 0$ to $f_{THT} = 30$ and to $f_{THT} = 50$, the absorption also increased between the two peaks of the spectra. Furthermore the addition of the THT fraction has also resulted in harvesting of more photons at the longer wave length compared to the pristine TQN while the low energy peak positions has not been affected. This may be due to aggregation and increase in conjugation length of the polymers and narrowing the bandgap of the polymers. In addition, similar to the TQTHT copolymers, the absorption of TQNTHT copolymers has also showed decrease in absorption at high energy position.

Figure 4.2.3 shows the UV-Vis spectra of TQN and copolymers with 30% and 50% THT mole fraction blended with [70]PCBM acceptor material. As shown in Figure 4.2.3, when the polymers are blended with [70]PCBM acceptor, the plateau nature of the absorption spectra has increased because of the contribution in absorption by the acceptor at low wavelength region [175, 202]. This absorption contribution by acceptor molecule may also enhance the photovoltaic performance of polymer solar cells by generating additional excitons during photoabsorption by active layer.

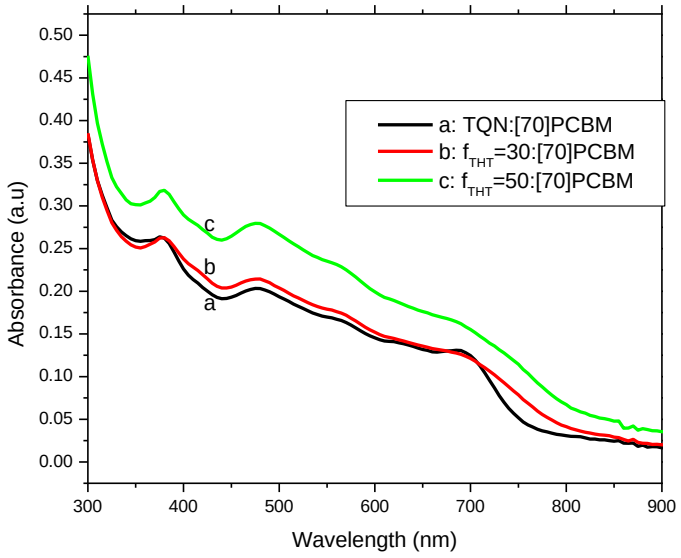

Figure 4.2.3. *UV-Vis spectra of TQN and TQNTHT copolymers blended with $PC_{70}BM$ acceptor.*

Table 4.2.1 shows the electrochemical parameters of TQN and TQNTHT copolymers determined from the square wave voltammetry [206]. Compared to TQ1, the HOMO and LUMO values of TQN have shifted away from vacuum level. This is due to the incorporation of the stronger electron withdrawing imine-nitrogen in to the acceptor moiety of TQN. This downshift of the HOMO energy level of TQN is expected to increase the V_{OC} of solar cells of the polymer [217]. Similarly, the HOMO and LUMO energy levels of TQNTHTs have also shifted away from the vacuum level compared to the HOMO and LUMO energy levels of the corresponding TQTHT copolymers. Generally, this down shift of energy levels of the TQN and TQNTHs compared to TQ1 series polymers may contribute to better photochemical stability for

solar cell application and also may enhance open circuit voltage for better photovoltaic performance of the copolymers.

Table 4.2.1. *Electrochemical parameters of TQN and TQNTHTs.*

S.No	Polymer	THT (%)	E_{ox} (eV)	HOMO (eV)	E_{red} (eV)	LUMO (eV)
1	TQN	0	0.87	-6.0	-1.43	-3.7
2	TQNTHT	30	0.77	-5.9	-1.53	-3.6
3	TQNTHT	50	0.47	-5.6	-1.63	-3.5

However, a too strong electron withdrawing results in decrease of the $LUMO_{polymer}$-$LUMO_{acceptor}$ offset which usually decreases efficiency of exciton dissociation and decreases current density of solar cells [219, 220]. Similar to TQTHTs, the HOMO and LUMO energy levels of TQNTHT copolymers have shifted towards the vacuum level compared to the pristine TQN polymer. This may be due to the electron donating nature of the THT that could increase electron density. This of course may affect the V_{OC} negatively and hence performance of solar cells fabricated from TQNTHT copolymers compared to that of pristine TQN similar to devices fabricated from TQTHTs copolymers.

4.2.2 Photochemical Stability

Under similar experimental conditions and procedures as that of TQ1 and its copolymers, the degradation of TQN and its copolymers was also studied by monitoring the bleaching of the UV-Vis absorption spectra. Figure 4.2.4 shows the UV-Vis spectra during bleaching experiment. As observed from UV-Vis spectra

measured at several times, it could be concluded that the TQN is much more stable than THT (Figure 4.2.4). $A_{max,\ remaining}$ was also used to monitor the degradation of TQN and TQNTHTs similar to TQ1 and TQ1THTs. When $A_{max,\ remaining}$ is reduced to 74% after 5 h and to ~25% after 24 h for THT, it reduces to ~95% after 5 h and to 66% after 50 h for TQN. This also indicates that TQN is much more stable than THT.

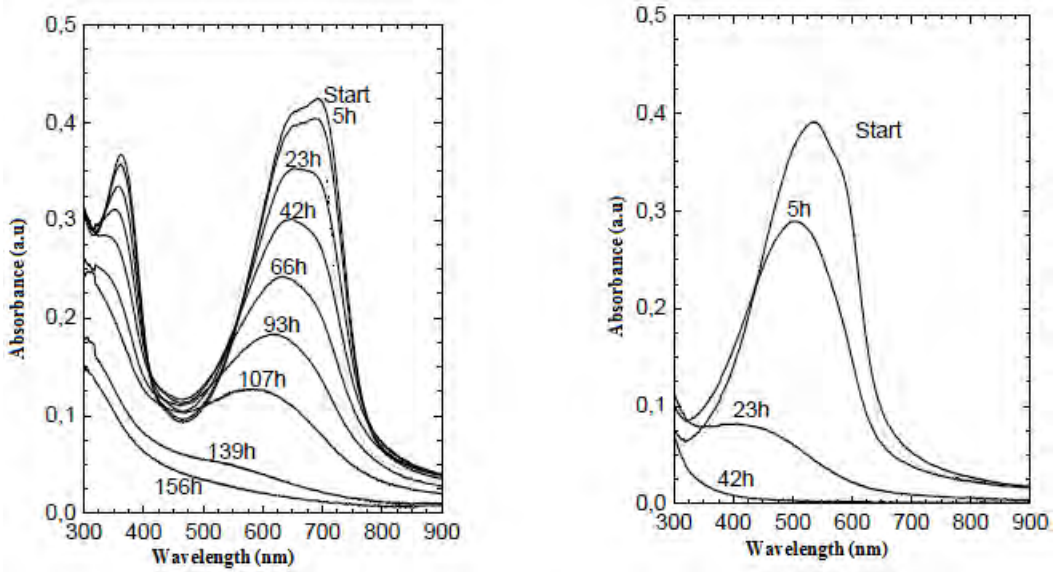

Figure 4.2.4. *UV-Vis spectra measured after ageing for indicated times under the solar simulator for TQN (left) and THT (right). Dotted line indicates the spectra before pre-heating.*

The data also shows that TQN is also more stable than TQ1 for which $A_{max,\ remaining}$ reduced to ~93% after 5h and to 53% after 50 h under similar conditions. This may be due to the difference in the energy positions of the HOMO as well as the LUMO (Table 4.1.1 and 4.2.1) of the two polymers [205, 221]. Both

energy levels of TQ1 lay closer to vacuum than that of TQN. The difference in stability may also be due to different degrees of packing of the polymers during film formation to limit oxygen and moisture diffusion in to the film.

To investigate if increasing f_{THT} influences the stability of the copolymers, the same stability test as described for TQTHT copolymers was performed on TQNTHT copolymers (Figure 4.2.5).

Figure 4.2.5. $\boldsymbol{A_{max,\ remaining}}$ *measured by UV-Vis after ageing under simulated solar irradiation is plotted against time for TQ with 0 mol% (stars), 30 mol% (diamonds), 50 mol% (triangles) THT with respect to TQN. As a reference the normalized maximum peak absorbance (circles) for THT is added.*

For TQNTHTs it would also be expected that the stability of the copolymers decrease with increasing f_{THT} as the stability of the reference polymer (THT) is very low. However, the stability of TQNTHTs is more or less similar to that of TQN as it can be seen from Figure 4.2.5. This similar stability of TQN and TQNTHTs even though the TQNTHTs has energy levels closer to vacuum than TQN could be due to the strong packing of the polymers during film formation and limit oxygen diffusion into the films [222]. In addition to increase in absorption with increase in THT fraction, this better stability of TQNTHT compared to TQTHT copolymers can be taken as an advantage for photovoltaic applications.

4.2.3 Photovoltaic Properties

Solar cell devices were fabricated by blending TQN and TQNTHTs with [70]PCBM acceptor similar to TQ1 and TQTHTs. The first and important step in characterizing the photovoltaic properties of new polymers is to optimize the donor-acceptor ratio for optimum donor-acceptor nanomorphology formation and better performance. Table 4.2.2 shows the performance of devices with different donor-acceptor ratios for TQN and TQNTHTs based polymers. As can be seen from Table 4.2.2, the maximum performing devices were obtained when the blend ratio between the polymers and [70]PCBM is 1:3. So it is this blend ratio which has formed the optimum nanomorphology between the donors and acceptor for better performance of the devices.

Table 4.2.2. *Performance of solar cells fabricated from TQN and TQNTHTs with different donor-acceptor ratios.*

S. No	Polymer	Polymer: [70]PCBM ratio	J_{SC} (mA/cm^2)	V_{OC} (V)	FF	PCE(%) (max)
1	TQN	1:1	3.03	0.56	0.28	0.48
		1:2	3.12	0.60	0.38	0.72
		1:3	3.36	0.62	0.42	0.89
		1:4	2.67	0.62	0.42	0.71
2	f_{THT} = 30	1:1	6.21	0.54	0.33	1.11
		1:2	5.30	0.51	0.42	1.13
		1:3	6.49	0.50	0.41	1.34
		1:4	4.97	0.52	0.47	1.22
3	f_{THT} = 50	1:1	8.66	0.54	0.35	1.62
		1:2	9.89	0.48	0.37	1.75
		1:3	10.03	0.49	0.44	2.17
		1:4	7.00	0.51	0.50	1.78

Figure 4.2.6 shows the current density-voltage (*J-V*) curves for devices with maximum performance fabricated from TQN and TQNTHTs blended with [70]PCBM. The summary of the photovoltaic parameters of these devices and that of reference device with the same blend ratio i.e. 1:3 for comparison are shown in Table 4.2.3. The photovoltaic performance of the polymers has increased as the fraction of the THT is increased in contrary to that of TQTHTs compared with TQ1. As it can be

observed from Figure 4.2.6 and Table 4.2.3, the increase in current density has major contribution to the increase in photovoltaic performance of the devices as THT fraction increases. This increase in current density is of course as expected and is in agreement with the increase in absorption of the donor polymers, coverage of the valleys between the high and low energy peaks, with increase in THT fraction (Figure 4.2.2).

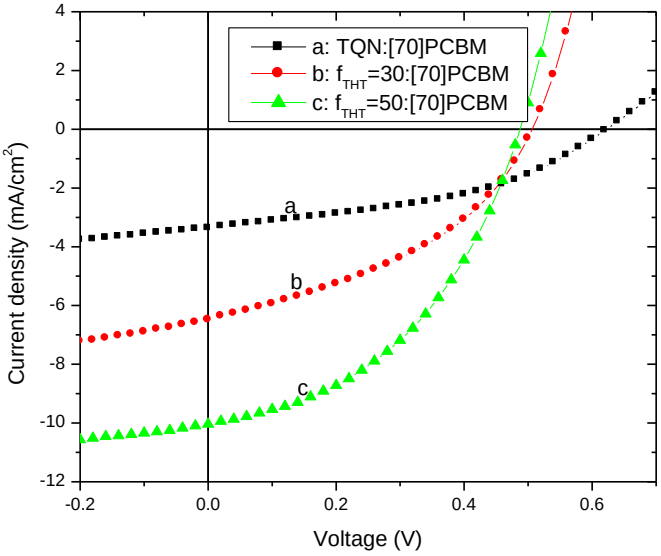

Figure 4.2.6. *J-V curves of solar cells with maximum performance fabricated from TQN and TQNTHTs blended with [70]PCBM acceptor.*

Table 4.2.3. *Summary of the photovoltaic parameters of the best performing devices fabricated from TQN, TQNTHTs, and that of THT with same blend ratio.*

S. No	Polymer	Polymer: [70]PCBM ratio	J_{SC} (mA/cm^2)	V_{OC} (V)	FF	PCE(%) (max)
1	TQN	1:3	3.36	0.62	0.42	0.89
2	$f_{THT} = 30$	1:3	6.49	0.50	0.41	1.34
3	$f_{THT} = 50$	1:3	10.03	0.49	0.44	2.17
4	THT	1:3	5.19	0.47	0.36	0.87

The V_{OC} of the devices are however decreased with increase of fraction of THT. This is also as expected from the electrochemical properties of the polymers (Table 4.2.1). That is with increase of fraction of THT, the HOMO energy level of the polymers has up-shifted and this minimizes the gap between the HOMO of the donor materials and the LUMO of the acceptor which directly influences the V_{OC} of the devices. The fill factors of the devices are more or less similar.

As stated above, TQN was synthesized by modifying the structure of TQ1 and the main modification was by incorporation of strong electron withdrawing imine-nitrogen group on the acceptor moiety [217]. This has also resulted in shift of HOMO energy level away from the vacuum level compared to TQ1 (Table 4.1.1 and 4.2.1). From this electrochemical property of the polymers, it is expected that the V_{OC} of device fabricated from TQN would be greater than that of TQ1. However, in contrary to the electrochemical properties of the two pristine polymers, the V_{OC} of device

fabricated from TQN (0.62 V) is less than that of TQ1 (0.78 V). Since pyridine-based materials are well-known to form complexes with metals and also fullerenes [223], it could be this type of interaction that has limited the V_{OC} and performance of TQN-based devices. Another factor that is able to influence the voltage is the well-known acidity of PEDOT-PSS, which protonate the pyridine-nitrogen at the polymer-PEDOT:PSS interface and there by altering the electronic properties of the materials interface. Kroon et al. [217] tested this by exchanging PEDOT:PSS for MoO_3, after which the devices showed ~50% increase in V_{OC} and therefore in its performance. For TQNTHTs, the pyridine-nitrogen interaction with PEDOT:PSS might be hindered sterically by increase in THT fraction which increases the pendent hexylthiophene side chains leading to better photovoltaic performance compared to the pristine TQN, the pyridine-nitrogen of which is not hindered, based devices.

In order to show the photoresponse of devices at different wavelengths, corresponding external quantum efficiency (EQE) of the PSCs was measured under the illumination of a monochromatic light source as shown in Figure 4.2.7. Similar to the UV-Vis spectra of the polymers (4.2.2), the devices have given good response between the wavelengths 300 - 700 nm. As observed from Figure 4.2.7, the devices fabricated from TQN and TQNTHTs efficiently harvest photons in the wavelength rage of about 350 nm to 550 nm and convert them in to electrical current while photon-to-current conversion of the devices decreased beyond about 550 nm to the longer wavelengths. However, the UV-Vis spectra of the polymers (Figure 4.2.2) show maximum absorbance between 550 nm and 700 nm where the devices lost

efficient photon-to-current conversion. This might also be due to the interaction of pyridine-nitrogen with metal and acidic PEDOT:PSS which could have changed the electronic structure of the polymers and resulted in poor performance of the devices [217].

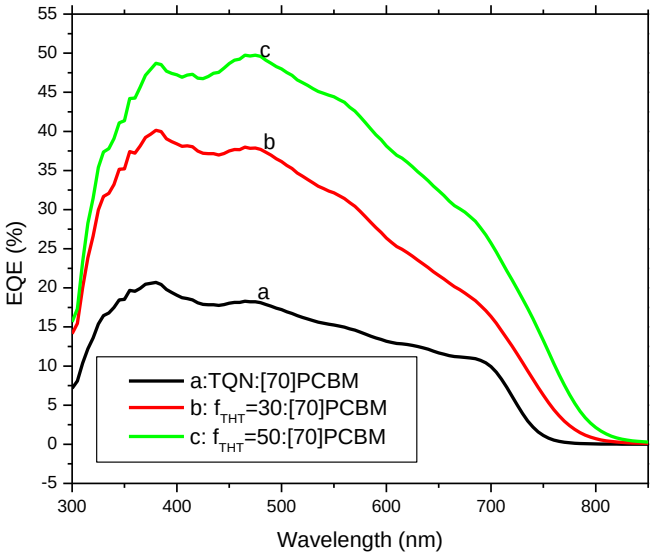

Figure 4.2.7. *EQE spectra of TQN, f_{THT} = 30, and f_{THT} = 50 solar cell devices with maximum PCEs.*

As described in the experimental section, the device structure in our study was glass/Al/TiOx/active layer/HC-PEDOT:PSS/Ag. To avoid the interaction of pyridine-nitrogen with acidic PEDOT:PSS, the acidic HC-PEDOT:PSS was replaced by neutral HC-PEDOT:PSS. Table 4.2.4 shows the values of photovoltaic parameters of devices fabricated from TQN and TQNTHTs using acidic and neutral HC-PEDOT:PSS as electrode.

Table 4.2.4. *Photovoltaic parameters of devices fabricated from TQN and TQNTHTs using acidic and neutral HC-PEDOT:PSS as anode electrode.*

S. No	Polymer	HC-PEDOT:PSS	J_{SC} (mA/cm^2)	V_{OC} (V)	FF	PCE(%) (max)
1	TQN	acidic	3.36	0.62	0.42	0.89
		neutral	2.8	0.52	0.37	0.54
2	f_{THT} = 30	acidic	6.49	0.50	0.41	1.34
		neutral	5.3	0.48	0.39	0.98
3	f_{THT} = 50	acidic	10.03	0.49	0.44	2.17
		neutral	9.2	0.45	0.36	1.50

As observed from Table 4.2.4, replacing the acidic HC-PEDOT:PSS electrode with neutral HC-PEDOT:PSS even worsened the performance of the devices. Replacing the acidic HC-PEDOT:PSS by neutral HC-PEDOT:PSS degrades all the photovoltaic parameters. Moet et al. [224] demonstrated that neutralization of PEDOT:PSS leads to reduced work function which results in a lower open circuit voltage of devices based on a polyfluorene derivative with a higher ionization potential. So, this could happen also in the case of the TQN and TQNTHTs based devices as the open circuit voltage is one of which degraded most when the acidic HC-PEDOT:PSS was replaced with the neutral one. Furthermore, replacing of acidic PEDOT:PSS with neutral PEDOT:PSS might have resulted in bad morphology of the blend films as all photovoltaic parameters are degraded.

To investigate the effect of THT on the blend morphology of pyridopyrazine based copolymers, AFM height image of the blend films were taken and is shown in Figure 4.2.8. The RMS values of the pyridopyrazine based blends are shown in the caption of Figure 4.2.8 in comparison with the blend of the reference material THT. Compared to the TQ1 and TQTHTs in general, TQN and TQNTHTs copolymer blends show rougher morphology structure. This could be due to the development of larger grain size crystals and self-aggregation of the components resulting from low miscibility of the components.

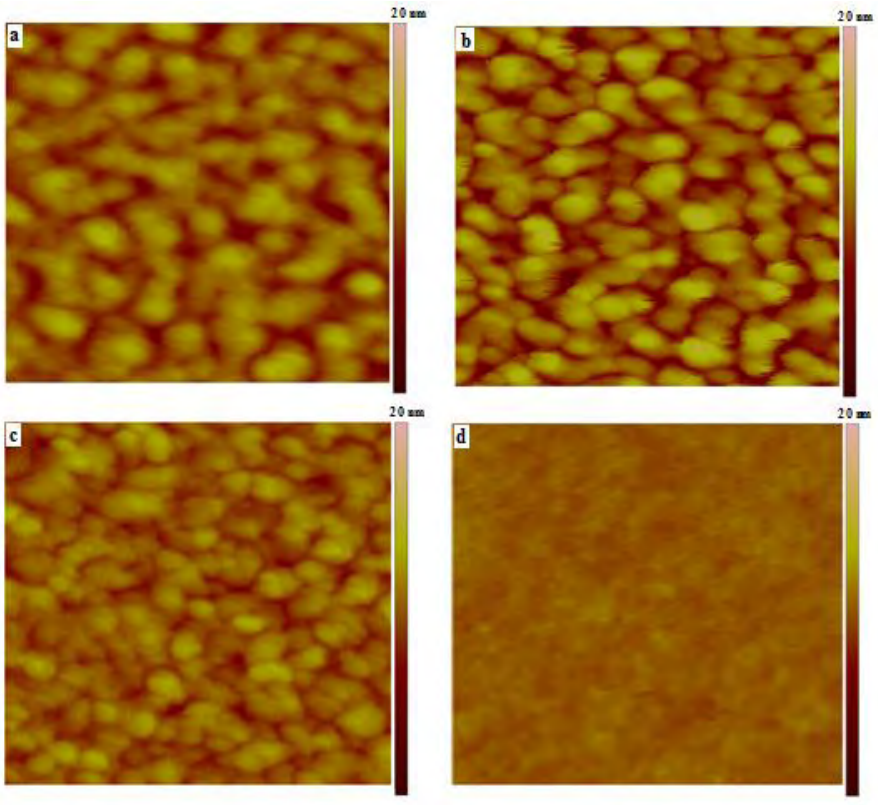

Figure 4.2.8. *AFM height image (1µm x 1µm) of: a) TQN, b) f_{THT} = 30, c) f_{THT} = 50, and d) THT blended with [70]PCBM. The root-mean-square (RMS) values are 1.42, 1.92, 1.16 and 0.365, respectively.*

Therefore, morphologies containing large phase structures are observed from Figure 2.2.8 indicating poor nanomorphology of the blends. The large grain structures showed reduction from TQN:[70]PCBM to (f_{THT} = 30):[70]PCBM and (f_{THT} = 50):[70]PCBM which is also one of the contributing factors for performance enhancement of TQNTHTs based devices. The large grain size structures of the blends largely affect exciton dissociation as they decay radiatively or non-radiatively before reaching donor-acceptor interfaces. Generally, this poor morphology of the blend films have contributed in hampering photovoltaic parameters like J_{SC}, FF, and V_{OC} resulting in poor performance of the devices fabricated from these copolymers.

To further investigate the nanomorphology of the blend films, photoluminescence experiment was also carried out and the PL spectra of the blends are shown in Figure 4.2.9.

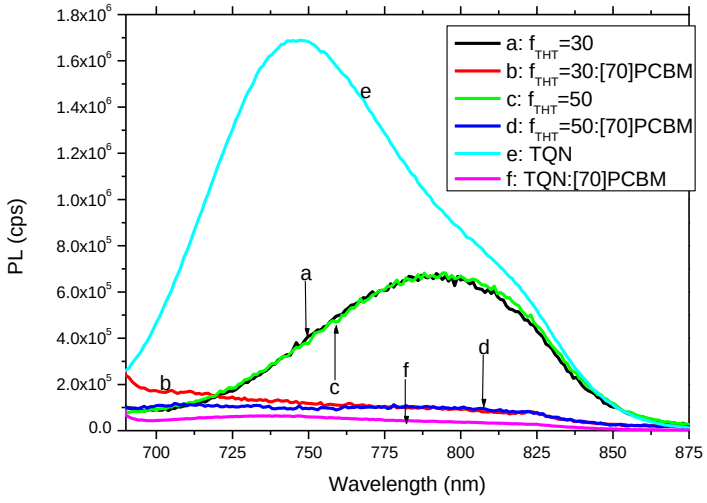

Figure 4.2.9. *Photoluminescence spectra of TQN, TQNTHTs, and their blends with [70]PCBM.*

As observed from the PL spectra of the blend films, the quenching efficiency of the PL spectra of the pyridopyrazine based copolymers is less compared to the corresponding quinoxaline based copolymers when blended with the same acceptor material. This is mostly due to the larger grain size of the polymer resulting in exciton radiative recombination before it reaches the donor-acceptor interface and this degrades the performance of the solar cell devices. This also complements the poor nanomorphology observed from the AFM height image.

Similar to quinoxaline based devices, stability measurement of devices fabricated from pyridopyrazine were also carried out to compare with photochemical stability of films of these polymers. Figure 4.2.10 shows the stability of the solar cell devices fabricated from pyridopyrazine based polymers. The stability of the devices was measured also by storing the devices in dark ambient condition and measuring their PCE starting from the date of fabrication at different time intervals. As one can observe from Figure 4.2.10, devices fabricated from the pyridopyrazine based polymers have more or less similar stability regardless of the fraction of THT and showed a little tendency of increase in stability as THT fraction increases. This little increase in stability with increase in THT fraction may be explained due to the steric hindrance of interaction of imine-nitrogen with acidic HC-PEDOT:PSS limiting the possibility of protonation and complex formation with metals. Compared to the corresponding conventional devices, the inverted solar cell devices are here also showed much better stability similar to devices fabricated from quinoxaline based copolymers.

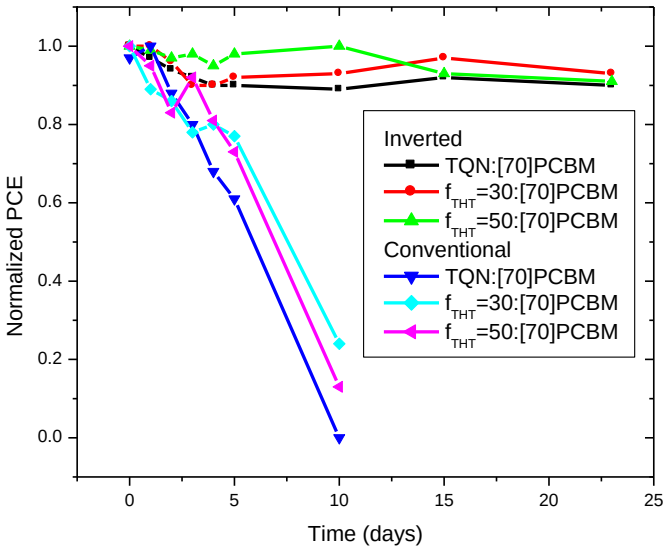

Figure 4.2.10. *Device stability of inverted (Glass/Al/TiOx/PFPA-1/active layer/HC-PEDOTPSS/Ag paste and conventional (ITO/PEDOT-PSS/active layer/Al) polymer solar cells fabricated from TQN and TQNTHTs.*

The inverted solar cell devices have retained more than 90% of their performance after 23 days storage in ambient atmosphere while the corresponding conventional solar cell devices lost 80% of their performance in 10 days under similar condition. This is also a further confirmation for conclusion made that fabrication of polymer solar cells in inverted geometry is a convenient architecture for large scale production and commercialization [82].

4.2.4 Conclusion

As expected, copolymerization of the pyridopyrazine monomer with thiophene-hexylthiophene monomer has resulted in copolymers with enhanced absorption in the valley of the absorption of TQN. As thiophene-hexylthiophene monomer has electron donating property, incorporation of the monomer in to the TQN polymer has up-shifted the HOMO and LUMO energy levels of the copolymers. Unlike the copolymers of TQ1, the incorporation of thiophene-hexylthiophene in to TQN copolymer has not affected the photochemical stability and the copolymers had similar stability compared to the pristine TQN polymer. Furthermore, the copolymers have shown better photovoltaic performance compared to that of TQN. Therefore, the pyridopyrazine based copolymers with incorporated thiophene-hexylthiophene are advantageous for photovoltaic applications compared to the pristine TQN while the photochemical stabilities of the copolymers are more or less the same with TQN.

4.3 Photochemical Stability and Photovoltaic Performance of Quinoxaline Based Copolymers with Low Thiophene-Hexylthiophene Composition

The effect of incorporation of large fraction of thiophene-hexylthiophene (30% and 50%) in to both quinoxaline and pyridopyrazine based copolymers have been studied in our previous work [206] under section 4.1 and 4.2. According to the findings incorporation of THT in to quinoxaline based copolymers affected negatively both their photochemical stability and photovoltaic performance. However, incorporation of the same fraction of THT as in that of quinoxaline based copolymers in to pyridopyrazine based copolymers increased their photovoltaic performance without affecting the photochemical stability. Therefore, the incorporation of large fraction of THT in to quinoxaline and pyridopyrazine based copolymers affected their photochemical stability and photovoltaic performance differently. However, the effects of incorporation of low fraction of thiophene-hexylthiophene in to quinoxaline based copolymers were not investigated. This investigation is required to see whether or not the loading of low mole fraction of THT in to the quinoxaline based polymer affect photochemical stability and photovoltaic performance in similar fashion with the high mole fraction of THT loaded in to the same polymer. This is because nature of chemical structure of polymer materials can affect their film nature that in turn affects the photochemical stability and photovoltaic performance of polymers. Therefore, here in this study the effect of incorporation of low fraction of THT (1% and 2.5%) in to quinoxaline based copolymers on their photochemical stability and photovoltaic performance were studied.

4.3.1 Photophysical and Electrochemical Properties

Quinoxaline based copolymers (TQTHTs) possessing THT fraction of 1% is named as $f_{THT} = 1$, and TQTHT with THT fraction of 2.5% is named as $f_{THT} = 2.5$. Figure 4.3.1 shows the UV-Vis absorption spectra of TQ1 and the copolymers with small fraction of THT fraction. As observed from the spectra (Figure 4.3.1a) all the polymers possess two distinct absorption peaks at low and high energy regions. For TQ1 it was reported that the peak at high energy region is due to the π-π* electronic transitions and the peak at low energy region is due to intramolecular charge transfer from the donor moiety (thiophene) to the acceptor moiety (quinoxaline) of the polymer along the backbone [203, 204], respectively. Similarly the two peaks observed from UV-Vis spectra of TQTHT copolymers (Figure 4.3.1a) with low fraction of THT at high and low energy regions are also due to π-π* electronic transitions and intramolecular charge transfer between the donor-acceptor moieties, respectively. When the UV-Vis absorption spectra of the TQTHT copolymers with low fraction of THT are compared to that of the TQ1, the valleys between the high and low energy regions are not covered as expected by incorporation of the THT fraction which was known to absorb in this region. This could be due to the low fraction of the THT in the copolymers that did not affect the absorption feature significantly. However in our previous work high fraction of THT (30% and 50%) in the quinoxaline and pyridopyrazine based copolymers showed absorption increment between the two absorption peaks.

Figure 4.3.1b shows also UV-Vis spectra of the copolymers blended with [70]PCBM. Blending the copolymers with [70]PCBM largely enhanced the absorption between the two peaks. This is due to absorption contribution from the [70]PCBM making the absorption spectra more plateau [175, 202] similar to the previous works.

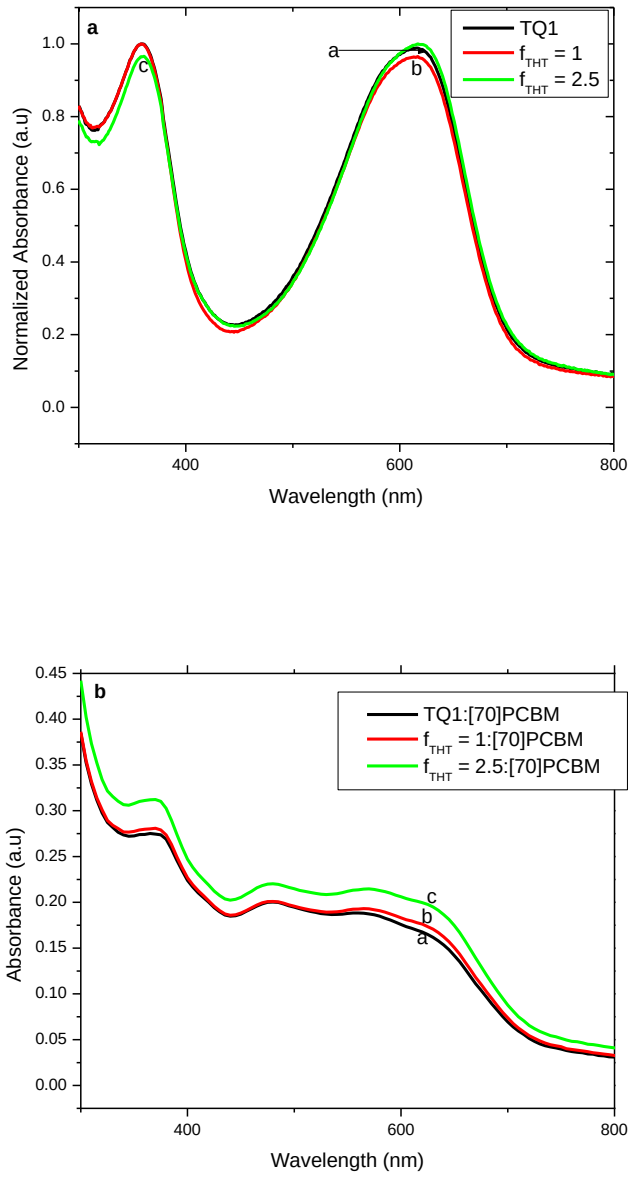

Figure 4.3.1. *UV-Vis spectra of: a) films of copolymers and b) films of copolymers blended with [70]PCBM.*

Table 4.3.1 shows the electrochemical values of the copolymers determined from square wave voltammetry (SWV) [206]. As observed from Table 4.3.1, the electrochemical values of the copolymers are not affected compared to TQ1. This is also due to the small fraction of the THT incorporated in to the copolymers that insignificantly affects the electronic structure. However, significant fraction of THT incorporated in to quinoxaline based copolymers was shown to largely affect the electrochemical values and in turn largely affected the photochemical stability and also photovoltaic performance of solar cell devices mainly the V_{OC} of the solar cells.

Table 4.3.1. *Electrochemical values of TQ1 and TQTHT copolymers.*

S.No	Polymer	THT (%)	E_{ox} (eV)	HOMO (eV)	E_{red} (eV)	LUMO (eV)
1	TQ	0	0.63	-5.76	-1.77	-3.36
2	$f_{THT} = 1$	1	0.63	-5.76	-1.77	-3.36
3	$f_{THT} = 2.5$	2.5	0.63	-5.76	-1.77	-3.36

4.3.2 Photochemical Stability

As described in the experimental section, photochemical stability of the copolymers was studied by comparing the UV-Vis bleaching of films. The films were aged under 1 sun solar simulator for different time interval while being annealed at 85^{o}C [181]. Figure 4.3.2 shows the bleaching UV-Vis absorption spectra of TQ1 and TQTHT with low fraction of THT copolymers aged under 1 sun solar simulator at different time intervals. From Figure 4.3.2 it can be observed that for prolonged ageing while

the films were being heated at 85°C, the absorption peak at low energy region get decreased and showed blue shift. This indicates that the conjugation length get decreased when the polymer is subjected to photo-induced oxidation, probably due to chain scission. The direction of the arrows show ageing time from 0 h to 92 h during bleaching experiment.

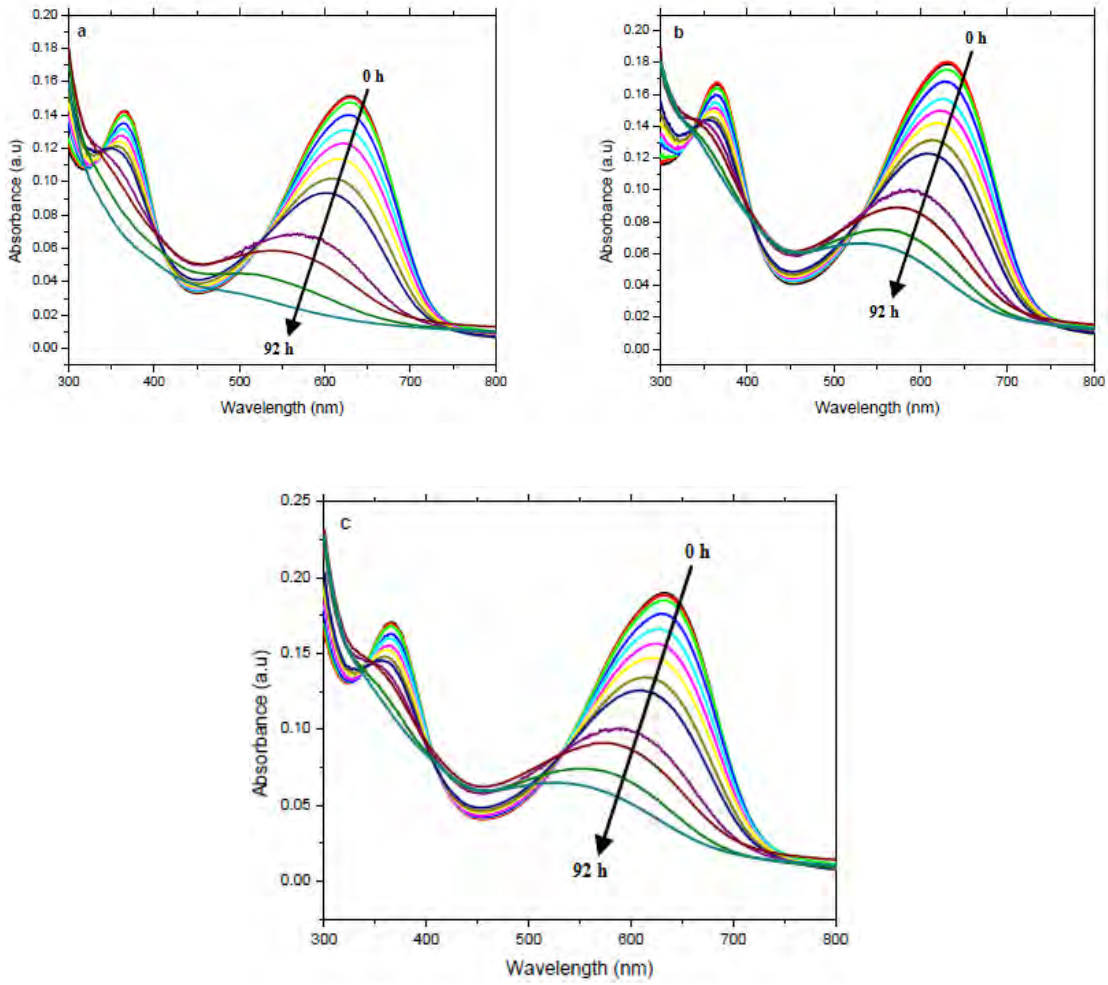

Figure 4.3.2. *UV-Vis spectra of: a) TQ1, b) f_{THT} = 1, and c) f_{THT} = 2.5 copolymers aged under 1 sun solar simulator for 0 h, 0.5 h, 3 h, 7 h, 12 h, 18 h, 26 h, 36 h, 44 h, 63 h, 72 h, 82, and 92 h.*

It can also be seen from Figure 4.3.2 that at low energy region TQ1 bleaches faster than the copolymers with low fraction of THT. Furthermore the low-energy absorption peak decreases faster than the high-energy peak i.e. the ratio between the peaks is changed for all polymers. Accordingly, the rate of decrease in absorbance during bleaching of peaks at low and high energy regions further confirms that it is TQ1 polymer that bleaches faster at low energy region compared to the other copolymers as it possesses steep slope than the others do.

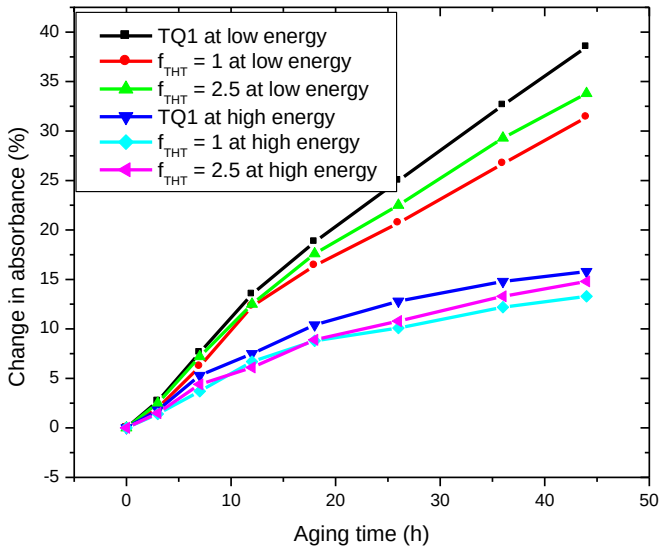

Figure 4.3.3. *Change in absorbance of TQ1 and TQTHTs with low fraction of THT at low and high energy regions of their corresponding bleaching UV-Vis spectra.*

As observed from the bleaching UV-Vis spectra of the copolymers, polymers with low fraction of THT shows descent decrease in the absorption peak at low energy region compared to the copolymer without THT fraction (TQ1). To monitor the

degradation and remaining peak absorbance of the copolymers at low energy region $A_{max,\ remaining}$ was used similar to the previous works.

Figure 4.3.4 shows the plot of $A_{max,\ remaining}$ of the copolymers with and without THT fraction aged under 1 sun solar simulator for different time intervals.

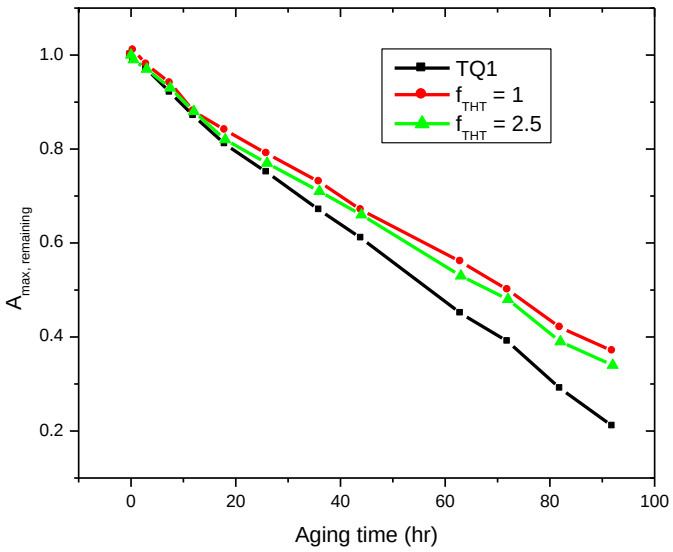

Figure 4.3.4. *Plot of $A_{max,\ remaining}$ of the copolymers (TQ1, f_{THT} = 1 and f_{THT} = 2.5) aged under 1 sun solar simulator for 0 h, 0.5 h, 3 h, 7 h, 12 h, 18 h, 26 h, 36 h, 44 h, 63 h, 72 h, 82, and 92 h.*

As it can be observed from Figure 4.3.4, the small fraction of THT has improved the photochemical stability of the copolymers compared to pristine TQ1. This improvement in photochemical stability of the copolymers with low fraction of THT could be due to increased in stiffness of the films of the copolymers. Compact and

dense films decrease rate of diffusion of oxygen and moisture in to the film and as a result decreases rate of degradation [222].

4.3.3 Photovoltaic Performance

To see the effect of the small fraction of THT on photovoltaic performance of the copolymers, solar cell devices were fabricated from blend solutions of the copolymers with [70]PCBM. Table 4.3.2 shows the summary of the photovoltaic parameters of the devices during optimization. As can be seen from Table 4.3.2 the optimum donor-acceptor ratio for all the copolymers is 1:2 which resulted in best performing devices.

Table 4.3.2. *Summary of photovoltaic parameters of TQ1 and TQTHTs with low fraction of THT based devices with different donor-acceptor ratios.*

Device	Ratio	J_{SC} (mA/cm^2)	V_{OC} (V)	FF	PCE (max)
TQ1:[70]PCBM	1:2	10.23	0.77	0.55	4.33
	1:3	10.12	0.74	0.52	3.89
f_{THT} = 1:[70]PCBM	1:1	8.43	0.84	0.42	2.99
	1:2	10.12	0.77	0.57	4.45
	2:5	9.11	0.80	0.56	4.08
	1:3	9.41	0.79	0.56	4.14
	1:4	9.64	0.74	0.52	3.69
f_{THT} = 2.5:[70]PCBM	1:1	8.47	0.83	0.39	2.72
	1:2	10.80	0.75	0.57	4.64
	2:5	10.05	0.75	0.57	4.34
	1:3	9.99	0.75	0.60	4.50
	1:4	9.73	0.72	0.55	3.86

Figure 4.3.5 shows the *J-V* curves and Table 4.3.3 is the summary of the photovoltaic parameters of the best performing devices of TQ1 and TQTHTs based solar cells with low fraction of THT. As it can be observed from Table 4.3.3 and the curves, the small fraction of THT incorporated in to the copolymers has decently affected the photovoltaic performance of the devices. Devices fabricated from the copolymer with 2.5% THT have shown better performance compared to the others. The enhancement has mainly arisen from the improved current density and fill factor compared to devices fabricated from TQ1. The improved current density could be due to the enhancement of UV-Vis absorption spectra of the blend shown in Figure 4.3.1.

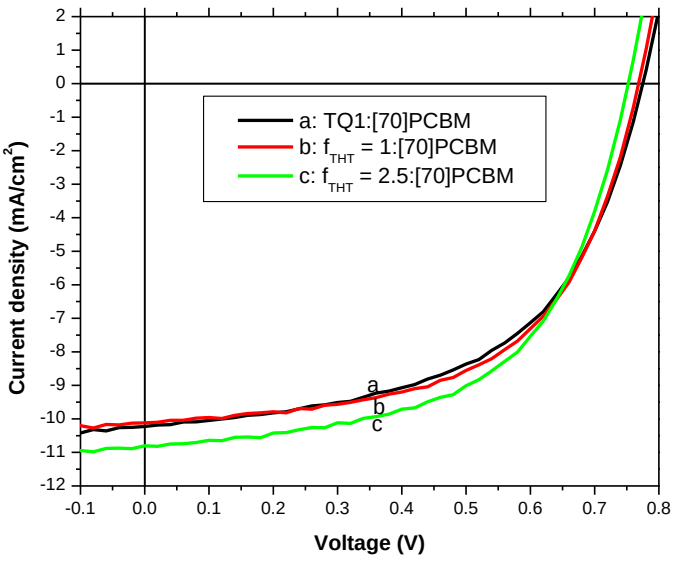

Figure 4.3.5. *J-V curves of best performing solar cell devices fabricated from blend solutions of copolymers of TQ1 and TQTHTs with low fraction of THT.*

However, devices fabricated from copolymer with 2.5% THT showed descent decrease in V_{OC} compared to devices fabricated from other copolymers. Compared to the TQ1 based solar cell devices, devices fabricated from the copolymers containing 1% and 2.5% THT showed better fill factor which has also contributed to their better performance. This could also be due to the better interpenetrating network formation of the blends between the two electrodes that largely facilitates charge carriers transportation. Moreover, the copolymer with THT fraction of 2.5% has resulted in better current density which contributed to the better photovoltaic performance for the device fabricated from the copolymer. The enhanced current density may also be due to the better degree of ordering of the film. Generally, incorporation of small fraction of THT in to TQ1 copolymer showed descent improvement of the performance of devices fabricated from the copolymers compared to the pristine TQ1 based devices.

Table 4.3.3. *Summary of photovoltaic parameters of best performing solar cell devices fabricated from blend solutions of TQ1 and TQTHTs with low fraction of THT.*

Device	Ratio	J_{SC} (mA/cm^2)	V_{OC} (V)	FF	PCE (max)
TQ1:[70]PCBM	1:2	10.23	0.77	0.55	4.33
$f_{THT = 1}$:[70]PCBM	1:2	10.12	0.77	0.57	4.45
$f_{THT = 2.5}$:[70]PCBM	1:2	10.80	0.75	0.57	4.64

The spectral responses of devices fabricated from the copolymers were also investigated by the external quantum efficiency (EQE) measurement. As can be seen from Figure 4.3.6 the spectral response of the devices at each and every wavelength was measured. Figure 4.3.6 clearly shows that all the devices show good spectral response over the whole wavelength range of the measurement of their corresponding UV-Vis spectra. The spectral response also agrees with the corresponding current densities of the best performing devices shown in Table 4.3.3 i.e. the spectral coverage of the device fabricated from the copolymer with THT fraction of 2.5% is higher compared to the spectral coverage of the devices fabricated from the other copolymers.

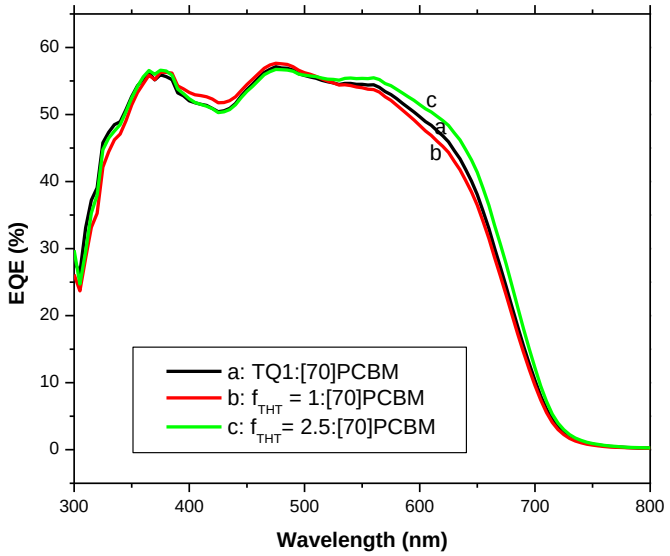

Figure 4.3.6. *EQE spectra of best performing devices fabricated from blend solutions of copolymers of TQ1 and TQTHTs with low fraction of THT.*

To see the effect of the incorporation of low fraction of THT in to TQ1 copolymer on morphology of the blend, height images of the blends were recorded using atomic force microscopy (AFM). Figure 4.3.7 shows the AFM images of blends of TQ1 and TQTHTs with small fraction of THT.

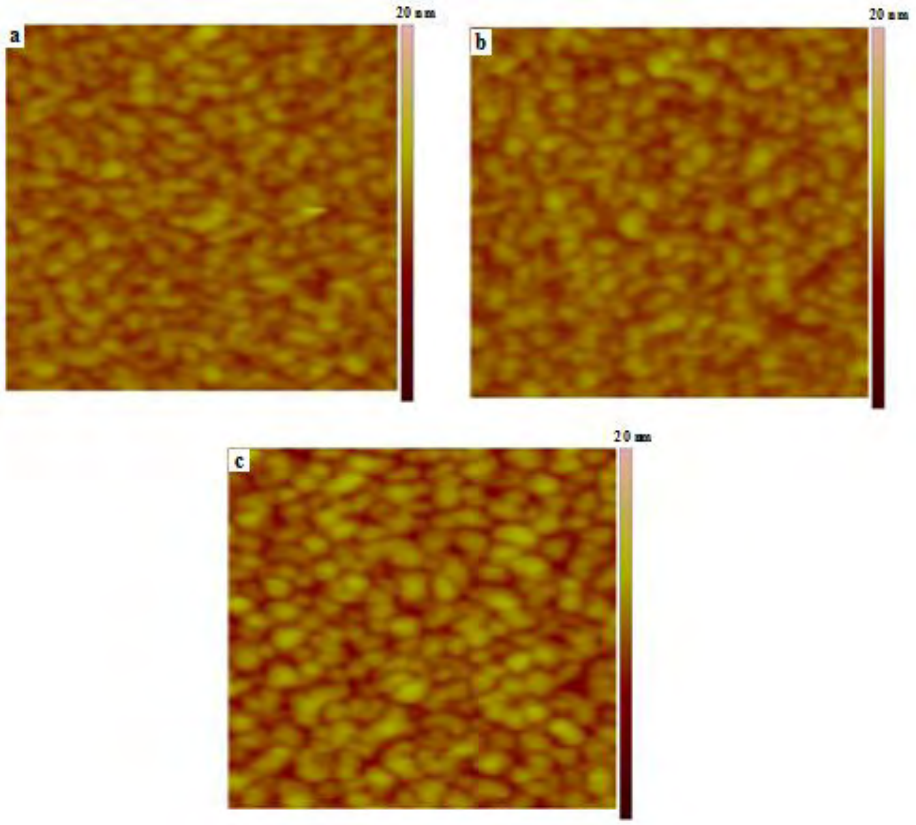

Figure 4.3.7. *AFM images (1µm x 1µm) of copolymers of: a) TQ1, b)* f_{THT} *= 1, and c)* f_{THT} *= 2.5 blended with [70]PCBM. The RMS values are 0.845 nm, 0.881 nm, and 1.26 nm respectively.*

As observed from Figure 4.3.7 the roughnesses of the blends get increased with increase in THT fraction. This may be due to the increase in crystallization due to

packing of the blend films up on increase in THT fraction. However, generally as observed from low RMS values of the blends, all the blends are very smooth indicating the copolymers are highly soluble in organic solvent and miscible with the acceptor material. However, the better degree of packing in copolymers with THT might have contributed to the better photochemical stability of the copolymers as packing decreases the rate of diffusion of moisture and oxygen in to the film [222].

To complement the AFM data of blends of TQ1 and TQTHTs with [70]PCBM, photoluminescence experiment was carried out. Figure 4.3.8 shows photoluminescence spectra of the blends.

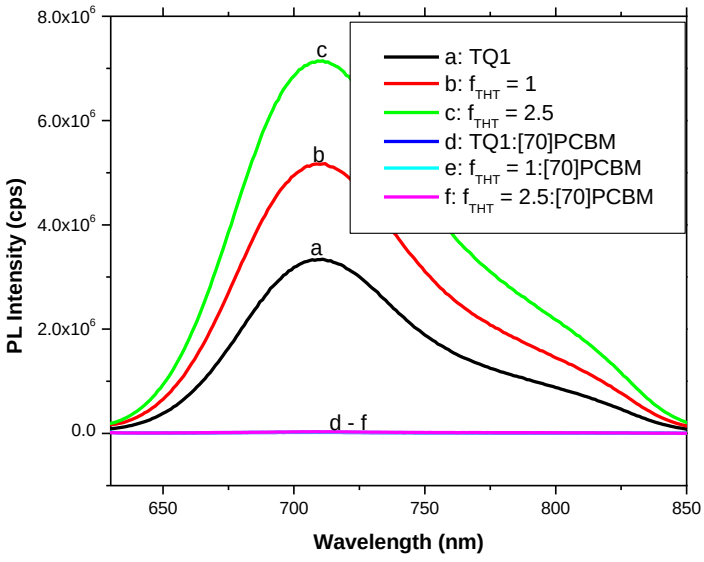

Figure 4.3.8. *Photoluminescence spectra of blends of TQ1 and TQTHTs with low fraction of THT with [70]PCBM.*

As observed from Figure 4.3.8 when all the copolymers are mixed with [70]PCBM, the photoluminescence of the copolymers were highly quenched. This further confirms that the copolymers are highly miscible with the acceptor material creating optimum nanomorphology for the excitons generated to diffuse to the donor-acceptor interface before decaying.

Figure 4.3.9 shows the device stability test of solar cells fabricated from copolymers with low fraction of THT for which the devices were stored in ambient dark environment before *J-V* test.

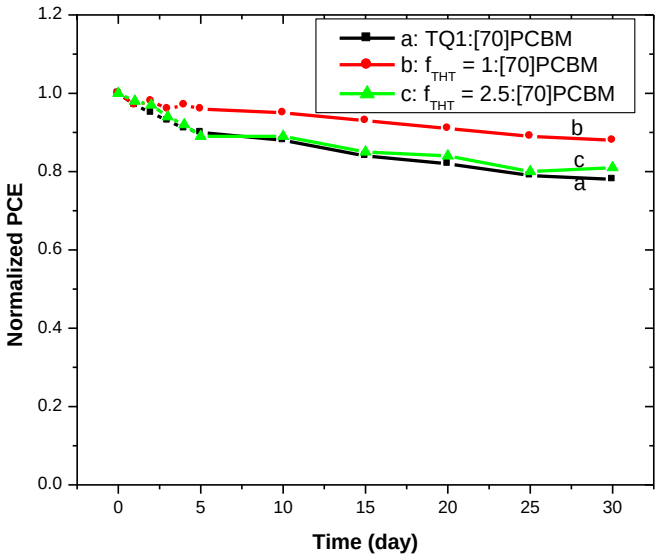

Figure 4.3.9: *Device stability of solar cells fabricated from low fraction of THT.*

As it can be seen from Figure 4.3.9 the device stability is more or less in agreement with the photochemical stability of the copolymers. The devices fabricated from

copolymers with THT have shown better stability compared to that of pristine TQ1. In addition, the solar cell fabricated from copolymer with THT fraction of 1% has shown better device stability compared to solar cell devices fabricated from the other copolymers.

4.3.4 Conclusion

The effect of incorporation of small fraction of THT in to quinoxaline based polymer on photochemical stability of the copolymers and photovoltaic performance of the solar cells were studied. Unlike the incorporation of large fraction of THT in to quinoxaline based polymer, the incorporation of the low fraction of THT in to quinoxaline based polymer has not affected the UV-Vis and the HOMO and LUMO energy levels of the copolymers. The incorporation of this low fraction of THT in to the quinoxaline based polymer however increased the photochemical stability and photovoltaic performance of solar cells fabricated from the copolymers compared to pristine TQ1 polymer. The increased photochemical stability of the copolymers with low fraction of THT could be due to formation of stiff films that decreases diffusion of oxygen and moisture in to the films.

4.4 Effect of Low Boiling Point Solvent Additives on Photovoltaic Performance of Bulk Heterojunction Polymer Solar Cells

Despite the two general rules of solvent additives [195, 199], there are limited reports on low boiling point solvent additives application for controlling of nanomorphology in organic solar cells. Among these, Chu et al. [225] reported the use of two dipolar solvents-dimethyl sulfoxide (DMSO, bp = 189^{o}C) and dimethyl formamide (DMF, bp = 153^{o}C) as processing additives in ortho-dichlorobenzene (*o*-DCB, bp = 186^{o}C). They improved the device performance of PCDTBT:$PC_{71}BM$ based solar cells from 6.0% to 7.1% and to 6.7% with an active area of 1.0 cm^2 using DMSO and DMF, respectively. According to their findings, the use of these additives had significant impact on the aggregation and packing of the PCDTBT molecules and thus affects the nanoscale morphology of the resulting BHJ films. This led to a fibrous nanoscale morphology which gives efficient exciton dissociation, improved hole mobility resulting in enhanced PCE. Similarly, Mahadevapuram et al. [226] also showed that a low-boiling point solvent additive tetrahydrofuran (THF, bp = 66^{o}C) in a high-boiling point parent solvent *o*-DCB was used to control nanomorphology in P3HT:PCBM cells. The use of this additive led to efficient charge extraction and fill factors (FF) as high as 69.5%. This is among the highest FF recorded (~ 68%) for the P3HT:PCBM system [191]. The overall efficiencies however were comparable for both, devices with THF additive (*o*-DCB-THF devices) and *o*-DCB-only devices, due to slight reduction in short circuit current density (J_{SC}) for *o*-DCB-THF device. Hence, the possibility of applications of the low boiling point solvent additives for controlling nanoscale morphology mentioned here above in polymer solar cells have also

motivated us to look for other low boiling point solvent additives in organic electronics applications. Here we studied the effect of low boiling point solvent additives iodomethane (IMe, bp = 42^{o}C), iodoethane (IEt, bp = 72^{o}C), and diiodomethane (DIMe, bp = 181^{o}C) in high boiling point host solvent *o*-DCB (bp = 186^{o}C) on poly[2,3-bis-(3-octyloxyphenyl)quinoxaline-5,8-diyl-alt-thiophene-2,5-diyl](TQ1):[6,6]-phenyl-C_{61}-butyric acid methyl ester ($PC_{61}BM$) and poly[N-9″-hepta-decanyl-2,7-carbazole-alt-5,5-(4′,7′-dithienyl-2′,1′,3′ benzothiadiazole)](PCDTBT):[6,6]-phenyl-C_{71}-butyric acid methyl ester ($PC_{71}BM$) based bulk heterojunction solar cells.

4.4.1 Photophysical Properties

Figure 4.4.1a shows the UV-Vis spectra of films of pristine TQ1:[60]PCBM and same blend containing 3% (v/v) solvent additives. As previously reported, the absorption spectrum of TQ1 film shows two distinct peaks one at high energy and the other at low energy regions [203]. The peak at high energy region is due to π-π* electronic transition of the polymer. The peak at low energy region is due to intramolecular charge transfer between the donor moeity (thiophene) and the acceptor moeity (quinoxaline) of the polymer [203]. Similarly, PCDTBT has also showed two distinct absorption peaks at high and low energy regions due to π-π* and charge transfer electronic transitions, respectively [227]. When the polymers are blended with PCBMs, the valley between the high and low energy peaks of the films is covered due to the absorption contribution from the PCBMs resulting in more plateau spectra. As the absorption contribution of [70]PCBM in visible region is more than

that of [60]PCBM [202, 228], the absorption valley between the high and low energy regions of PCDTBT is highly covered.

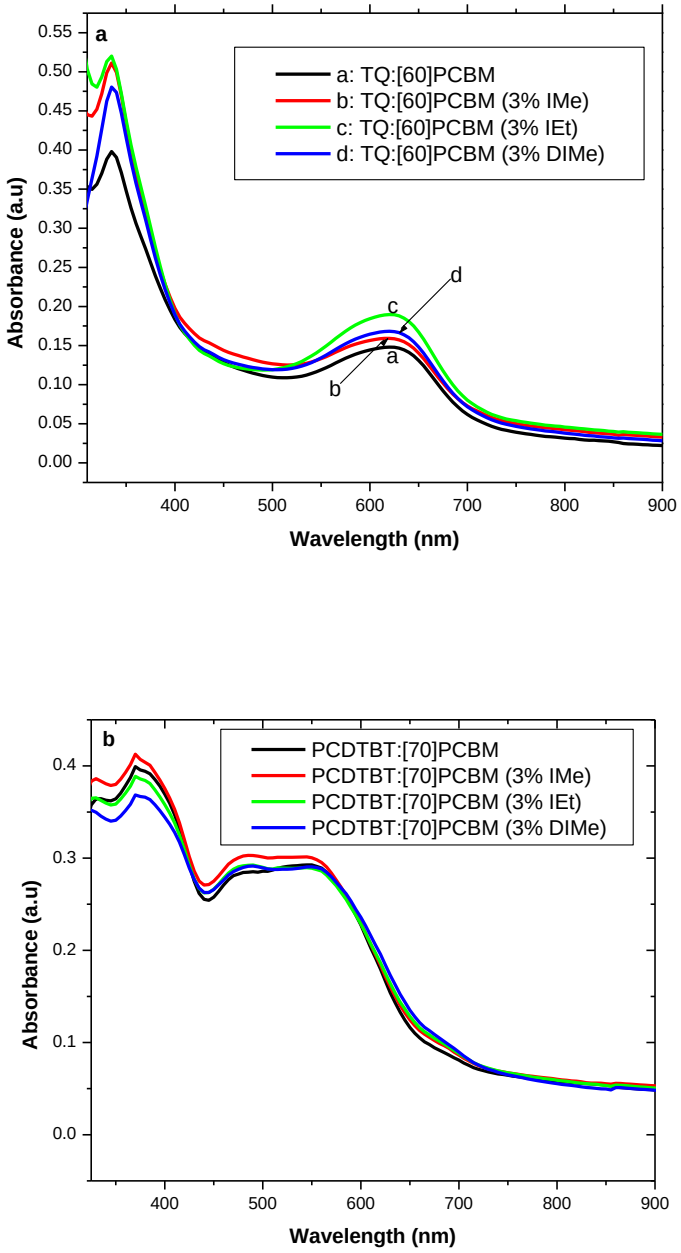

Figure 4.4.1. *UV-Vis absorption spectra of: a) TQ1:[60]PCBM and b) PCDTBT:[70]PCBM blend films containing 3% low boiling point solvent additives IMe, IEt, and DIMe.*

Moreover, blending of the polymers with PCBMs largely enhanced the high energy region peak of the polymers as the absorption maxima of PCBMs are in this region [202, 228]. Furthermore, the absorption band of films processed from TQ1:[60]PCBM blend solution containing 3% (v/v) solvent additives have shown significant increment in absorption intensity at low energy region compared to the pristine blend (Figure 4.4.1a). The absorption maxima of films processed from TQ1:[60]PCBM however did not show peak shift compared to the pristine TQ1:[60]PCBM which is at 620 nm. This fixed absorption maxima indicates that the thin films prepared using additives have amorphous phase [229]. Even though the exact mechanism of increment in absorption band up on addition of the solvent additives is not well known, it might be due to morphology change of the active layer [230, 231]. Hence, the increment in absorption of the blend films up on addition of these low boiling point solvent additives are expected to have contribution for improvement of current density compared to that of the pristine blend based solar cell devices. However, for PCDTBT:[70]PCBM blend films, significant increment of the absorption bands at low energy region up on addition of the low boiling point solvent additives was not observed (Figure 4.4.1b). This could be due to difference in interaction mechanism of the additives with the two blends.

Figure 4.4.2 shows the UV-Vis spectra of films of TQ1:[60]PCBM blend solutions containing the solvent additives with different composition in the optimization range.

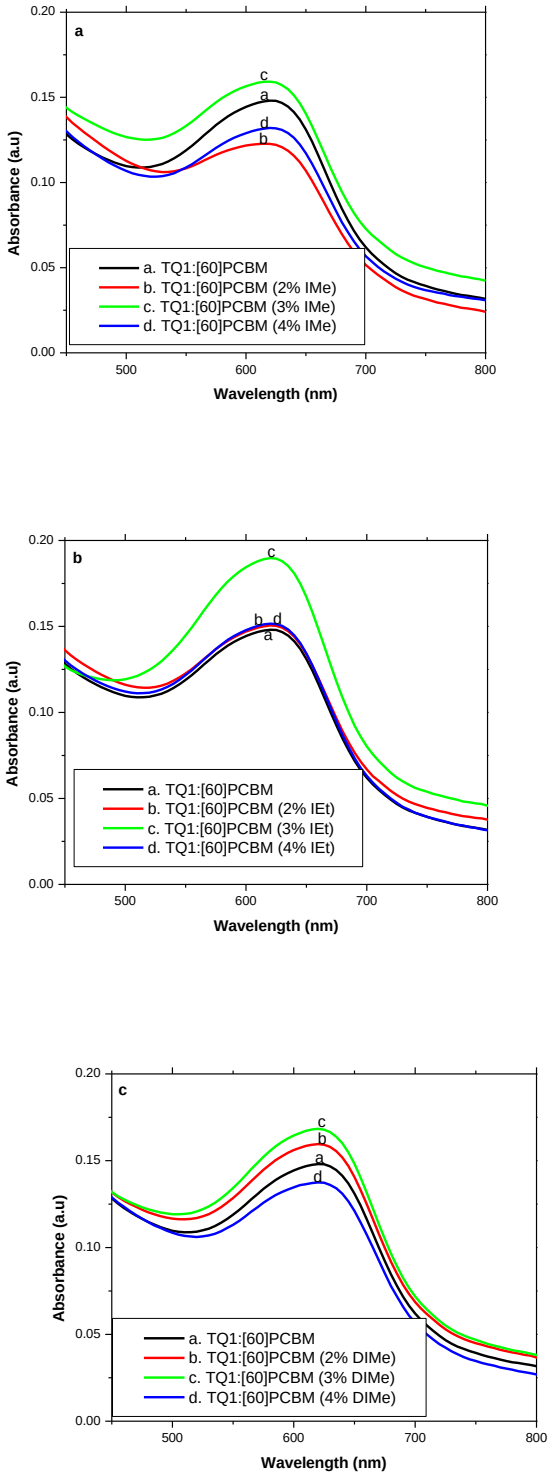

Figure 4.4.2. *UV-Vis absorption spectra of films of TQ1:[60]PCBM blend solution containing different composition of solvent additives: a) IMe, b) IEt, and c) DIMe.*

Additive composition optimization for photovoltaic performance of TQ1:[60]PCBM blend were carried out from 2% to 3% and to 4% for which the 3% solvent additive composition became optimum as it resulted in enhanced PCEs for all the additives (Figure 4.4.3 and Table 4.4.1). As 3% (v/v) low boiling point solvent additives have shown significant absorption band increment at low energy region, we were also interested to investigate the effect of the composition of the solvent additives on photophysical properties of TQ1:[60]PCBM blend solution in the optimization range. As it can be observed from Figure 4.4.2, the absorption increment is maximum for the optimum composition i.e. 3% (v/v) for all the solvent additives and the absorption band strength was weakened for 2% and 4% composition for same blend concentration and spin speed even though film thicknesses of blends with 2% solvent additives (IEt and DIMe) are greater than blends with 3% solvent additives (Table 4.4.1). Therefore, this difference in absorption intensity with different composition of additives could be due to morphology change of the active layer and the 3% additives might have resulted in more orderly arrangement of the blend films [230, 231].

4.4.2 Photovoltaic Properties

To look in to the effect of the low boiling point solvent additives on photovoltaic performance of TQ1:[60]PCBM blend, percent composition by volume optimization were carried out for each solvent additive. The *J-V* curves and the corresponding photovoltaic parameters of devices fabricated from different additive composition during optimization of each additive used are shown in Figure 4.4.3 and Table 4.4.1. During the optimization, solar cells based on TQ1:[60]PCBM blend solution were fabricated from *o*-DCB containing 2%, 3%, and 4% (v/v) of each solvent additive.

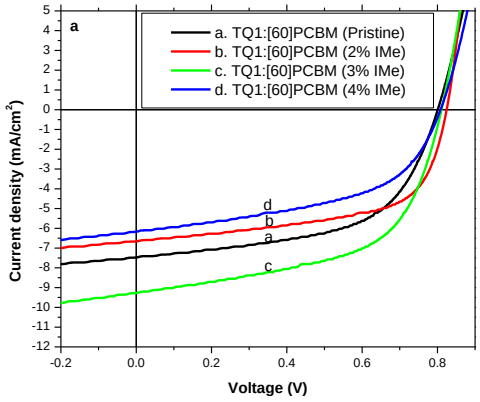

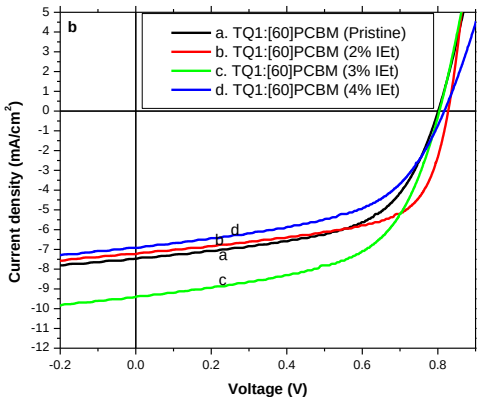

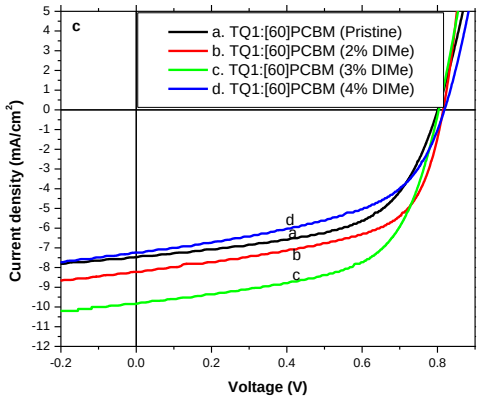

Figure 4.4.3. *J-V curves of solar cell devices fabricated from TQ1:[60]PCBM blend solution with different composition of additives: a) IMe, b) IEt, and c) DIMe.*

Values in parentheses of Table 4.4.1 are average values of four devices. As it can be seen from Figure 4.4.3 and Table 4.4.1 when the composition of the solvent additives became 2% significant increase in fill factors for all fabricated devices were observed with descent decrease of short circuit current for IMe and IEt [226].

Table 4.4.1. *Summary of Photovoltaic parameters of solar cell devices fabricated from TQ1:[60]PCBM blend solution with different composition of additives IMe, IEt, and DIMe.*

Device	J_{SC} (mA/cm^2)	V_{OC} (V)	FF	PCE (%)	Additive used	Thickness (nm)
TQ1:$PC_{61}BM$	7.48(7.60)	0.80(0.79)	0.57(0.55)	3.41(3.30)	No	80
	6.66(6.58)	0.82(0.82)	0.60(0.59)	3.29(3.18)	2% IMe	-
	9.27(8.99)	0.81(0.82)	0.57(0.58)	4.28(4.25)	3% IMe	-
	6.17(5.78)	0.81(0.81)	0.51(0.51)	2.54(2.39)	4% IMe	-
	7.23(7.13)	0.83(0.82)	0.61(0.61)	3.65(3.59)	2% IEt	84
	9.40(9.33)	0.80(0.80)	0.57(0.58)	4.41(4.35)	3% IEt	85
	6.92(6.67)	0.82(0.83)	0.53(0.53)	3.00(2.90)	4% IEt	75
	8.22(7.54)	0.82(0.82)	0.58(0.59)	3.88(3.62)	2% DIMe	85
	9.84(9.49)	0.80(0.80)	0.59(0.60)	4.66(4.55)	3% DIMe	80
	7.24(6.86)	0.82(0.80)	0.52(0.53)	3.08(2.90)	4% DIMe	75

However, devices fabricated from DIMe containing blend solution showed little increase in short circuit current. The increase in fill factor for devices fabricated from

the blend solution containing 2% of the low boiling point solvent additives has shown the potential of the additives for the application of controlling nanoscale morphology in BHJ solar cells as in literature [225, 226]. Further increase in composition of the additives to 3% has largely improved the short circuit current density and average fill factor of all the devices resulting in enhanced PCEs. However, when the composition of the additives is increased further to 4%, short circuit current densities and fill factors of all devices for all additives are largely degraded. The decrease in absorption band intensities for 2% and 4% composition of the additives (Figure 4.4.2) could have contributed for the decrease in short circuit current density of the corresponding solar cell devices. However, in all additive composition, the V_{OC} of the solar cells are more or less the same. Accordingly, the optimum percent composition by volume of all additives resulted in best performing solar cell devices was found to be 3%.

Figure 4.4.4 and Table 4.4.2 show *J-V* curves and the summary of photovoltaic parameters of the best performing solar cell devices fabricated from blends containing 3% (v/v) of each low boiling point solvent additive. Therefore, optimization of the composition of the solvent additives IMe, IEt, and DIMe have resulted in enhancement of PCE of TQ1:[60]PCBM based solar cell devices from 3.41% to 4.28%, to 4.41%, and 4.66%, respectively. This showed the potential of these low boiling point solvent additives in controlling nanomorphology of BHJ solar cells resulting in large interface area between the donor and acceptor materials for efficient exciton dissociation as confirmed from morphology study of the blend films (Figure 4.4.5).

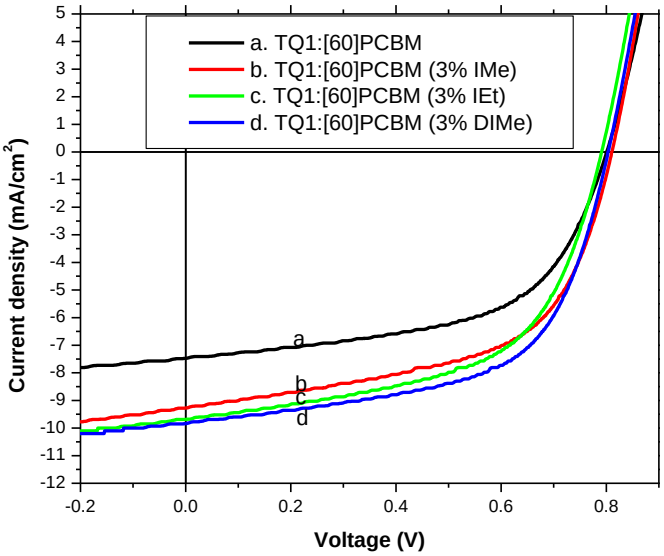

Figure 4.4.4. *J-V curves of solar cell devices fabricated from TQ1:[60]PCBM based blend solution containing 3% low boiling point solvent additives.*

Table 4.4.2. *Summary of the photovoltaic parameters of devices fabricated from pristine and 3% solvent additives containing TQ1:[60]PCBM blend solutions.*

S.No	TQ1:[60]PCBM	J_{SC} (mA/cm^2)	V_{OC} (V)	FF	PCE (%)
1	Pristine	7.48(7.60)	0.80(0.79)	0.57(0.55)	3.41(3.30)
2	3% IMe	9.27(8.99)	0.81(0.82)	0.57(0.58)	4.28(4.25)
3	3% IEt	9.40(9.33)	0.80(0.80)	0.57(0.58)	4.41(4.35)
4	3% DIMe	9.84(9.49)	0.80(0.80)	0.59(0.60)	4.66(4.55)

The AFM height image of films processed from blend solutions containing 2%, 3%, and 4% IEt and 2%, 3%, 4%, and 10% DIMe were recorded in taping mode. As observed from Figure 4.4.5 addition of 2% solvent additives enhanced formation of networked nanomorphology structures compared to the pristine blend.

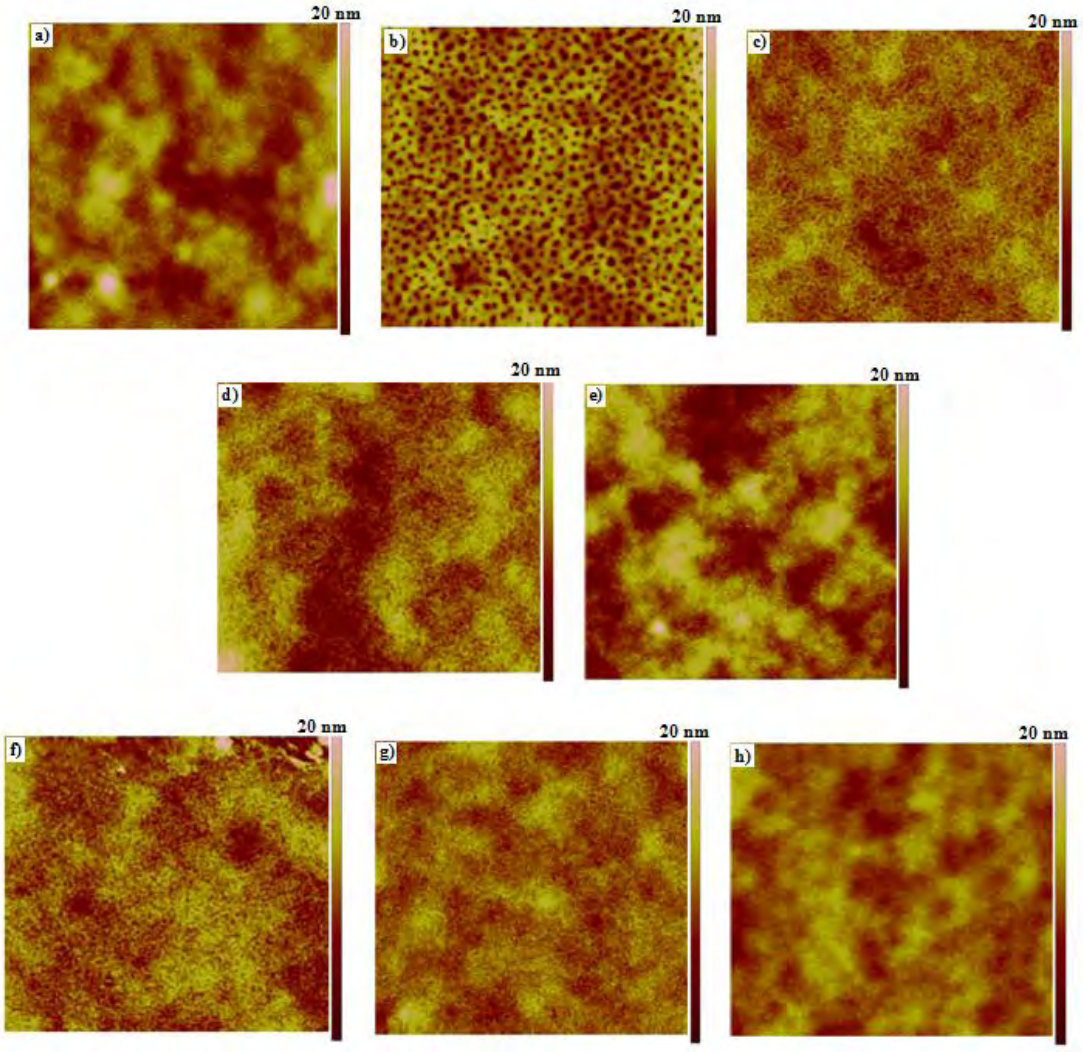

Figure 4.4.5. *AFM height images (5µm x 5µm) of: (a) pristine TQ1:[60]PCBM (RMS = 2.46 nm) and (b - h) processed from 2% DIM (RMS = 2.63 nm), 3% DIM (RMS = 1.62 nm), 4% DIM (RMS = 2.36 nm), 10% DIM (RMS = 2.82 nm), 2% IEt (RMS = 2.18 nm), 3% IEt (RMS = 1.54 nm), and 4% IEt (RMS = 1.58 nm), respectively.*

For blend film processed from both DIMe and IEt with 3% (v/v) more fine and interpenetrated networks are observed which largely contributed for the improvement of J_{SC} and FF by creating large interface area between D-A components and extending the network between the electrodes for better charge carriers' transport and enhanced PCEs of the solar cells. However, when the composition of additives increases to 4% (for both IEt and DIMe) and 10% (for DIMe) large grains and bloating are observed indicating formation of bad morphology of the blends hampering the performance of the solar cells [232]. This shows the potential of the low boiling point solvent additives to control the nanomorphology of active layer in polymer solar cells. The AFM images were also complemented with PL spectra measurement of the TQ1:[60]PCBM based blends with and without solvent additives to investigate further the formation of nanoscale morphology (Figure 4.4.6).

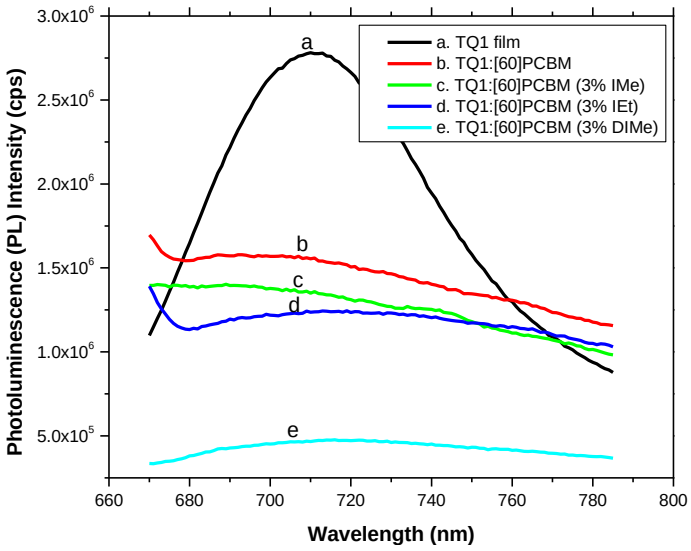

Figure 4.4.6. *Photoluminescence spectra of TQ1 polymer film, pristine TQ1:[60]PCBM, and TQ1:[60]PCBM blend films containing 3% IMe, IEt, and DIMe.*

As observed from Figure 4.4.6, PL intensity of TQ1 was decreased up on addition of the solvent additives. This increased quenching efficiency of PL of the polymer up on addition of the solvent additives is due to formation of better nanoscale morphology and creation of large interface area between donors and acceptors. The large interface area between donors and acceptors is an advantage for generation of excitons at close vicinity to the donor-acceptor interface and their diffusion to the interface to dissociate efficiently before decaying [191]. Therefore, the increase in PL quenching efficiencies of the polymers processed from blend solutions containing solvent additives are indicative of formation of better nanoscale morphology in BHJ solar cells leading to improved PCEs of the solar cells.

To see the response of TQ1:[60]PCBM based solar cell devices at each and every absorption wavelengths, IPCE measurements were made (Figure 4.4.7).

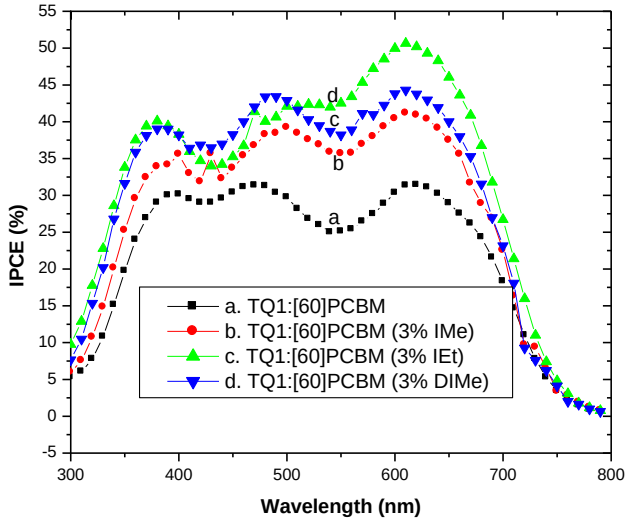

Figure 4.4.7. *IPCE spectra of solar cell devices fabricated from pristine and blend solutions of TQ1:[60]PCBM containing 3% solvent additives IMe, IEt, and DIMe.*

It can be seen from Figure 4.4.7 that the solar cell devices fabricated from TQ1:[60]PCBM based blend solutions have shown good spectral response over the wide range of absorption wavelengths. Moreover, the action spectra are very similar to their corresponding UV-Vis spectra indicating the devices are responsive over all absorption wavelengths. Furthermore, the action spectra also indicate that the responses of the devices are more pronounced with addition of solvent additives that agrees with increase in short circuit current density of the devices fabricated from the blend solutions containing the low boiling point solvent additives.

To see the applicability of the solvent additives on wide range of materials, solar cell devices based on PCDTBT:[70]PCBM blend solution were also fabricated. Optimizations of the low boiling point solvent additives were not carried out for this blend solution. However, the optimum additive composition used for TQ1:[60]PCBM based BHJ solar cells was applied. Figure 4.4.8 shows the *J-V* curves of solar cells fabricated from PCDTBT:[70]PCBM based blend solution containing 3% (v/v) solvent additives and the corresponding photovoltaic parameters are summarized in Table 4.4.3. As it can also be observed from Table 4.4.3, addition of 3% additive to the blend has also improved short circuit current density and fill factor of the devices compared to that of pristine device fabricated from PCDTBT:[70]PCBM blend solution. This is similar to that of TQ1:[60]PCBM based devices. However, devices fabricated from PCDTBT:[70]PCBM blend solution containing 3% IMe additive has shown 60 - 70 mV decrease in V_{OC} while the other additives do not affect the V_{OC} of the solar cell devices. The enhancement in PCE of the PCDTBT:[70]PCBM based

solar cell devices further confirm that the additives can be applied on the wide range of materials.

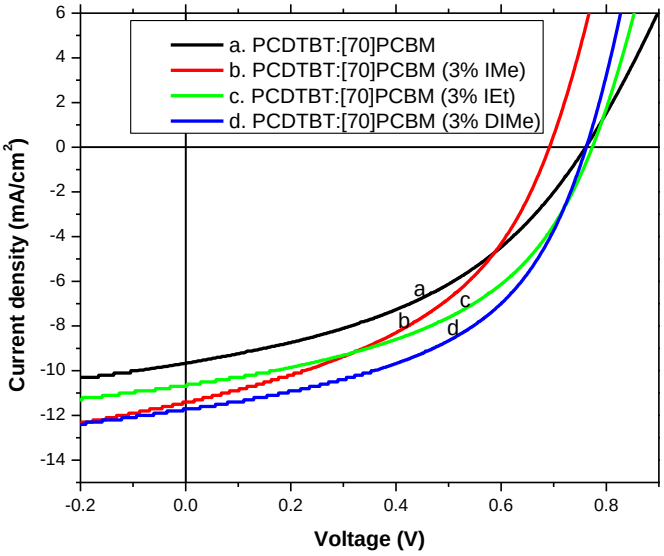

Figure 4.4.8. *J-V curves of solar cells fabricated from PCDTBT:[70]PCBM based blend solutions containing 3% low boiling point solvent additives.*

Table 4.4.3. *Photovoltaic parameters of solar cells fabricated from PCDTBT:[70]PCBM based blend solutions containing 3% low boiling point solvent additives.*

S.No	PCDTBT:[70]PCBM	J_{SC} (mA/cm^2)	V_{OC} (V)	FF	PCE (%)
1	Pristine	9.66(9.92)	0.76(0.74)	0.42(0.40)	3.08(2.97)
2	3% IMe	11.4(11.00)	0.69(0.68)	0.43(0.43)	3.39(3.21)
3	3% IEt	10.7(10.9)	0.77(0.76)	0.46(0.45)	3.80(3.71)
4	3% DIMe	11.7(11.6)	0.76(0.75)	0.49(0.48)	4.37(4.22)

In general, the study showed that the low boiling point solvent additives IMe, IEt, and DIMe could be applied for wide range of materials for controlling nanomorphology of active layer in BHJ solar cells.

Figure 4.4.9 also shows the action spectra of PCDTBT:[70]PCBM based devices. To see the spectral response of the devices fabricated from PCDTBT:[70]PCBM based solar cell devices, the incident-photon-to-current-conversion efficiency (IPCE) measurements were carried out.

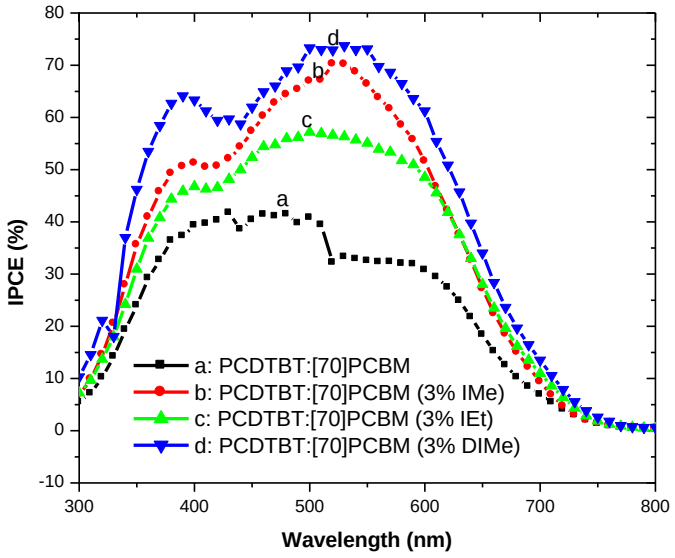

Figure 4.4.9. *IPCE spectra of solar cell devices fabricated from pristine and blend solutions of PCDTBT:[70]PCBM containing 3% solvent additives IMe, IEt, and DIMe.*

As observed from the Figure 4.4.9, the solar cell devices fabricated from PCDTBT:[70]PCBM blend solutions have also shown good spectral response over the wide range of absorption wavelengths. Furthermore, the action spectra, similar to

the action spectra of TQ1:[60]PCBM based devices, also indicate that the responses of the devices are enhanced with addition of solvent additives that agrees with increase in short circuit current density of the devices fabricated from the blend solutions containing the low boiling point solvent additives. To see the effect of the solvent additives on nanoscale morphology formation of PCDTBT:[70]PCBM blend, PL spectra measurement was also carried out (Figure 4.4.10).

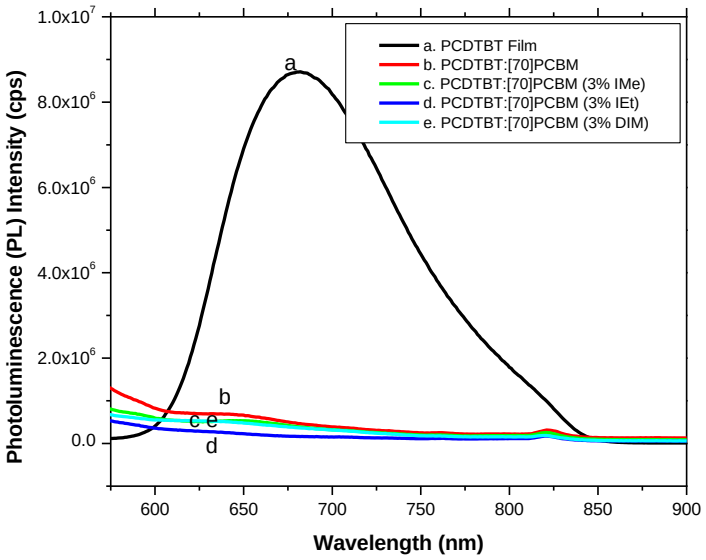

Figure 4.4.10. *Photoluminescence spectra of PCDTBT polymer film, pristine PCDTBT:[70]PCBM blend films, and PCDTBT:[70]PCBM blend films containing 3% IMe, IEt, and DIMe.*

Similar to the TQ1:[60]PCBM based films, PL intensities of PCDTBT was decreased up on addition of the solvent additives. This increased quenching efficiency of PL of the polymers up on addition of the solvent additives is also due to formation of better

nanoscale morphology and creation of large interface area between donors and acceptors fastening charge transfer before decaying radiatively or non-radiatively [191].

To see how the additives affected the performance of BHJ solar cells for TQ1:[60]PCBM and PCDTBT:[70]PCBM blend solutions, we carried out solubility test of pristine blend films in IEt and DIMe additives [195]. Figure 4.4.11 shows UV-Vis spectra of pristine blends and blends soaked for 5 seconds in solvent additives [195]. As can be seen from the UV-Vis spectra of the blends (Figure 4.4.11a and 4.4.11b), the absorption region at lower wavelengths were decreased and the valleys at these wavelengths get deeper after the pristine films were soaked in the additives. As PCBMs absorb at lower wavelengths [202, 228], the decrease in absorption band intensity at lower wavelengths indicates that the PCBMs were washed out up on soaking in the additives and as a result their absorption feature were disappeared. This further confirms that the additives selectively dissolve the PCBMs verifying the selective solubility rule of the general additive design [195, 199]. The UV-Vis spectral feature obtained after soaking the films in the solvent additives have almost the same structure as that of the UV-Vis spectra of their corresponding polymer films used as references. This similarity in spectral feature of the soaked films with films of the polymers indicates that the later films are less or not soluble in the solvent additives used.

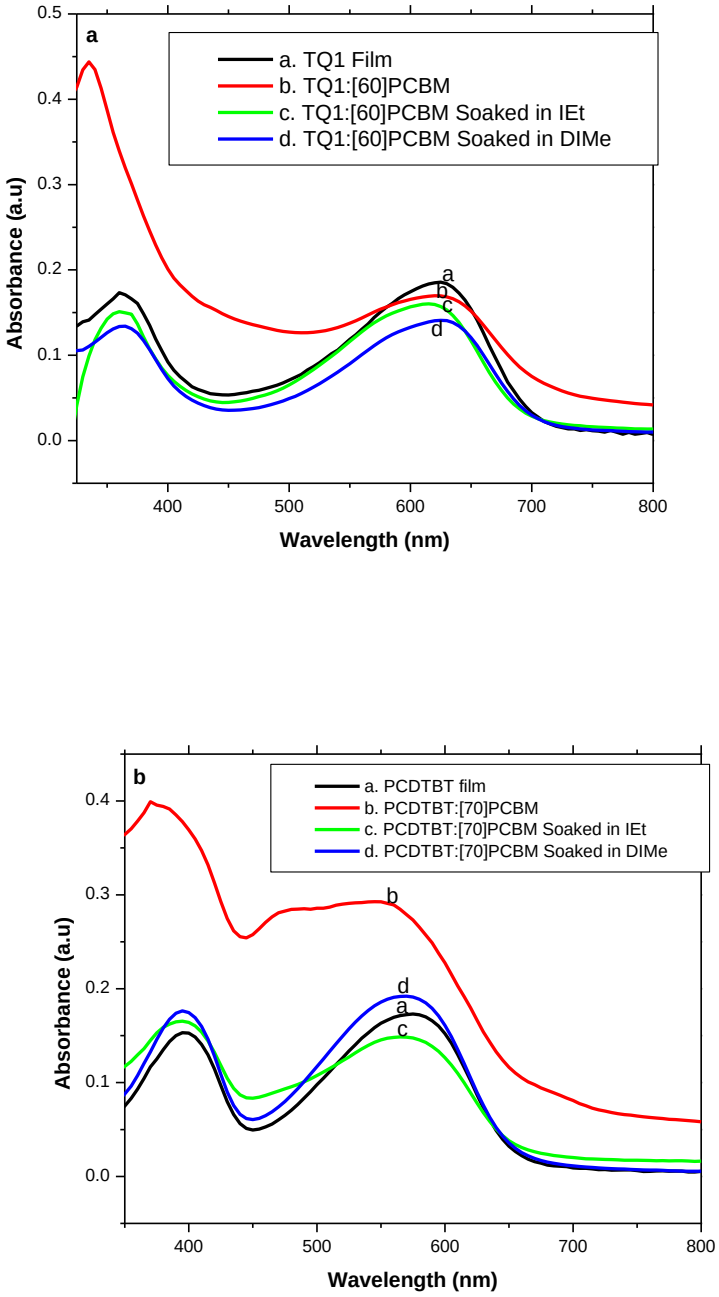

Figure 4.4.11. *UV-Vis spectra of: a) TQ1:[60]PCBM and b) PCDTBT:[70]PCBM blend films in pristine form and after soaked in IEt and DIMe for 5 seconds. UV-Vis of the corresponding films of the polymers are also included for comparison.*

Figure 4.4.12a and 4.4.12b are the corresponding PL spectra of the soaked films, the UV-Vis of which are depicted in Figure 4.4.11a and 4.4.11b, respectively. PL experiments were carried out to further confirm that PCBMs were washed out to complement the results found from UV-Vis experiments. PCBMs are efficient acceptors of electrons in BHJ solar cells [24]. When polymers get excited with photon energy at a given wavelength in the presence of PCBMs in the blend, the intensity of PL of polymer decreases. Therefore, the PL spectra of the soaked films in Figure 4.4.12a and 4.4.12b obtained are evidence for the decrease of the concentration of the quenchers as the PL intensities of the polymers get increased compared to the PL spectra of the corresponding pristine (unsoaked) blends. This also confirms that it is the PCBMs which were washed out up on soaking. Additionally, the PL spectra also give information that it is DIMe which strongly interacts with PCBMs as the intensities of PL spectra of the films soaked in it for both blends are about one order of magnitude greater than the other additives. This strong interaction of DIMe could be due to the presence of two partially negatively charged iodides which can strongly interact with electron deficient PCBM acceptors. This is also in agreement with the high fill factors and current densities (Table 4.4.2 and 4.4.3) obtained for solar cells fabricated from both TQ1:[60]PCBM and PCDTBT:[70]PCBM blend solutions processed in DIMe compared to IMe and IEt.

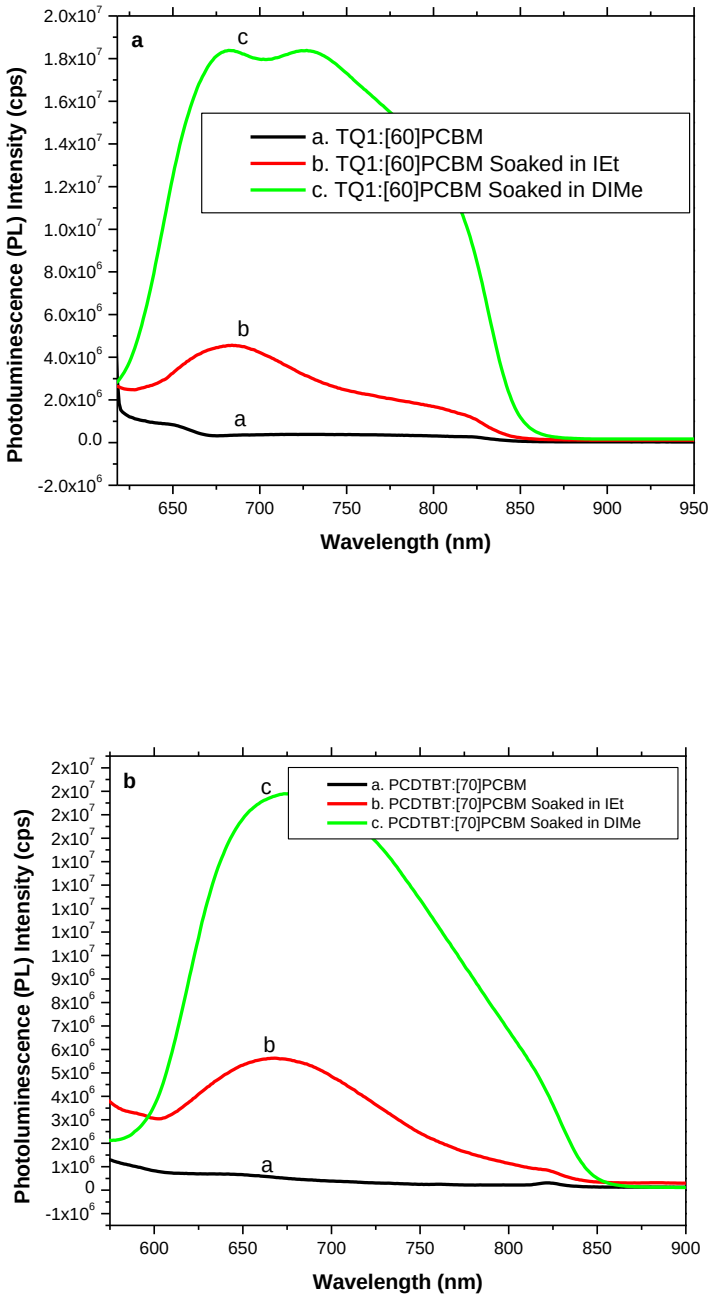

Figure 4.4.12. *Photoluminescence spectra of a) TQ1:[60]PCBM and b) PCDTBT:[70]PCBM blend films in pristine form and after soaked in IEt and DIMe for 5 seconds.*

4.4.3 Conclusion

In this study it was shown that TQ1:[60]PCBM and PCDTBT:[70]PCBM bulk heterojunction devices processed from low boiling point solvent additives exhibited enhanced PCE compared to that of devices fabricated from the corresponding pristine blend solutions. Accordingly, devices fabricated from TQ1:[60]PCBM blend containing 3% of the low boiling point solvent additives iodomethane, iodoethane, and diiodomethane have shown PCEs of 4.28%, 4.41%, and 4.66%, respectively as compared to devices without solvent additive (3.41%). Similarly, devices fabricated from PCDTBT:[70]PCBM blend solutions containing 3% IMe, IEt, and DIMe have also shown enhanced PCEs from 3.08% (control device) to 3.39 to 3.80 and to 4.37%, respectively. The reason for the enhancement of PCE of devices fabricated from both blends is mainly due to the improvement of fill factors and short circuit current densities up on addition of the solvent additives. In both cases addition of the solvent additives has not affected the V_{OC} of the devices. The improvement of fill factors and short circuit current densities clearly shows that the low boiling point solvent additives control the nanoscale morphology of the blend films. This leads to increase in interface area between donors and acceptors for efficient exciton dissociation before decaying. The additives might also enhance the percolation of donors and acceptors to electrodes for efficient charge carriers transport to respective electrodes. Generally, we have here shown that low boiling point solvent additives IMe, IEt, and DIMe have potential in controlling nanoscale morphology for BHJ solar cell applications and enhance PCEs of OSC devices.

References

1. F.C. Krebs, *Polymer Photovoltaics: A Practical Approach*, SPIE Press, Bellingham, **2008**.
2. P.G. Nicholson, F.A. Castro, *Nanotechnology*, **2010**, 21, 1.
3. L.L. Gui, L.G. Hao, Y.X. Niu, Z.E. Le, *Chinese Science Bulletin,* **2007**, 52, 145.
4. W. Tang, J. Hai, Y. Dai, Z. Huang, B. Lu, F. Yuan, J. Tang, F. Zhang, *Sol. Energy Mater. Sol. Cells,* **2010**, 94, 1963.
5. Y. Wang, W. Wei, X. Liu, Y. Gu, *Sol. Energy Mater. Sol. Cells*, **2012**, 98, 129.
6. J.E. Slota, X. He, W.T.S. Huck, *Nano Today*, **2010**, 5, 231.
7. S. Sista, Z. Hong, L.-M. Chenx, Y. Yang, *Energy Environ. Sci*., **2011**, 4, 1606.
8. R.E. Smalley, *MRS Bull.*, **2005**, 30, 412.
9. N.S. Lewis, *MRS Bull.*, **2007**, 32, 808.
10. E. Becquerel, *C. R. Acad. Sci.*, **1839**, 9, 561.
11. D.M. Chapin, C.S. Fuller, G.L. Pearson, *J. Appl. Phys*., **1954**, 25, 676.
12. M.A. Green, K. Emery, Y. Hishikawa, W. Warta, E.D. Dunlop, *Prog. Photovolt: Res. Appl*., **2015**, 23, 1.
13. M.A. Green, K. Emery, Y. Hishikawa, W. Warta, E.D. Dunlop*, Prog. Photovolt: Res. Appl*., **2015**, 23, 805.
14. M. Jørgensen, K. Norrman, S.A. Gevorgyan, T. Tromholt, B. Andreasen, F.C. Krebs, *Adv. Mater.,* **2012**, 24, 580.
15. S. Hegedus, *Prog. Photovoltaics,* **2006**, 14, 393.

16. A. Slaoui, R.T. Collins, *MRS Bull*., **2007**, 32, 211.

17. H. Akamatsu, H. Inokuchi, Y. Matsunaga, *Nature*, **1954**, 173, 168.

18. H. Shirakawa, E.J. Louis, A.G. MacDiarmid, C.K. Chiang, A.J. Heeger, *J. Chem. Soc. Chem. Commun.*, **1977**, 579.

19. D. Hertel, H. Baessler, *ChemPhysChem*., **2008**, 9, 666.

20. G.A. Chamberlain, *Solar Cells,* **1983**, 8, 47.

21. C.W. Tang, *Appl.Phys. Lett.,* **1986**, 48, 183.

22. R.H. Smalley, *Rev.Mod.Phys.*, **1997**, 69, 723.

23. N.S. Sariciftci, L. Smilowitz, A.J. Heeger, F. Wudl, *Science*, **1992**, 258, 1474.

24. G. Yu, J. Gao, J.C. Hummelen, F. Wudl, A.J. Heeger, *Science,* **1995**, 270, 1789.

25. B. Kippelen, J.-L. Bredas, *Energy Environ. Sci*., **2009**, 2, 251.

26. A.J. Epstein, *Synth.Met.*, **1987**, 18, 303.

27. W.R. Salaneck, R.H. Friend, J.L. Bredas, *Physics Reports,* **1999**, 319, 231.

28. R.J. Waltman, J. Bargon, *Can. J. Chem*., **1986**, 64, 76.

29. K.M. Molapo, P.M. Ndangili, R.F. Ajayi, G. Mbambisa, S.M. Mailu, N. Njomo, M. Masikini, P. Baker, E.I. Iwuoha, *Int. J. Electrochem. Sci.,* **2012**, 7, 11859.

30. A.J. Heeger, *Synth. Met.,* **2001**, 125, 23.

31. A.J. Heeger, *J. Phys. Chem.* B*,* **2001**, 105, 8476.

32. B. Bolto, R. McNeill, D. Weiss, *Aust.J.Chem.,* **1963**, 16, 1090.

33. A. Facchetti, *Chem. Mater*., **2011**, 23, 733.

34. C. Deibel, V. Dyakonov, *Rep. Prog. Phys*., **2010**, 73, 1.

35. R.H. Friend, D.C. Bott, D.D.C. Bradley, C.K. Chai, W.J. Feast, P.J.S. Foot, J.R.M. Giles, M.E. Horton, C.M. Pereira, P.D. Townsend, *Phil. Trans. R. Soc. Lond.* A, **1985**, 314, 37.

36. A.G. MacDiarmid, *Angew. Chem. Int. Ed*., **2001**, 40, 2581.

37. A.G. MacDiarmid, R.J. Mammone, R.B. Kaner, S.J. Porter, *Phil. Trans. R. Soc. Lond.*A, **1985**, 314, 3.

38. A. Moliton, R.C. Hiorns, *Polym.Int.,* **2004**, 53, 1397.

39. K.D. Tapan, S. Prusty, *Polymer-Plastics Technology and Engineering*, **2012**, 51, 1487.

40. M. Ates, T. Karazehir, A.S. Sarac, *Current Physical Chemistry*, **2012**, 2, 224.

41. K. Gurunathan, A.V. Murugan, R. Marimuthu, U.P. Mulik, D.P. Amalnerkar, *Materials Chemistry and Physics*, **1999**, 61, 173.

42. H. Sirringhaus, *Nat. Mater*., **2003**, 2, 641.

43. A. Pron, P. Rannou, *Polym. Sci*., **2002**, 27, 135.

44. H.E. Katz, *Chem. Mater*., **2004**, 16, 4748.

45. S. Allard, M. Forster, B. Souharce, H. Thiem, U. Scherf, *Angew. Chem., Int. Ed*., **2008**, 47, 4070.

46. R. Hamilton, C. Bailey, W. Duffy, M. Heeney, M. Shkunov, D. Sparrowe, S. Tierney, I. McCulloch, R.J. Kline, D.M. DeLongchamp, M. Chabinyc, *Proc. SPIE;Int. Soc. Opt. Eng*., **2006**, 6336, 158.

47. J.J.M. Halls, C.A. Walsh, N.C. Greenham, E.A. Marsegila, R.H. Friend, S.C. Moratti, A.B. Holmes, *Nature*, **1995**, 376, 498.

48. C.J. Brabec, S. Gowrisanker, J.J. Halls, D. Laird, S. Jia, S.P. Williams, *Adv. Mater.* **2010**, 22, 3839.

49. W. Li, R. Qin, Y. Zhou, M. Andersson, F. Li, C. Zhang, B. Li, Z. Liu, Z. Bo, F. Zhang, *Polymer*, **2010**, 51, 3031.

50. C. Li, M. Liu, N.G. Pschirer, M. Baumgarten, K. M¨ullen, *Chem. Rev*., **2010**, 110, 6817.

51. J. Chen, Y. Cao, *Acc. Chem. Res*., **2009**, 42, 1709.

52. L. Akcelrud, *Prog. Polym. Sci*., **2003**, 28, 975.

53. B. W. D'Andrade, S.R. Forrest, *Adv. Mater*., **2004**, 16, 1585.

54. H. Hoppe, S.C. Sariciftci, *J. Mater. Res*., **2004**, 19, 1924.

55. W. Yu, L. Huang, D. Yang, P. Fu, L. Zhou, J. Zhang, C. Li, *J. Mater. Chem.* A, **2015**, 3, 10660.

56. X. Ouyang, R. Peng, L. Ai, X. Zhang, Z. Ge, *Nat. Photonics*, **2015**, 9, 520.

57. C. Chen, W. Chang, K. Yoshimura, K. Ohya, J. You, J. Gao, Z. Hong, Y. Yang, *Adv. Mater*., **2014**, 26, 5670.

58. A.R.M. Yusoff, D. Kim, H.P. Kim, F.K. Shneider, W.J. Silva, J. Jang, *Energy Environ. Sci*., **2015**, 8, 303.

59. J. You, C.C. Chen, Z. Hong, K. Yoshimura, K. Ohya, R. Xu, S. Ye, J. Gao, G. Li, Y. Yang, *Adv. Mater*., **2013**, 25, 3973.

60. K.S. Liao, S.D. Yambem, A. Haldar, N.J. Alley, S.A. Curran, *Energies,* **2010**, 3, 1212.

61. H. Sun, J. Weickert, H.C. Hesse, L.S. Mende, *Sol. Energy Mater. Sol. Cells*, **2011**, 95, 3450.

62. N. Grossiord, J.M. Kroon, R. Andriessen, P.W.M. Blom, *Org. Electron.,* **2012**, 13, 432.

63. M. Jørgensen, K. Norrman, F.C. Krebs, *Sol. Energy Mater. Sol. Cells,* **2008**, 92, 686.

64. S. Lattante, *Electronics,* **2014**, 3, 132.

65. Z. Liang , Q. Zhang , O. Wiranwetchayan , J. Xi , Z. Yang , K. Park , C. Li , G. Cao, *Adv. Funct. Mater.,* **2012**, 22, 2194.

66. B. Park, Y.C. Kim, S.H. Yun, *J. Mater. Chem.* A, **2013**, 1, 2030.

67. K.-G. Lim, M.-R. Choi, H.-B. Kim, J.H. Park, T.-W. Lee, *J. Mater. Chem*., **2012**, 22, 25148.

68. C.-P. Chen, Y.-D. Chen, S.-C. Chuang, *Adv. Mater.,* **2011**, 23, 3859.

69. J. Zou, H.-L. Yip, Y. Zhang, Y. Gao, S.-C. Chien, K. O'Malley, C.-C. Chueh, H. Chen, A.K.-Y. Jen, *Adv. Funct. Mater.,* **2012**, 22, 2804.

70. T. Yuan, D. Yang, X. Zhu, L. Zhou, J. Zhang, G. Tu, C. Li, *RSC Adv*., **2014**, 4, 50988.

71. L. Hou, E. Wang, J. Bergqvist, B.V. Andersson, Z. Wang, C. Müller, M. Campoy-Quiles, M.R. Andersson, F. Zhang, O. Inganäs, *Adv. Funct. Mater.,* **2011**, 21, 3169.

72. E.G. Wang, Z.F. Ma, Z. Zhang, P. Henriksson, O. Inganäs, F.L. Zhang, M.R. Andersson, *Chem. Commun.,* **2011**, 47, 4908.

73. G. Adam, A. Pivrikas, A.M. Ramil, S. Tadesse, T. Yohannes, N.S. Sariciftci, D.A.M. Egbe, *J. Mater. Chem*., **2011**, 21, 2594.

74. E.G. Wang, Z.F. Ma, Z. Zhang, P. Henriksson, O. Inganäs, F.L. Zhang, M.R. Andersson, *J. Am. Chem. Soc.,* **2011**, *133*, 14244.

75. M.P. de Jong, L.J. van IJzendoorn, M.J.A. de Voigt, *Appl. Phys. Lett.,* **2000**, 77, 2255.

76. K.H. Yim, Z. Zheng, R.H. Friend, W.T.S. Huck, J.S. Kim, *Adv. Funct. Mater.,* **2008**, 18, 2897.

77. E. Pavlopoulou, G. Fleury, D. Deribew, F. Cousin, M. Geoghegan, G. Hadziioannou, *Org. Electron.,* **2013**, 14, 1249.

78. D.R. Baigent, R.N. Marks, N.C. Greenham, R.H. Friend, S.C. Moratti, A.B. Holmes, *Appl. Phys. Lett.,* **1994**, 65, 2636.

79. Z. Xu, L.-M. Chen, G. Yang, C.-H. Huang, J. Hou, Y. Wu, G. Li, C.-S. Hsu, Y. Yang, *Adv. Funct. Mater*., **2009**, 19, 1227.

80. M. Campoy-Quiles, T. Ferenczi, T. Agostinelli, P.G. Etchegoin, Y. Kim,T.D. Anthopoulos, P.N. Stavrinou, D.D. C. Bradley, J. Nelson, *nat.mater.*, **2008**, 7, 158.

81. S.K. Hau, H.-L. Yip, A.K.-Y. Jen, *Polymer Reviews*, **2010**, 50, 474.

82. F. Zhang, X. Xu, W. Tang, J. Zhang, Z. Zhuo, J. Wang, J. Wang, Z. Xu, Y. Wang, *Sol. Energy Mater. Sol. Cells*, **2011**, 95, 1785.

83. L.-M. Chen, Z. Hong, G. Li, Y. Yang, *Adv. Mater*., **2009**, 21, 1434.

84. A.C. Arias, M. Granstr¨om, D.S. Thomas, K. Petritsch, R.H. Friend, *Phys.Rev.* B*,* **1999**, 60, 1854.

85. T. Nyberg, *Synth. Met.,* **2004**, 140, 281.

86. T. Ameri, G. Dennler, C. Waldauf, P. Denk, K. Forberich, M.C. Scharber, C.J. Brabec, K. Hingerl, *J. Appl. Phys.,* **2008**, 103, 084506.

87. J. Yuan, X. Huang, H. Dong, J. Lu, T. Yang, Y. Li, A. Gallagher, W. Ma, *Org. Electron.,* **2013**, 14, 635.

88. A.K.K. Kyaw, D.H. Wang, D. Wynands, J. Zhang, T.-Q. Nguyen, G.C. Bazan, A.J. Heeger, *Nano Lett.*, **2013**, 13, 3796.

89. F.-C. Chen, J.-L. Wu, Y. Hung, *Appl. Phys. Lett*., **2010**, 96, 193304.

90. P.C. Yang, J.Y. Sun, S.Y. Ma, Y.M. Shen, Y.H. Lin, C.P. Chen, C.F. Lin, *Sol. Energy Mater. Sol. Cells*, **2012**, 98, 351.

91. X. Liu, C. Liu, R. Sun, K. Liu, Y. Zhang, H.-Q. Wang, J. Fang, C. Yang, *ACS Appl. Mater. Interfaces,* **2015**, 7, 18904.

92. P. de Bruyn, D.J.D. Moet, P.W.M. Blom, *Org. Electron.*, **2010**, 11, 1419.

93. T. Yang, M. Wang, C. Duan, X. Hu, L. Huang, J. Peng, F. Huang, X. Gong, *Energy Environ. Sci.*, **2012**, 5, 8208.

94. T.Yuan, X. Zhu, L. Zhou, J. Zhang, G. Tu, *Appl.Phys. Lett*., **2015**, 106, 083302.

95. X. Gong, *Polymer*, **2012**, 53, 5437.

96. K. Zhang, C. Zhong, S. Liu, C. Mu, Z. Li, H. Yan, F. Huang, Y. Cao, *ACS Appl. Mater. Interfaces*, **2014**, 6, 10429.

97. R. Xia, D.-S. Leem, T. Kirchartz, S. Spencer, C. Murphy, Z. He, H. Wu, S. Su, Y. Cao, J.S. Kim, J.C. de Mello, D.D.C. Bradley, J. Nelson, *Adv. Energy.Mater*., **2013**, 3, 718.

98. H.R. Yeom, J. Heo, G.-H. Kim, S.-J. Ko, S. Song, Y. Jo, D.S. Kim, B. Walker, J.Y. Kim, *Phys. Chem. Chem. Phys.*, **2015**, **17**, 2152.

99. Y. Zhou, H. Cheun, W.J. Potscavage, J.C. Fuentes-Hernandez, S.-J. Kim, B. Kippelen, *J. Mater. Chem*., **2010**, 20, 6189.

100. T. Kuwabara, H. Sugiyama, M. Kuzuba, T. Yamaguchi, K. Takahashi, *Org. Electron.*, **2010**, 11, 1136.

101. Y. Liu, T.T. Larsen-Olsen, X. Zhao, B. Andreasen, R.R. Søndergaard, M. Helgesen, K. Norrman, M. Jørgensen, F.C. Krebs, X. Zhan, *Sol. Energy Mater. Sol. Cells*, **2013**, 112, 157.

102. R.R. Søndergaard, M. Hosel, D. Angmo, T.T. Larsen-Olsen, F.C. Krebs, *Materials Today*, **2012**, 15, 36.

103. J.E. Carle´, T.R. Andersen, M. Helgesen, E. Bundgaard, M. Jørgensen, F.C. Krebs, *Sol. Energy Mater. Sol. Cells*, **2013**, 108, 126.

104. R.R. Søndergaard, M. Hosel, F.C. Krebs, *J Polym.Sci. Part B: Polym. Phys.*, **2013**, 51, 16.

105. M. Hosel, R.R. Søndergaard, M. Jørgensen, F.C. Krebs, *Energy Technol*. **2013**, 1, 102.

106. Z. Xue, X. Liu, Y. Lv, N. Zhang, X. Guo, *ACS Appl. Mater. Interfaces,* **2015**, 7, 19960.

107. M. Manceau, D. Angmo, M. Jørgensen, F.C. Krebs, *Org. Electron.*, **2011**, 12, 566.

108. S. Wilken, D. Scheunemann, V. Wilkens, J. Parisi, H. Borchert, *Org. Electron.*, **2012**, 13, 2386.

109. A. De Sio, K. Chakanga, O. Sergeev, K. Maydell, J. Parisi, E. von Hauff, *Sol. Energy Mater. Sol. Cells*, **2012**, 98, 52.

110. S. Wilken, T. Hoffmann, E. von Hauff, H. Borchert, J. Parisi, *Sol. Energy Mater. Sol. Cells,* **2012**, 96, 141.

111. S.K. Hau, H.-L. Yip, J. Zou, A. K.-Y. Jen, *Org. Electron.*, **2009**, 10, 1401.

112. D. Angmo, F.C. Krebs, *J. Appl. Polym. Sci*., **2013**, 129, 1.

113. B. Azzopardi, C.J.M. Emmott, A. Urbina, F.C. Krebs, J. Mutale, J. Nelson, *Energy Environ. Sci*., **2011**, 4, 3741.

114. C.J.M. Emmott, A. Urbina, J. Nelson, *Sol. Energy Mater. Sol. Cells*, **2012**, 97, 14.

115. A. Anctil, C.W. Babbitt, R.P. Raffaelle, B.J. Landi, *Prog. Photovolt: Res. Appl*., **2012**, 20, 1.

116. N. Formica, P. Mantilla-Perez, D.S. Ghosh, D. Janner, T.L. Chen, M. Huang, S. Garner, J. Martorell, V. Pruneri, *ACS Appl. Mater. Interfaces*, **2015**, 7, 4541.

117. G. Li, R. Zhu, Y. Yang, *Nat. Photonics*, **2012**, 4, 153.

118. X. Wang, D. Liu, J. Li, *Front. Chem. China*, **2010**, 5, 45.

119. S.J. Martin, D.D.C. Bradley, P.A. Lane, H. Mellor, P.L. Burn, *Phys. Rev.* B, **1999**, 59, 15133.

120. H. Hoppe, N. Arnold, N.S. Sariciftci, D. Meissner, *Sol. Energy Mater. Sol. Cells,* **2003**, 80**,** 105.

121. E. Lioudakis, A. Othonos, I. Alexandrou, Y. Hayashi, *J. Appl. Phys.,* **2007**, 102**,** 083104.

122. A.V. Gavrilenko, T.D. Matos, C.E. Bonner, S.-S. Sun, C. Zhang, V.I. Gavrilenko, *J. Phys. Chem.* C, **2008***,* 112, 7908.

123. S.H. Park, A. Roy, S. Beaupre, S. Cho, N. Coates, J.S. Moon, D. Moses, M. Leclerc, K. Lee, A.J. Heeger, *Nat.Photon.*, **2009**, 3, 297.

124. H.Y. Chen, J. Hou, S. Zhang, Y. Liang, G. Yang, Y. Tang, L. Yu, Y. Wu, G. Li *Nat. Photon.,* **2009**, 3, 649.

125. P. Heremans, D. Cheyns, B.P. Rand, *Acc. Chem. Res.*, **2009**, 42, 1740.

126. G. Chidichimo, L. Filippelli, *International Journal of Photoenergy,* **2010**, 2010, 1.

127. E. Bundgaard, F.C. Krebs, *Sol. Energy Mater. Sol.Cells,* **2007***,* 91, 954.

128. R. Kroon, M. Lenes, J.C. Hummelen, P.W.M. Blom, B. De Boer, *Polym. Rev.,* **2008***,* 48**,** 531.

129. K.M. Coakley, M.D. McGehee, *Chem. Mater.,* **2004**, 16, 4533.

130. A.J. Moule, K. Meerholz, *Appl. Phys.* B, **2007**, 86, 721.

131. J. Gilot, I. Barbu, M.M. Wienk, R.A. J. Janssen, *Appl. Phys. Lett*., **2007**, 91, 113520.

132. H.D. Ko, J.R. Tumbleston, L. Zhang, S. William, J.M. De Simone, R. Lopez, E.T. Samulski, *Nano Lett.,* **2009**, 9, 2742.

133. M. Niggemann, M. Glatthaar, P. Lewer, C. Muller, J. Wagner, A. Gombert, *Thin Solid Films,* **2006***,* 511**,** 628.

134. A. Meyer, H. Ade, *J. Appl. Phys.,* **2009***,* 106, 113101.

135. S.R. Forrest, *Nature,* **2004***,* 428, 911.

136. J.L. Brédas, J. Cornil, A.J. Heeger, *Adv. Mater.,* **1996**, 8, 447.

137. S.F. Alvarado, P.F. Seidler, D.G. Lidzey, D.D.C. Bradley, *Phys. Rev. Lett.,* **1998**, 81, 1082.

138. L.W. Barbour, R.D. Pensack, M. Hegadorn, S. Arzhantsev, J.B. Asbury, *J. Phys. Chem.* C, **2008**, 112, 3926.

139. D.E. Markov, C. Tanase, P.W.M. Blom, J. Wildeman, *Phys. Rev.* B, **2005**, 72, 045217.,

140. V. Choong, Y. Park, Y. Gao, T. Wehrmeister, K. Mullen, B.R. Hsieh, C.W. Tang *Appl. Phys. Lett.*, **1996**, 68, 3120.

141. J.J.M. Halls, K. Pichler, R.H. Friend, S.C. Moratti, A.B. Holmes, *Appl. Phys. Lett.*, **1996**, 68, 3120.

142. J.J.M. Halls, R.H. Friend, *Synth. Met.,* **1997**, 85**,** 1307.

143. D.E. Markov, E. Amsterdam, P.W.M. Blom, A.B. Sieval, J.C. Hummelen, *J. Phys. Chem.* A, **2005**, 109, 5266.

144. P. Peumans, A. Yakimov, S.R. Forrest, *J. Appl. Phys.,* **2003**, 93, 3693.

145. R.A. Marsh, C. Groves, N.C. Greenham, *J. Appl. Phys.,* **2007**, 101, 083509.

146. P.K. Watkins, A.B. Walker, G.L.B. Verschoor, *Nano Lett.,* **2005**, 5, 1814.

147. P. Schilinsky, C. Waldauf, C.J. Brabec, *Appl. Phys.Lett.,* **2002**, 81, 3885.

148. S. Gunes, H. Neugebauer, N.S. Saricifti, *Chem. Rev.,* **2007**, 107, 1324.

149. C.J. Brabec, G. Zerza, N.S. Sariciftci, G. Cerullo, S. DeSilvestri, S. Luzatti, J.C. Hummelen, *Chem. Phys. Lett.*, **2001**, 340, 232.

150. I.-W. Hwang, D. Moses, A.J. Heeger, *J. Phys. Chem.* C, **2008**, 112, 4350.

151. H. Ohkita, S. Cook, Y. Astuti, W. Duffy, S. Tierney, W. Zhang, M. Heeney, I. McCulloch, J. Nelson, D.D.C. Bradley, J. R. Durrant, *J. Am. Chem. Soc.*, **2008**, 130, 3030.

152. D. Veldman, S.C.J. Meskers, R.A.J. Janssen, *Adv. Funct. Mater.,* **2009**, 19, 1939.

153. M. Koeler, M.C. Santos, M.G.E. da Luz, *J. Appl. Phys*., **2006**, 99, 053702.

154. G.L. Gaines, M.P. O'Neil, W.A. Svec, M.P. Niemczyk, M.R. Wasielewski, *J. Am. Chem. Soc.,* **1991**, 113, 719.

155. Sze S M 1981 *Physics of Semiconducting Devices* (New York:Wiley).

156. D.I. Parker, *J. Appl. Phys.,* **1994**, 75**,** 1656.

157. V. Coropceanu, J. Cornil, D.A. da Silva Filho, Y. Olivier, R. Silbey, J.-L. Bre´das, *Chem. Rev*., **2007**, 107, 926.

158. F.A. Castro, J. Heier, F. Nuesch, R. Hany, *IEEE J. Sel.Top. Quantum,* **2010**, 99**,** 1.

159. F. Nuesch, F. Rotzinger, L. Si-Ahmed, L. Zuppiroli, *Chem. Phys. Lett.,* **1998**, 288, 861.

160. M. Kemerink, J.M. Kramer, H.H.P. Gommans, R.A.J. Janssen, *Appl. Phys. Lett.,* **2006**, 88, 192108.

161. T.-W. Lee, O.O. Park, *Adv. Mater.,* **2000**, 12, 801.

162. B. Qi, J. Wang, *Phys.Chem. Chem. Phys.,* **2013**, 15, 8972.

163. K. Vandewal, K. Tvingstedt, A. Gadisa, O. Inganäs, J.V. Manca, *Nature Materials*, **2009**, 8, 904.

164. S. Zhang, X. Yang, Y. Numata, L. Han, *Energy Environ. Sci*., **2013**, 6, 1443.

165. T.L. Benanti, D. Venkataraman, *Photosynthesis Research*, **2006**, 87, 73.

166. C.J. Brabec, A. Cravino, D. Meissner, N.S. Sariciftci, T. Fromherz, M.T. Rispens, L. Sanchez, J.C. Hummelen, *Adv. Funct. Mater*., **2001**, 11, 374.

167. M.C. Scharber, D. Műhlbacher, M. Koppe, P. Denk, C. Waldauf, A.J. Heeger, C.J. Brabec, *Adv. Mater*., **2006**, 18, 789.

168. R. Tipnis, J. Bernkopf, S. Jia, J. Krieg, S. Li, M. Storch, D. Laird, *Sol. Energy Mater. Sol. Cells,* **2009**, 93, 442.

169. X.N. Yang, J. Loos, S.C. Veenstra, W.J.H. Verhees, M.M. Wienk, J.M. Kroon, M.A.J. Michels, R.A.J. Janssen, *Nano Lett.* **2005**, 5, 579.

170. D.M. Tanenbaum, H.F. Dam, R. Rösch, M. Jørgensen, H. Hoppe, F.C. Krebs, *Sol. Energy Mater. Sol. Cells,* **2012**, 97, 157

171. F.C. Krebs, H. Spanggaard, *Chem. Mater.,* **2005**, 17, 5235.

172. C.H. Peters, I.T. Sachs-Quintana, J.P. Kastrop, S. Beaupré, M. Leclerc, M.D. McGehee, *Adv. Energy Mater.,* **2011**, 1, 491.

173. S. Beaupre, M. Leclerc, *Journal of Materials Chemistry* A, **2013**, 1, 11097.

174. K. Zweibel, *Energy Policy*, **2010**, 38, 7519.

175. K. Norrman, F.C. Krebs, *Sol. Energy Mater. Sol. Cells*, **2006**, 90, 213.

176. F.C. Krebs, K. Norrman, *Progress in Photovoltaics: Research and Applications*, **2007**, 15, 697.

177. M. Girtan, M. Rusu, *Sol. Energy Mater. Sol. Cells*, **2010**, 94, 446.

178. R. Pacios, A.J. Chatten, K. Kawano, J.R. Durrant, D.D.C. Bradley, J. Nelson, *Advanced Functional Materials*, **2006**, 16, 2117.

179. K. Kawano, R. Pacios, D. Poplavskyy, J. Nelson, D.D.C. Bradley, J.R. Durrant, *Sol. Energy Mater. Sol. Cells*, **2006**, 90, 3520.

180. X. Yang, J.K.J. Duren, M.T. Rispens, J.C. Hummelen, R.A.J. Janssen, M.A.J. Michels, J. Loos, *Advanced Materials*, **2004**, 16, 802.

181. M. Manceau, E. Bundgaard, J.E. Carlé, O. Hagemann, M. Helgesen, R. Søndergaard, M. Jørgensen, F.C. Krebs, *Journal of Materials Chemistry*, **2011**, 21, 4132.

182. F.C. Krebs, *Sol. Energy Mater. Sol. Cells*, **2009**, 93, 2009.

183. M. Manceau, A. Rivaton, J.-L. Gardette, S. Guillerez, N. Lemaître, *Polymer Degradation and Stability*, **2009**, 94, 898.

184. H. Hintz, H.-J. Egelhaaf, H. Peisert, T. Chassé, *Polymer Degradation and Stability*, **2010**, 95, 818.

185. M. Manceau, S. Chambon, A. Rivaton, J.-L. Gardette, S. Guillerez, N. Lemaˆıtre, *Sol. Energy Mater. Sol. Cells*, **2010**, 94, 1572.

186. A. Rivaton, S. Chambon, M. Manceau, J.-L. Gardette, N. Lemaître, S. Guillerez, *Polymer Degradation and Stability,* **2010**, 95, 278.

187. S. Chambon, A. Rivaton, J.-L. Gardette, M. Firon, L. Lutsen, *Journal of Polymer Science: Part A: Polymer Chemistry*, **2007**, 45, 317.

188. D.M. de Leeuw, M.M.J. Simenon, A.R. Brown, R.E.F. Einerhand, *Synth, Met,*, **1997**, 87 53.

189. T.D. Anthopoulos, G.C. Anyfantis, G.C. Papavassiliou, D.M. de Leeuw, *Applied Physics Letters*, **2007**, 90, 122105.

190. S.J. Lou, J.M. Szarko, T. Xu, L. Yu, T.J. Marks, L.X. Chen, *J. Am. Chem.Soc.*, **2011**, 133, 20661.

191. G. Dennler, M.C. Scharber, C.J. Brabec, *Adv. Mater.,* **2009**, 21, 1323.

192. T. Wang, A.J. Pearson, D.C. Lidzey, R.A. Jones, *Adv. Funct. Mater.,* **2011**, 21, 1383.

193. G. Li, Y. Yao, H. Yang, V. Shrotriya, G. Yang, Y. Yang, *Adv. Funct. Mater.,* **2007**, 17, 1636.

194. S.H. Lin, S. Lan, J.Y. Sun, C.F. Lin, *Org. Electron.*, **2013**, 14, 26.

195. J.K. Lee, W.L. Ma, C.J. Brabec, J. Yuen, J.S. Moon, J.Y. Kim, K. Lee, G.C. Bazan, A.J. Heeger, *J. Am. Chem. Soc*., **2008**, 130, 3619.

196. Y. Kim, H.R. Yeom, J.Y. Kim, C. Yang, *Energy Environ. Sci.*, **2013**, 6, 1909.

197. C.V. Hoven, X.D. Dang, R.C. Coffin, J. Peet, T.Q. Nguyen, G.C. Bazan, *Adv. Mater.,* **2010**, 22, 63.

198. L. Ye, Y. Jing, X. Guo, H. Sun, S. Zhang, M. Zhang, L. Huo, J. Hou, *J. Phys. Chem. C*, **2013**, 117, 14920.

199. A. Pivrikas, H. Neugebauer, N.S. Sariciftci, *Sol. Energy,* **2011**, 85, 1226.

200. Z. Tang, L.M. Andersson, Z. George, K. Vandewal, K. Tvingstedt, P. Heriksson, R. Kroon, M.R. Andersson, O. Inganas, *Adv. Mater*, **2012**, 24, 554.

201. Y. Zhou, D.A. Gedefaw, S. Hellström, I. Krätschmer, F. Zhang, W. Mammo, O. Inganäs, M.R. Andersson, *IEEE J.Selected Topics in Quantum Electronic*, **2010**, 16, 1565.

202. M.M. Wienk, J.M. Kroon, W.J. Verhees, J. Knol, J.C. Hummelen, P.A. van Hal, R.A. Janssen, *Angewandte Chemie*, **2003**, 42, 3371.

203. E. Wang, L. Hou, Z. Wang, S. Hellström, F. Zhang, O. Inganäs, M.R. Andersson, *Adv. Mater*., **2010**, 22, 5240.

204. T. Yamamoto, B.L. Lee, H. Kokubo, H. Kishida, K. Hirota, T. Wakabayashi, H. Okamoto, *Macromol. Rapid. Commun.*, **2003**, 24, 440.

205. J.E. Carlé, M. Jørgensen, M. Manceau, M. Helgesen, O. Hagemann, R. Søndergaard, F.C. Krebs, *Sol. Energy Mater. Sol. Cells*, **2011**, 95, 3222.

206. P. Henriksson, C. Lindqvist, B. Abdisa, E. Wang, Z. George, R. Kroon, C. Müller, T. Yohannes, O. Inganäs, M.R. Andersson, *Sol. Energy Mater. Sol. Cells*, **2014**, 130, 138.

207. V.V. Pavlishchuk, A.W. Addison, *Inorg. Chim. Acta*, **2000**, 298 97.

208. A.J. Bard, L.R. Faulkner, *Electrochemical Methods: Fundamentals and Applications*, Wiley, New York, **2001**.

209. E. Wang, Z. Ma, Z. Zhang, P. Henriksson, O. Inganäs, F. Zhang, M.R. Andersson, *Chem. Commun.***, 2011**, 47, 4908.

210. S. Hellström, F.L. Zhang, O. Inganäs, M.R. Andersson, *Dalton Trans.*, **2009**, 10032.

211. J.D.A. Lin, J. Liu, C. Kim, A.B. Tamayo, C.M. Proctor, T.Q. Nguyen, *R. Soci. Chem. Adv.,* **2014**, 4, 14101.

212. Y. Liang, D. Feng, Y. Wu, S.T. Tsai, G. Li, C. Ray, *J. Am. Chem. Soc*., **2009**, 131, 7792.

213. W.Y. Huang, C.C. Lee, S.G. Wang, Y.K. Han, M.Y. Chang, *Journal of The Electrochemical Society*, **2010**, 157, 1336.

214. F. Liu, Y. Gu, J.W. Jung, W.H. Jo, T.P. Russell, *Journal of Polymer Science, Part B: Polymer Physics*, **2012**, 50, 1018.

215. J. Bergqvist, S.A. Mauger, K. Tvingstedt, H. Arwin, O. Inganas, *Sol. Energy Mater. Sol. Cells*, **2013**, 114, 89.

216. O.V. Mikhnenko, H. Azimi, M. Scharber, M. Morana, P.W.M. Blom, M.A. Loi, *Energy Environ. Sci.*, **2012**, 5, 6960.

217. R. Kroon, R. Gehlhaar, T.T. Steckler, P. Henriksson, C. Müller, J. Bergqvist, A. Hadipour, P. Heremans, M.R. Andersson, *Sol. Energy Mater. Sol. Cells*, **2012**, 105, 280.

218. H.A.M. van Mullekom, J.A.J.M. Vekemans, E.E. Havinga, E.W. Meijer, *Materials Science and Engineering: R: Reports,* **2001**, 32, 1.

219. S. Shoaee, T.M. Clarke, C. Huang, S. Barlow, S.R. Marder, M. Heeney, I. McCulloch, J.R. Durrant, *J. Am. Chem. Soc*., **2010**, 132, 12919.

220. T.M. Clarke, A. Ballantyne, S. Shoaee, Y.W. Soon, W. Duffy, M. Heeney, I. McCulloch, J. Nelson, J.R. Durrant, *Adv. Mater.*, **2010**, 22, 5287.

221. B.S. Ong, Y. Wu, P. Liu, S. Gardner, *J. Am. Chem. Soc*., **2004**, 126, 3378.

222. W.R. Mateker, T. Heumueller, R. Cheacharoen, I.T. Sachs-Quintana, M.D. McGehee, *Chem. Mater*., **2015**, 27, 6345.

223. A. Laiho, R.H.A. Ras, S. Valkama, J. Ruokolainen, R. O¨sterbacka, O. Ikkala, *Macromolecules*, **2006**, 39, 7648.

224. D.J.D. Moet, P. de Bruyn, P.W.M. Blom, *Appl. Phys. Lett.*, **2010**, 96, 153504.

225. T.Y. Chu, S. Alem, S.W. Tsang, S.C. Tse, S. Wakim, J. Lu, G. Dennler, D. Waller, R. Gaudiana, Y. Tao, *Appl. Phys. Lett.,* **2011**, 98, , 253301.

226. R.C. Mahadevapuram, J.A. Carr, Y. Chen, S. Bose,K.S. Nalwa, J.W. Petrich, S. Chaudhary, *Synth. Met.,* **2013**, 185, 115.

227. N. Blouin, A. Michaud, M. Leclerc, *Adv. Mater*., **2007**, 19, 2295.

228. F. Zhang, J. Bijieveld, E. Perzon, K. Tvingstedt, S. Barrau, O. Inganäs, M.R. Andersson, *J. Mater. Chem.,* **2008**, 18, 5468.

229. M. Ito, K. Palanisamy, A. Kumar, V.S. Murugesan, P.K. Shin, N. Tsuda, J. Yamada, S. Ochiai, *Int. J. Photoenergy,* **2014**, 2014, 1.

230. R. Lin, M. Wright, A. Uddin, *Phys. Status Solidi A*, **2013**, 210, 1785.

231. N. Ni, B. Qu, D. Tian, Z. Cong, W. Wang, C. Gao, L. Xiao, Z. Chen, Q. Gong , W. Wei, *Macromol. Chem. Phys.,* **2013**, 214, 985.

232. J. Bergqvist, S.A. Mauger, K. Tvingstedt, H. Arwin, O. Inganäs, *Sol. Energy Mater. Sol. Cells,* **2013**, 114, 89.